Copolymer-based membrane stabilizers for Duchenne Muscular Dystrophy

A Dissertation
SUBMITTED TO THE FACULTY OF
UNIVERSITY OF MINNESOTA
BY

Evelyne Morgane Houang

IN PARTIAL FULFILLMENT OF THE REQUIREMENTS
FOR THE DEGREE OF DOCTOR OF PHILOSOPHY

Joseph M. Metzger

April 2016

Acknowledgements

I feel lucky to say that my graduate studies have been one of the best times in my life, both in terms of academic accomplishment and personal life satisfaction. I understand and fully appreciate that it is not often the case for most people. For that, I am grateful to the people that have been on this journey with me.

I would first like to acknowledge my advisor and mentor, Joe Metzger. I first heard about Joe around 2008, at the time pursuing undergraduate research on Duchenne Muscular Dystrophy while still finishing my chemistry degree. Joe has been an eminent researcher in the field of DMD and heart disease and at the time, as I was wondering where my young research career would take me, if anywhere, he was one of the few people in this country that I had actual interest in working for. That opportunity would come serendipitously. It turned out that about a week before I accepted another research job at the Center for Drug Design at the U, someone from Joe's lab just happened to walk into my new boss' office out of the blue asking to collaborate on a project. That eventually turned into me joining the IBP program to work for Joe. Joe's continuous support and unwavering passion and excitement for research will always inspire me to keep my head up when times are difficult, always trudge on when things don't go my way, and to always be excited about any discoveries, small and large, that are made. His passion (and competitiveness) is contagious, and I thank him for guiding me with it.

Another person who has made an enormous impact on my graduate career is my old boss, Yuk Sham, a computational chemist at the Center for Drug Design. At a time when I was completely unsure whether I even wanted to go to graduate school or into research, his pure excitement for science in general, his way of thinking (way) outside the box in often amusing ways, and for solving any problems that came his way, sealed the deal for me. The one I go to every time I am stuck in the computational part of my project, he is that character in the movies that you trust is going to show up at the very last minute and save you from impending doom. Without fail, that has been the case. For that, I thank him. Also, thanks for keeping me well fed many, many times, sensei.

I also want to thank the rest of my committee, DeWayne Townsend, Frank Bates and Dawn Lowe. DeWayne was the person who led this project before I joined and his advice and support for me through it has been invaluable. Frank, for his unabated excitement for all things polymers, which bled into my thesis. And finally Dawn, who has been a support ever since my undergraduate years and who is one of the reasons why I love muscle physiology.

Finally, I want to thank my friends, especially the ones who were in this graduate school path with me. Some were with me since the beginning, others I met throughout. All have been invaluable and are cherished. I want to particularly thank Dalay and Cheryl, I had no idea when we first met that we would become this little core that would go through everything together. They are literally the main reason I made it this far while still having so much fun. I wouldn't have given you up for anything. I'd also like to thank Brian Thompson and Anthony (Tony) Vetter for being my bay companions. I have learned so much from both of you and our conversations and debates have made my days in lab so much more fun than they should have been. Whether it is cheering me up with hilarious gifs found on the internet or with a drink of whiskey after a rough day, I am so glad that if I had to spend so much time in a small space with anyone during my working days, it was with the both of you. You will however never convince me that American football is better than real football. Lastly, I would like to thank all the other friends I made throughout grad school. You are the only people who truly appreciate the corny science jokes and banter we trade with each other, and who appreciate that science is not just one protein or one gene or one disease, but rather a way of thinking and learning about the whole world around us. I had so much fun learning about astrophysics, dinosaurs, emerging viruses and insects with people who appreciate all that as much as I do. One motto that I strive to live by is "if you walk into a room and you are the smartest person there, you are in the wrong room". I am quite proud to say that I never, ever, was in the wrong room.

Dedication

This thesis is dedicated to my parents, who have unconditionally supported me through everything. Your complete dedication and love is the reason I am here. You have made me the person I am today and I have no idea who I would be without you. I love you.

Abstract

The overarching objective of this work centers on a structure-function approach to investigate the mechanism of action of synthetic copolymer-based membrane stabilization in the context of Duchenne Muscular Dystrophy (DMD). The guiding theme is the investigation of mechanism of interaction of membrane stabilizing copolymers using cellular and whole animal physiology, chemical engineering, and supercomputational approaches.

DMD is an X-linked recessive disease of marked striated muscle deterioration affecting 1 in 3500-5000 boys. DMD results from the lack of the cytoskeletal protein dystrophin, which is essential for maintaining the structural integrity of the muscle cell membrane. DMD patients develop severe skeletal muscle degeneration, along with clinically significant cardiomyopathy. There is no cure for DMD patients, or any effective treatment to halt, prevent or reverse DMD striated muscle deterioration. The primary pathophysiological defect in DMD is the marked susceptibility to contraction-induced membrane stress and the subsequent muscle damage and degeneration that occurs due to loss of muscle membrane barrier function. In this context, a unique therapeutic approach is the use of synthetic membrane stabilizers to prevent muscle damage by directly stabilizing the dystrophin-deficient muscle membrane. The triblock copolymer poloxamer 188 (P188) has numerous features that make it an attractive synthetic membrane stabilizer candidate for DMD treatment and has been demonstrated to target and stabilize damaged membranes in various pathophysiological contexts.

The efficacy of P188 in protecting the dystrophic myocardium has been well established, but its effect on the dystrophic skeletal muscle has remained unclear. This work for the first time demonstrates that P188 stabilizes the dystrophic skeletal muscle membrane in vivo and protects it against the mechanical stress associated with lengthening contractions. This result validates P188 as a therapeutic strategy to directly target the hallmark of DMD: impaired membrane stability in all striated muscles.

Very little is known on how P188 interacts with and stabilizes biological membranes. To fundamentally probe the mechanism of action of synthetic copolymers as membrane stabilizers, a structure-function approach was undertaken. The aim was to gain insight into the essential critical chemical parameters of copolymers in terms of membrane interacting properties. This work shows for the first time that copolymer mass, composition, architecture, and functional end group chemistries significantly define mechanism of action at the membrane. Based on these insights, an "anchor and chain" model is advanced whereby membrane interaction is critically dependent on end group hydrophobicity.

Finally, leveraging the power of supercomputational approaches, Molecular Dynamics simulations were developed to further evaluate and understand copolymer-membrane interactions at atom level resolution. Using increases in surface tension applied to the lipid bilayer, an area-per- lipid dependence of adsorption vs. insertion was uncovered, supporting the hypothesis that copolymers insert into areas of decreased lipid density and then are "squeezed-out" once membrane integrity is restored. Collectively, these findings shed new light on block copolymer dynamic interaction with biological membranes.

Table of Contents

List of Tables

List of Figures

Chapter One

Chapter Two

Chapter Three

Chapter Four

Chapter Six

CHAPTER 1
INTRODUCTION

Overview

The central focus of this dissertation is the investigation of copolymer-based membrane stabilizers to protect striated muscle membranes against the mechanical forces associated with contraction in the context of Duchenne Muscular Dystrophy (DMD). The purpose of this chapter is to describe DMD and the role of dystrophin, as well as introduce a potential synthetic copolymer-based therapeutics to the disease.

1.1 Duchenne Muscular Dystrophy

Duchenne Muscular Dystrophy is an X-linked neuromuscular disease of muscle degeneration which results from the lack of the dystrophin protein at the muscle membrane (sarcolemma)[1]. It was first described in 1852 by Meryon and later by Duchenne in 1868[2]. As the most common of the human muscular dystrophies, it affects 1 in 3500 males every year[3] or ~20 000 new patients worldwide each year, with typical onset between the ages of 2 and 5 years that is characterized by delay in achieving childhood motor milestones. The disease presents as a prominent and progressive weakness in the lower limbs muscles and postural muscles[4], leading to spinal scoliosis, and decrease in exercise capacity. Weakness of the knees and hip extensors are displayed through the Gower's sign, a maneuver through which the affected child will right himself from a supine position by using his hands and arms to extend the hips and bring the torso to an upright position[5]. Other physical symptoms include reduced muscle bulk, pseudo-

hypertrophy and contractures of the calf muscles and joints[6]. Bone fragility and osteoporosis also contribute to the development of scoliosis[7].

Concurrent with the decline in orthopedic condition is loss of respiratory function brought on by significant diaphragm wasting[8] leading patients to be placed on positive pressure nocturnal ventilation. Current clinical diagnosis is made via genetic testing to probe for absence of the dystrophin protein or mutation in dystrophin gene, as well as measurements of plasma levels of creatine kinase (CK)[9,10], a striated-muscle specific enzyme marker of membrane damage. Loss of ambulation and wheelchair dependency occur by their early teens[11], and patients typically succumb in their late second decade of life due to respiratory failure.

In addition to the skeletal muscle pathology, DMD patients also develop progressively severe cardiomyopathy, with 10-20% of cases presenting as dilated cardiomyopathy[12] with arrhythmias and eventually heart failure occurring in the latter half of the second decade of life[11]. With increases in patient lifespan as a result of palliative glucocorticoid treatment and improvements in respiratory care and orthopedic corrections[9,13], cardiomyopathy is an increasingly important but underappreciated contributor to DMD mortality despite cardiomyopathy being present in 90% of DMD patients by age 18 and confirmed by the finding of significant myocardial fibrosis in autopsies[14–17]. Interestingly, the cardiomyopathy usually remains subclinical at early age and cardiac disease progression typically proceeds at a slower rate compared to the skeletal muscle degeneration[18]. The incidence and evolution of cardiomyopathy in Duchenne muscular dystrophy is presumably due to lesser strain on the heart when physical activity is limited once the patient is wheelchair bound. Clinical symptoms include rhythmic, structural and hemodynamic abnormalities with defects in both systolic and diastolic functions[19]. Electrocardiography reveals some electrical conduction impairment such as sinus tachycardia, premature atrial contractions and fast atrioventricular node conduction[11].

Gastrointestinal manifestations related to smooth muscle dysfunction also occur more commonly as a secondary pathology to respiratory infection, cardiac failure or recent surgery although spontaneous smooth muscle dysfunction has been observed in the latter stages of the disease[11]. Smooth muscle of the gastrointestinal tract of DMD patients show both loss and atrophy and fibrosis[11].

Cognitive impairment is also seen in varying degrees in DMD patients indicating that dystrophy affects brain function although the impairment is neither progressive nor correlated with the severity of the musculoskeletal symptoms[20]. Boys with DMD have been observed to perform more poorly on tests requiring attention to complex verbal information and the mean IQ for DMD patients is one standard deviation below normal, with 1/3 patients having an IQ below 75. The causes of the IQ impairment remains unclear although studies have revealed abnormal dendritic development and arborisation of nerve axons branching[21].

1.2 Dystrophin

Extensive genetic analysis of DMD patients determined that disruption of the dystrophin gene is causal for the disease[1]. Dystrophin is the largest discovered human gene and is located on the short arm of the X-chromosome, consists of 79 exons and is over 2.3 million base pairs in size. It also has one of the highest known spontaneous mutations rates of all human genes. There are three full-length isoforms with three different promoters in striated muscle, brain and cerebellar Purkinje neurons. Other isoforms are generated via alternative splicing events[22]. The dystrophin gene has four internal promoters, dp260, dp140, dp116 and dp71 that have tissue specific expressions[1,23]. Deletion of one or more exons is the most common defect in the DMD gene, with duplications, point mutations (missense, nonsense, and splice site variations) and rearrangement (insertions, deletions or inversion) being less common defects. While

the vast majority of DMD mutations results in the complete absence of dystrophin, certain mutations result in low levels of a truncated but partially functional dystrophin protein with individuals affected by a milder form of the disease (Becker muscular dystrophy).

The dystrophin protein is a 427 kDa, 3685 amino acids rod-shaped cytoskeletal protein found on the intracellular surface of the muscle membrane that links cytoskeletal γ-actin to the extracellular matrix. Dystrophin consists of four major functional domains: an actin-binding domain at the N-terminus, a central rod domain consisting of 24 spectrin-like repeats separated by four hinge regions, that has been shown to unfold and give flexibility in response to mechanical stretch[24], a cysteine-rich domain that interacts with the transmembrane protein β-dystroglycan, and a C-terminal domain, the latter being important for dystrophin's interaction with other sub-sarcolemmal proteins. Carefully designed transgenic studies have determined that the domains most critical to the DMD pathology are the cysteine-rich domain and the N-terminal domain, which are those directly associated with mechanically linking the extracellular matrix and the cytoskeleton[25].

Dystrophin is part of a large membrane-spanning complex of glycoproteins (Dystrophin-Glycoprotein complex or DGC) that also include sarcoglycans (α, β, γ, δ), dystroglycans (α and β), dystrobrevins, syntrophins and sarcospan (**Figure 1**). The essential function of dystrophin in striated muscle is to stabilize the muscle membrane against the forces associated with contraction thereby acting as a "molecular shock absorber" or molecular force dampener of the muscle membrane.

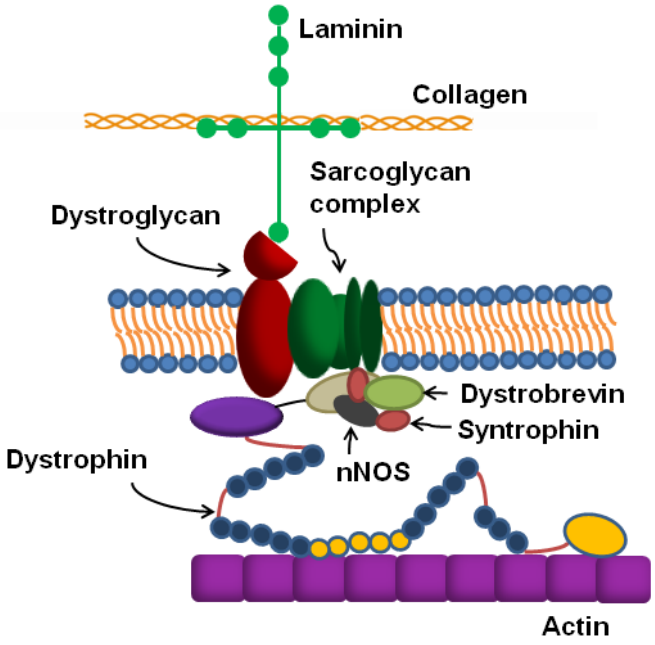

Figure 1: Dystrophin-glycoprotein complex (DGC) at the sarcolemma.

Loss of dystrophin affects many aspects of muscle function and the precise molecular mechanisms leading to membrane injury and muscle degeneration is not fully resolved. The importance of dystrophin's molecular reinforcement at the membrane is evident in studies showing that dystrophin-deficient muscle fibers where the membrane was experimentally removed show no difference in contractile function compared to normal skeletal muscle fibers, indicating a defect in the membrane-cytoskeleton linkage rather than in the contractile apparatus[27]. The DGC is found to be enriched at the costamere, a sub-sarcolemmal protein complex which assembles at regular intervals along the sarcomere and stabilizes the cytoskeletal apparatus via the intermediate filament network through the membrane, to the extracellular matrix[28,29]. In cardiac myocytes, dystrophin appears to also co-localize with t-tubules[30]. Dystrophin is crucial for maintenance of the DGC in skeletal muscle[31], the lack of dystrophin leading to marked reduction of all DGC components at the sarcolemma. In contrast and for unclear

reasons, DGC expression is not significantly affected by loss of dystrophin in cardiac muscle[32].

Dystrophin plays a critical role mechanically linking the extracellular matrix to the sarcomeres and the extracellular matrix transmits the force generated at the sarcomeres to the muscle tendon[33–35]. In striated muscle, force is transmitted laterally from the Z-discs at the sarcomere through the membrane to the extracellular matrix[33,36]. These studies suggest that force is lost during transmission from cell-to-cell independent of loss in membrane integrity[37,38].

Dystrophin has a homolog protein, utrophin, with which it shares significant sequence and structural homology[39]. While utrophin is not part of the DGC complex itself, it is highly expressed in muscle during development but its expression becomes restricted to only the neuromuscular junction and myotendinous junctions in normal adult skeletal muscle. However, utrophin expression has been found to be upregulated at the sarcolemma along the entire myofiber and was found to mitigate the severity of the pathogenesis in some DMD animal models, suggesting that this adaptation is beneficial and leading to the proposition of utrophin upregulation as a potential therapeutic goal for DMD.

In addition to mechanical and anchoring roles, DGC members also act as scaffolding proteins for various signaling pathways. Syntrophins, which bind to homologous sequences in the C-terminal domain of dystrophin, contain a PDZ domain which recruits nitric oxide synthase (nNOS), aquaporin-4, diacylglycerol kinase-ζ, and various ion channels to the DGC. Here nNOS is of particular interest in DMD as a well-known signaling molecule involved amongst other cellular processes, in the regulation of blood flow to skeletal muscle by synthesizing nitric oxide from the oxidation of L-arginine to L-citrulline. Nitric oxide diffuses to vascular smooth muscle cells and opposes exercise-induced α-adrenergic constriction and this process was found to be impaired in DMD[40]. Effectively, nNOS is lost from the sarcolemma when dystrophin is absent and is reduced in both total content and activity[41,42]. As such, dystrophic skeletal

muscle is susceptible to ischemic insults, and therefore decreased perfusion, during contractile events[43]. Moreover, nNOS is expressed at high level in fast type II skeletal muscle fibers which may explain the increased susceptibility of this fiber type to injury in DMD[44]. These results point to a deleterious effect of unopposed adrenergic vasoconstriction on dystrophic muscle perfusion both in terms of energetic depletion due to ischemia as well as restricted perfusion of potential therapeutics to affected muscles.

1.3 Muscle mechanics

1.3.1 Muscle structure

Skeletal muscles are made up of myofibers, which themselves contain bundles of myofibrils made up of proteins including actin and myosin filaments arranged in repeat myofilament units named sarcomeres. The arranged repetitive units of sarcomeres along the length of the myofibril give skeletal muscles their characteristic striated appearance. The functional unit of the myofibril is named a sarcomere, which consists of thick filaments made up of the protein myosin and thin filaments made up of actin. The globular heads on myosin are also known as cross-bridges as their role is to bind and pull actin thin filaments past the thick filament in what is known as the sliding filament mechanism of muscle contraction.

1.3.2 Excitation-contraction coupling

At the initiation of contraction, electrical impulses are transmitted from nerve terminal endings of motor neurons to the motor end plates of muscle fibers. This causes depolarization of the cell membrane and propagation of the action potential through the transverse tubule system leading to activation of voltage-gated Ca^{2+} channels and release

of Ca^{2+} from the sarcoplasmic reticulum (SR) of the muscle cell. This leads to a transient increase in cytoplasmic Ca^{2+}, activation of the contractile apparatus, and generation of muscle tension. This process linking the depolarization of the muscle sarcolemma to the release of Ca^{2+} from the sarcoplasmic reticulum (SR) of the muscle cell is referred to as excitation-contraction (EC) coupling[45]. EC coupling differs between skeletal and cardiac muscle. In skeletal muscle, the action potential passes along the sarcolemma and into the sarcolemmal invaginations of the t-tubule system. Depolarization is sensed by voltage-sensitive Ca^{2+} channels, the dihydropyridine receptor (DHPR), which isoforms differ between cardiac and skeletal muscle. The skeletal muscle DHPR only mediates a small influx of extracellular Ca^{2+} and activates Ca^{2+} release from the SR via direct mechanical coupling with the ryanodine receptor type 1. In contrast, in a cardiac muscle cell, the extracellular Ca^{2+} flowing through the DHPR binds to and activates the ryanodine receptor type 2 on the SR, leading to Ca^{2+} release from the SR in a "Ca^{2+} induced Ca^{2+} release" process.

At resting intracellular Ca^{2+} concentrations, the contractile apparatus remains in an inactivated state in which myosin heads on the thick filaments cannot bind actin on the thin filaments due to tropomyosin interacting with and blocking actin-myosin binding sites on actin. Upon SR Ca^{2+} release, the resulting rise in cytoplasmic Ca^{2+} leads to Ca^{2+} binding to troponin C, the sensory component of the three part protein complex troponin, on the thin filaments which then allosterically moves tropomyosin to reveal the myosin binding sites on actin. Myosin heads then bind actin and initiate the ATP-dependent cross-bridge cycling process which is the basic process for muscle force production and contraction.

1.3.3 Types of muscle contractions

Excitation-contraction coupling leads to a twitch response from muscle units and the contraction of whole muscle groups is derived from both temporal and spatial

summation of single twitches. Repeated and rapid stimuli create a maximal sustained contraction called tetanus. There are three types of muscle contractions: shortening (or concentric), isometric, and lengthening (or eccentric). Shortening contractions occur when the force produced by the muscle exceeds the force applied to the muscle resulting in shortening of the muscle. Isometric contractions are characterized by constant muscle length during activation, with the force generated dependent on the muscle length at time of activation. Maximal isometric force is generated at the muscle optimal length (L_o) where the maximum numbers of cross bridges are available. Lengthening contractions occur when the force applied to the muscle exceeds the force generated by the muscle, resulting in lengthening of the muscle. Repetitive lengthening contractions can cause damage to myofibers by injuring elements of the EC coupling machinery[36,46].

1.4 Cell membrane structure, function, and susceptibility to mechanical injury

1.4.1 Biological lipid membranes

Biological membranes are asymmetrical bilayers approximately 5-6 nm thick and composed of various lipids including phospholipids, sphingolipids, glycolipids and sterols, with compositions varying between different cell types and in diseased states. The cell membrane is also typically composed of 20-30% proteins responsible for ion conduction, various signaling pathways, and structural integrity[47]. Regardless of the cell type and function, the primary role of the cellular membrane is to segregate the intracellular milieu from the outside environment to actively preserve intracellular homeostasis. Its constituent proteins are essential for normal transmembrane passage of ions, allowing maintenance of physiological ionic gradients at affordable metabolic cost. Failure to maintain this barrier function leads to exhaustion of the metabolic energy of the cell, biochemical arrest, and eventual cellular demise. The membrane bilayer is held

together via hydrophobic effect with the surrounding polar environment as well as van der Waals forces, hydrogen bonding, and electrostatic interactions. Membrane constituents are allowed various intra-bilayer motions, such as lateral diffusion, rotation of lipids around their major axes, and oscillations[48–50]. These motions as well as degree of packing the bilayer components are collectively described as "membrane fluidity"[48], which is modified by a number of factors such as lipid composition, sterol enrichment, and temperature, and which is commonly assessed using fluorescence polarization methods, electron spin resonance and other spectroscopic methods[51–54]. It has been proposed that lipid fluidity and membrane conformation influences the activity and dynamics of membrane proteins[52]. Along with membrane fluidity, the structure and composition of the bilayer can be described by parameters such as rigidity, elasticity, and tensile strength, all of which make up the membrane physical property known as plasma membrane order[50,55]. Data from various studies have proposed that an optimal level of membrane order is essential for normal myocyte function[49,56]. Of particular interest to muscle, nicotinic acetylcholine receptors (nAChRs), which are present at neuromuscular junctions of muscle cells, require optimal membrane order to retain normal function[57] and alterations to the membrane either during mechanical stress or in diseased states such as in DMD could have important ramifications on action potential generation and propagation during muscle contraction.

1.4.2 Membrane permeability and mechanical injury in DMD

Electron microscopy analysis of DMD muscle revealed absent or disrupted sections of the muscle membrane thereafter named delta lesions[58,59]. This led to the theory that the loss of dystrophin and associated proteins at the sarcolemma renders the muscle susceptible to muscle contraction-induced injury. Indeed, the finding of the soluble enzyme creatine kinase released from the injured muscle into the serum is a clinical hallmark of the disease[60]. Moreover, the ongoing degeneration-regeneration

process leads to satellite cells exhaustion and replacement of muscle with fibrotic and fatty connective tissues leaving small islands of intact muscle cells. The membrane permeability associated with the lack of dystrophin leads to loss of homeostasis within the cell, with influx of ions such as Ca^{2+} from the extracellular fluid, which in turns activates pathological pathways inside the cell such as inflammatory immune cell infiltration, cytokines and proteolytic enzyme activation, leading to apoptosis and necrosis[61,62].

Membrane permeability is further exacerbated by mechanical stress, particularly with lengthening contractions of skeletal muscles such as during downhill walking/running[34]. In DMD patients, muscle biopsies reveal ongoing degeneration and regeneration of muscle fibers and creatine kinase is persistently elevated. It is unclear what the precise nature of membrane disruptions after lengthening contractions look like, however, the release of intracellular enzymes such as creatine kinase and the uptake of large proteins such as albumin and vital dyes like Procion orange[34] and Evans blue dye[63] into non necrotic muscle fibers indicate that the membrane disruption is sufficiently large to permit the transmembrane passage of large macromolecules[60].

Lengthening injury is particularly apparent in the diaphragm which contracts to expand the lungs during breathing, with ventilatory muscles of DMD animal models and patients having impaired contractility and increased fibrosis[64]. Dystrophin also plays a crucial role in buffering against cardiac myocyte extension. This occurs when the ventricle fills with blood during diastole, and its absence leads to the formation of small membrane tears as evidenced by uptake of extracellular molecules[37]. Moreover, the consequences of membrane disruptions and increased permeability to extracellular ions such as Ca^{2+} are intrinsically different between cardiac and skeletal muscle as the process of Ca^{2+} induced Ca^{2+} release from the ryanodine receptors is amplified in the heart[65]. As such, with increases in contractility and larger passive extensions, subsequently more unregulated Ca^{2+} entry into the cell eventually results in terminal contracture of the dystrophic myocyte[37].

Along with its barrier maintaining function, the cell membrane is responsible for transmitting and propagating action potentials generated at the neuromuscular junction to the transverse tubule (t-tubule). In dystrophic muscles, this network is directly affected by lengthening stretches as it runs perpendicular to the axis of contraction and anchors along the contractile unit of the muscle (sarcomere)[66]. The t-tubules contain the voltage-gated Ca2+ channels required to activate muscle contraction and are required for proper propagation of action potentials generating from the nerve terminals to the whole muscle. As lengthening stretch disrupts the sarcomeres of weakened muscle membranes, the t-tubules are also laterally disrupted, affecting electrical conduction during muscle contraction.

1.4.3 Calcium homeostasis

It is strongly suggested that Ca^{2+} homeostasis may be perturbed in dystrophic muscle and that this may be an important initiator of the pathological processes leading to muscle cell death. Intracellular calcium levels are reported to be elevated in both *mdx* skeletal muscle fibers and cardiomyocytes[37,67–69]. It is still unclear what causes this rise in intracellular Ca^{2+}, with some studies suggesting Ca^{2+} entering the cell due to increased sarcolemmal permeability or "breaches"[37], and other studies showing evidence for the activation of Ca^{2+} leak channels or stretch-activated channels[70]. Regardless of the initial mechanism of entry, this abnormal elevation in Ca^{2+} has consequences to muscle structure and function due to activation of pathological Ca^{2+} sensitive cellular pathways such as activation of the calpain proteases[71] and perturbation of calcium-activated signaling pathways including calmodulin[72], calcineurin[73], and the mitochondrial permeability transition[74]. A pathological rise in cytosolic Ca2+ also contributes to membrane damage via activation of phospholipase A2 and promotion of reactive oxygen species (ROS) production by the mitochondria[75]. ROS in turns leads to peroxidation of membrane lipids[76,77]. Consequently, maintaining intracellular Ca^{2+} homeostasis by

preventing deleterious influx of extracellular Ca^{2+} is crucial to maintaining sarcolemmal integrity and survival of the dystrophic myocyte.

1.4.3 Endogenous cellular membrane repair mechanisms

For pure lipid bilayers such as liposomal and vesicular assemblies, resealing of injured bilayers occurs in a spontaneous, thermodynamically driven manner at a rate dependent on membrane tension, with higher membrane tension having slower rate of repair[78,79]. On the other hand, the presence of a cortical cytoskeleton in living cells results in a baseline surface tension that is not existent in simple lipid bilayers and which prevents spontaneous resealing[80,81]. Loss of membrane integrity compromises its function in maintaining cellular homeostasis and can lead to the demise of the cell. As membrane disruptions are common and normal events in the life of a cell, particularly in muscle cells[82], there must exist an innate repair mechanism to rapidly restore the integrity of the cell and prevent cell death.

It was found that resealing of living cells is immediately preceded by a decrease in membrane tension[79] and absolutely requires Ca^{2+} -dependent exocytosis to deliver vesicles to the site of disruption to fuse and form patches[79,83]. This decrease in membrane tension is, at least in part, due to expanding of membrane area by active insertion of internal vesicle membrane via exocytosis[82,84]. The protein dysferlin, which localizes to the plasma membrane[85], has been identified as having a pivotal role in the active membrane repair process in cardiac[86] and skeletal muscle[87]. Dysferlin is thought to regulate vesicle trafficking and fusion at the site of membrane injury in a Ca^{2+} dependent manner via association with annexins A1 and A2[88,89] and requires several other proteins including SNARE proteins[90] and synaptotagmins[91]. The absence of dysferlin leads to defective membrane resealing and certain types of muscular dystrophy classified as dysferlinopathies[92]. Another protein that was discovered to play an important role in membrane repair is the TRIM-family E3 ubiquitin ligase protein MG53. MG53 is

recruited to the injury site where it is proposed to be oxidized when exposed to the oxidative extracellular environment to form a disulfide-linked oligomerized scaffold[93,94]. This scaffold then serves as an assembly site to recruit MG53-tethered intracellular vesicles toward the injury site for fusion with the damaged membrane[94,95].

In DMD, increased susceptibility to membrane tearing eventually leads to cell death and muscle degeneration by eventual overwhelming of this cell repair processes[96]. Chronic damage resulting from a continual cycle of muscle degeneration and regeneration eventually leads to depletion of the skeletal muscle stem cell pool and muscle wasting.

1.5 Current therapeutic strategies for DMD

1.5.1 Palliative treatments

There is currently no cure for DMD and while current supportive therapies help improve lifespan and quality of life, development of new and improved palliative treatments is still critical. The most commonly prescribed treatments are ventilatory support, corticosteroids and β-blockers[6,97–99]. Nocturnal ventilatory support is provided in the earlier stages of the disease, but inevitably becomes constantly required as the disease worsens owing to loss of diaphragm function. Ventilatory support has been shown to maintain pulmonary function presumably by reducing diaphragm workload and significantly prolongs DMD patients' lifespan[8,99,100].

Corticosteroids have been used to treat DMD since the mid 1970s[97] and are the current standard therapy for the disease. Prednisolone and deflazacort are regularly administered soon after diagnosis and have been shown to slow the progression of the disease by improving muscle strength and exercise capacity thereby delaying loss of ambulation and improving both pulmonary and cardiac functions[16,97,101]. Glucocorticoids

have been shown to benefit both skeletal and cardiac muscle and while the precise mechanism through which corticosteroids improve muscle function remains unclear, it is hypothesized that it is beneficial via anti-inflammatory effects, increased expression of the dystrophin homolog utrophin, and increased skeletal muscle proliferation[97,98,102]. However, chronic corticosteroids use is associated with numerous adverse effects including weight gain, gastrointestinal symptoms, behavioral difficulties, cataracts and bone demineralization[98,103,104]. Despite the side effects and risks involved with long-term chronic use of steroids, corticosteroids continue to be the first-line treatment for DMD.

For the DMD heart disease, β-blockers are usually prescribed at the first signs of cardiomyopathy and in combination with ACE inhibitors have shown to improve left ventricular ejection fraction and reduced mortality[105–107]. β-blockers prescribed at the point of diagnosis as a cardioprotective pretreatment is currently under consideration. While these treatments help alleviate symptoms, they do not directly target the disease mechanism nor prevent its progression.

1.5.2 Animal models of DMD

The primary mouse model of DMD, the *mdx* mouse, was discovered not long after the discovery of the dystrophin gene, by the detection of muscle pyruvate kinase and creatine phosphokinase in serum in a screen for glycolytic enzyme mutants[108]. This mouse model harbors a naturally occurring non-engineered stop codon in exon 23 of the dystrophin gene causing the lack of dystrophin in all of its striated muscle. As such, the mdx mouse displays most of the hallmarks of DMD including decreased lifespan, muscle wasting, progressive cardiomyopathy, fibrosis, and leakage of muscle specific enzymes into the serum. However, the *mdx* mouse has a milder baseline phenotype presumably due to compensatory mechanisms in mice such as increased expression of the dystrophin homolog utrophin. *Mdx* mice do show many features of DMD with pathology being most

prominent in the diaphragm[64] where fiber loss and collagen deposition are significant and atrophy and fibrosis of limb muscles present in older *mdx* mice.

While the *mdx* phenotype does not fully recapitulate the human disease severity under normal conditions, physiological stresses induce significant cardiac and skeletal muscle dysfunction in *mdx* mice[37,34]. In terms of cardiac function alterations, *mdx* hearts have changes in ventricular geometry with significantly lowered systolic and diastolic volumes compared to normal hearts but largely maintain stroke volume[37]. The shift to lower volumes is hypothesized to be due to adaptation against the defect in passive distention in *mdx* cardiac myocytes, resulting in a relatively normal baseline cardiac function but little cardiac reserve, which is particularly evident during adrenergic stress testing[37]. The vast majority of studies have been carried out using this model making it the current standard model to evaluate therapeutic efficacy for DMD. More similarly to DMD patients, dystrophin/utrophin double knockout mice (*mdx:utr*$^{-/-}$) have a much more catastrophic phenotype at baseline and significantly reduced lifespan, with most dying prematurely between 9 and 10 weeks of age, with active degeneration/regeneration, widespread inflammation, sarcolemmal leakage and fibrosis starting at ~2 weeks of age[109,110].

In addition to the *mdx* and *mdx:utr*$^{-/-}$ mice models, several dystrophin-deficient dogs have been identified, with the golden retriever muscular dystrophy model (GRMD) showing the closest similarity to the human DMD skeletal muscle phenotype as well as a profound dilated cardiomyopathy with myocardial wasting, fibrosis, and contractile dysfunction [111–113]. As such, the GRMD is considered the current gold standard large animal model for DMD. However, the costs associated with GRMD dogs upkeep and care however limits the testing of potential treatments to only those that have passed pre-clinical efficacy in *mdx* and *mdx:utr*$^{-/-}$ mice models.

1.5.3 Current therapeutic avenues

Gene-based therapies

Replacement of dystrophin using viral gene therapy and exon skipping approaches are one of the main promising strategies targeted at treating DMD, via aiming to restore or complement dystrophin expression. Adeno-associated virus (AAV), which benefits include long-term gene expression, high transduction levels in muscle and muscle-specific serotypes, has emerged as the current transgene delivery tool of choice[114]. Recombinant AAV (rAAV) vectors however have limited packing capacity and the enormous size of the dystrophin cDNA has constrained investigators to perform detailed functional analysis of dystrophin structural domains to determine which regions can be deleted or recombined without significant consequences to function. Because Becker patients exhibit a milder phenotype and relatively normal lifespan, micro[115,116] and mini-dystrophins[24,117,118] constructs have been generated to mimic BMD deletions to render semi-functional dystrophins.

In addition, as structure-function of dystrophin and particularly, its interactions with other components of the DAPC has been uncovered, refinement of these dystrophin constructs have allowed to keep functionality of the transgene as close to the full-length dystrophin as possible. In addition to limited packaging size of the delivery vectors, there are still many hurdles including immunological barriers to the viral vector and/or the transgene, poor delivery to target tissues, and the roadblocks associated with producing high enough viral titres for clinical applications[114].

Utrophin, the homolog protein to dystrophin, is also a functional substitute for dystrophin and has been shown to be upregulated at the sarcolemma of dystrophic animal models[39]. Over-expression of utrophin or its truncated forms has been shown to completely prevent the dystrophic phenotype and is thus another potential therapeutic approach under investigation[119–122]. To overcome delivery vectors and immunogenicity

complications associated with rAAV delivery of dystrophin, one approach is to increase the expression of utrophin gene at a transcriptional level using small molecules such as SMTC110 to target already existing cellular mechanisms. One limitation however is that utrophin lacks an nNOS-binding site and is therefore unable to restore nNOS to the sarcolemma[123].

For exon skipping, the general strategy is to restore expression of the mutated dystrophin gene by skipping frame-disrupting mutations in the dystrophin gene using antisense oligonucleotides (AO), short nucleic acid analogues that attach to mRNA or single-stranded DNA, with a number of out-of-frame mutations rendered phenotypically mild through endogenous exon skipping and other alterations in splicing and post transcriptional-translational processing. This process leads to production of truncated but functional dystrophins. Exon skipping using small molecules has been demonstrated to ameliorate the severe phenotype in both canine and murine DMD models[124–128] while being well tolerated and non-immunogenic but this strategy is only applicable to the subset of DMD patients with the corresponding targeted mutation.

Several phase II/III clinical trials using antisense oligonucleotide (AO)-induced exon skipping targeting exon 51 (applicable to 13% of DMD patients) of dystrophin to restore its open reading frame have recently completed. Results from a recently completed Phase III randomized, double blond, and placebo controlled clinical study of Drisapersen. 2'-*O*-methyl phosphorothioate (2OMePS) AO, did not meet its primary endpoint, with no statistical improvement in the Six-Minute Walking Distance (6MWD) test in a trial of 186 boys nor improvements in secondary assessments of motor function[129–131]. Moreover, dosage is a limiting factor with Drisapersen, with renal toxicity observed at higher dosages[131], limiting the level of dystrophin production that can be achieved.

In a different trial conducted by Mendell *et al*. using Eteplirsen, an AO with a phosphorodiamidate morpholino (PMO) backbone that induces removal of exon 51 during the RNA splicing process, systemic delivery to a small cohort of DMD patients

resulted in a dose-dependent restoration of dystrophin production with upregulation of other dystrophin-associated proteins at the membrane, along with some improvement in patient walking ability compared to placebo controls[132,133]. However, this improvement was only observed in a small subset of the patient group, with dystrophin levels observed to be highly variable among all patients. Most preclinical studies have reported higher efficiency of AOs using the PMO backbone chemistry as well as apparent non-toxicity compared to the 2OMePS chemistry[124,127,134] but there are still concerns about their ability to produce a clinically therapeutic amount of dystrophin protein product as well as improving tissue targeting efficiency and uptake of AOs, particularly to the diaphragm and cardiac muscle.

Stop codon read-through using aminoglycosides such as gentamicin restore protein translation by causing misreading of the RNA and allowing alternative amino acids to insert at the site of the stop codon, with applicability to ~15% of DMD patients, but toxicity is a major concern. Other synthetic compounds discovered via screening for read-through are currently under evaluation.

The DMD gene has one of the highest rates of new mutations, complicating all gene targeting approaches that need to be applied to be able to treat all DMD patients. Gene editing using endonuclease-mediated gene repair allows for permanent repair of the patient's DNA to restore full-length dystrophin and is therefore applicable to all DMD patients regardless of mutation. Gene correction can be achieved using oligonucleotide-mediated genome repair, spliceosome-mediated RNA trans-splicing, and gene targeting.

Another very exciting area of research is the recent development of the CRISPR/Cas9 system for genome engineering, which couples a DNA double strand endonuclease to a short guide RNA to specifically target any site in the genome to disrupt, replace or modify the targeted gene[135,136]. In the context of DMD, this gene-editing approach induces exon deletion and reinstatement of dystrophin expression. Multiple studies have already shown efficacy in restoring dystrophin expression in myofibers, cardiomyocytes as well as satellite cells following both local and systemic

delivery using AAV[137–139]. Due to this technology being very new, there is still a lot of research to be done in optimizing the system and evaluating long term therapeutic benefits. Off-target effects at other sites of the genome are also a genuine concern in human clinical application.

Non gene-based therapies

Muscle augmentation via myostatin inhibition is another quickly advancing area. Myostatin is a transforming growth factor-β family member and a negative regulator of skeletal muscle mass. Inhibition of myostatin has been demonstrated to increase muscle mass in mdx mice[140–143] and GRMD dogs[144] and may be beneficial in DMD patients. A Phase I/II multicenter safety trial is currently being undertaken for MYO-029, a neutralizing antibody to myostatin[145]. Another muscle augmentation approach involves enhancing insulin-like growth factor I (IGF-1) to enhance muscle regeneration and protein synthesis[146,147]. A Phase I/II trial is currently assessing the impact of IGF-1 treatment in preserving motor function in DMD patients.

Another strategy includes the use of stem cell therapy to regenerate muscle. This strategy is attractive as it requires only the use of stimulatory signals and/or small molecules to expand large numbers of cells. Induced pluripotent stem cell (iPSC) technology is one leading area of focus in stem cell therapy as it allows derivation of patient-specific pluripotent stem cell preparations. This obviates both ethical and immunological concerns that are associated with embryonic stems cells. One recent study showed proof-of-principle application of *ex vivo* genetic correction of dystrophic iPS cells with a micro-utrophin transgene before transplantation back into dystrophin/utrophin double knockout mice[148]. They observed that engrafted muscle had large numbers of corrected myofibers, restoration of the DGC complex, and improved contractile strength. Moreover, they observed seeding of the transplanted cells within the satellite cell compartment. While these results are positive and exciting, this strategy still

has to overcome multiple important hurdles, such as improved survival of the cells post-injection, effective migration to the compromised muscles, and successful engraftment.

An alternative strategy involves targeting of the membrane repair machinery. Recent advances have identified another component of the membrane repair process, the protein Mitsugumin 53 (MG53, also known as TRIM72). MG53 is a tripartite motif family protein (TRIM) found primarily in striated muscle, and its role is to facilitate vesicle trafficking during the process of membrane repair and nucleates the assembly of the repair machinery through a redox-dependent mechanism[93,95,149,150]. Injections of recombinant MG53 have been shown to mitigate pathology in *mdx* mice by increasing membrane repair in muscle fibers and prevent muscle injury *in vivo*[151]. However, there are some concerns about the possible metabolic side effects of MG53 upregulation[152].

Collectively, while there are no current clinically approved treatments for DMD, there are many potential avenues that can be undertaken to target the disease pathology and potential combinations of these strategies may end up being optimal in treating the disease. Unfortunately, none of these potential strategies to ultimately cure DMD are likely to be ready for clinical application in human patients in the near future, as most require optimization in methods, delivery, safety, as well as the process of having to go through lengthy clinical trials. It is therefore crucial to find a therapeutic that can help improve and prolong quality of life in DMD patients.

1.5.4 Consequences to tissue specific treatment

Current palliative care regimens and new promising therapeutic strategies are largely directed at aiding respiratory function and prevent/slow skeletal muscle degeneration but it is critical to consider the interplay between the skeletal and cardiac myopathies (**Figure 2**). Leaving the skeletal myopathy untreated leads to blood flow adaptations and increased hemodynamic load on the heart while currently skeletal muscle centric therapeutic strategies for DMD also lead to increased stress on the untreated

myocardium presumably due to prolonged ambulation leading to increased cardiac demands[153]. A clear example is demonstrated in mice lacking both dystrophin and MyoD, a skeletal muscle specific key regulator of myofiber regeneration. Mice lacking dystrophin do not display cardiac abnormalities under baseline conditions but additional deletion of MyoD, which leads to impaired skeletal muscle regeneration and worsened skeletal phenotype, also induces severe cardiomyopathy[154].

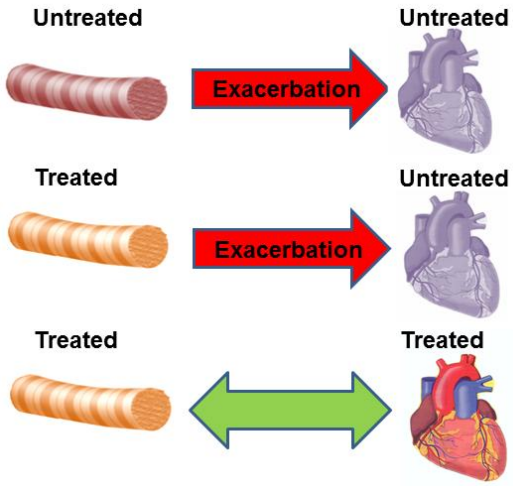

Figure 2: Interplay between the skeletal and cardiac myopathies. The optimal therapeutics will target all striated muscles simultaneously.

This is further evidenced in X-linked dilated cardiomyopathy, an inherited disorder caused by mutations in dystrophin that induces either the loss of dystrophin or production of an aberrant dystrophin in the heart but does not affect skeletal muscles[12] and that affects some female carriers of Duchenne, and in Becker's muscular dystrophy patients, develop cardiomyopathy despite retaining healthy skeletal muscle function[155]. BMD patients with less affected skeletal muscle appear to have more severe decline in cardiac function[156]. Moreover, growing evidence from animal studies raise concerns over skeletal muscle centric therapeutics worsening the cardiac disease[153]. *Mdx* mice treated with a skeletal muscle specific mini-dystrophin transgene were observed to have significantly enhanced voluntary wheel running activity compared to non-transgene

treated *mdx* mice suggesting that enhanced exercise capability from skeletal muscle treatment provides a setting for increased cardiac workload and heightened stress[157,158]. In agreement, the transgene treated *mdx* cohort had significant increase in left ventricular diastolic volume and greater incidence of myocardial necrosis and intracellular immunoglobulin accumulation[159].

This highlights the significance of a novel therapeutic that can alleviate the whole disease by targeting both cardiac and skeletal muscle. Cardiac and skeletal muscles have important differences in both structure and function which need to be kept in consideration when developing therapies for DMD.

1.6 Copolymer based membrane stabilizers for DMD

Poloxamer 188 (P188), the lead membrane stabilizer molecule of interest, belongs to the class of synthetic block copolymer surfactants generally known as poloxamers or Pluronics, which are tri-block copolymers comprised of a hydrophobic polypropylene oxide (PPO) core block flanked on both sides by hydrophilic polyethylene oxide (PEO) chains (**Figure 3**) in a A-B-A architecture. A wide range of copolymers with distinct physicochemical properties can be generated by varying the lengths of the PEO and PPO segments.

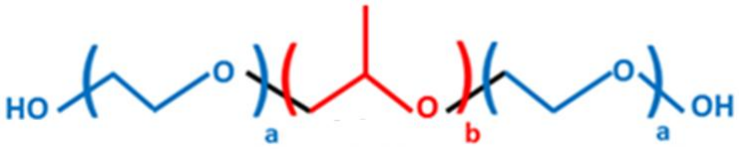

Figure 3: Schematic representation of an A-B-A triblock copolymer. Variation in PEO_a (blue) and PPO_b (red) block lengths leads to changes in physicochemical properties.

Poloxamers were the first commercially produced block copolymers, synthesized by Wyandotte Chemical Corporation in the late 1940s for industrial purposes, and now widely found in both industrial and consumer products. Poloxamers are mild, non-ionic

amphiphiles (having both hydrophilic and lipophilic properties) that exist at 10-80% wt. % poly(ethylene oxide) and 1-15000 g/mol molecular weights and have now been found to also have various biological applications such as drug delivery carriers, to enhance drug penetration in the treatment of multiple drug resistant tumors[160,161], or membrane interacting agents, either as lysis detergents[162–164] or cell membrane stabilizers[165,37,166], the latter being directly attributed to poloxamers' varying affinity for both the surrounding solvent and with the similarly amphiphilic phospholipid membranes[167–170]. The modulation of copolymer-phospholipid membrane interactions that results in therapeutic membrane stabilization *in vivo* is the major focus of this work.

1.6.1 Poloxamer 188

The most commonly studied poloxamer is P188, with the earliest reported use in clinical research as a rheological agent in blood[171,172]. P188 was used as a solubilizing agent of perfluorochemicals, which have significant O_2 carrying capacity, to create an emulsion used as an artificial blood substitute[173]. It was later determined that P188 reduces endothelial adherence and improves the rheology of sickled red blood cells[174], leading to P188 being pushed to clinical trial as a therapeutic agent for sickle cell anemia[175,176]. Its first FDA approved use in humans was as a skin wound cleanser due to its lack of toxicity to the cellular components of blood and its lack of interference to the wound's ability to heal and resist infection[177]. P188 was then first demonstrated to act as a cell membrane stabilizer when it was shown to reduce the electroporation-induced leakage of carboxyfluorescein dye from cells[165]. P188 was also observed to reduce membrane fluidity and improve cell survivability during shear stress in HB-32 hybridoma cell lines, presumably through direct membrane interaction[53] and has been widely deployed as a shear protective agent used in bioreactors[178]. Of note, P188 has been demonstrated to significantly lower apparent membrane tension and restore membrane resealing cells treated with the tetanus toxin, which prevents exocytosis at sites of

membrane disruption and blocks membrane resealing[84]. More recently, P188 has been reported to be protective against ischemic-reperfusion injury[179,180], thermal[181] and radiation burns[182,183], myocardial infarctions[184–186] and Duchenne muscular dystrophy cardiomyopathy[37,187,188].

1.6.2 Poloxamer 188 as a membrane stabilizer for DMD

Due to its membrane stabilizing capacity in various other membrane injury models, there has been strong interest in applying P188 to stabilize dystrophic muscle membranes. A first study has demonstrated that the acute application of P188 to isolated *mdx* cardiomyocytes restored myocyte compliance to wildtype levels while also reducing stretch-mediated calcium overload and preventing the intracellular uptake of the membrane probe FM1-43[37]. *Mdx* cardiac myocytes demonstrate increased passive tension when load is applied which results from the influx of extracellular Ca^{2+} and application of P188 completely normalizes passive compliance to normal levels. At the level of the whole organ, P188 decreases passive tension and thereby improves myocardial relaxation allowing for complete filling of the ventricles and return to normal working end diastolic and end systolic volumes[12]. Moreover, *in vivo* administration of P188 to *mdx* mice improved ventricular geometry and prevented acute cardiac failure during a dobutamine stress protocol[37]. Another study using the more diseased GRMD dog model demonstrated the effectiveness of chronic P188 administration at preventing left-ventricular remodeling, reducing myocardial fibrosis and blocking increased cardiac troponin I and brain type natriuretic peptide in the serum[187].

Another group has also demonstrated the effectiveness of chronic intermittent administration of P188 in protecting against beta-agonist isoproterenol induced cardiomyopathy in *mdx* mice[188]. In comparison, the ability of synthetic membrane stabilizers to protect fragile DMD skeletal muscles has been less clear. Early experiments with P188 have so far shown little to no efficacy in protecting dystrophic

limb skeletal muscle function *in vivo*[189,190]. However, P188 is effective in protecting hindlimb skeletal muscle in a range of other conditions, including electroporation injury[165,191], hindlimb ischemia-reperfusion injury[180,192], and in a model of dysferlin-deficiency[193].

Furthermore, P188 has been demonstrated to confer protection to dystrophic skeletal muscle *in vitro*[194]. These examples raise the possibility that the ineffectiveness exhibited by P188 in dystrophic skeletal muscle *in vivo* in past work is due to sub-optimal pharmacodynamics of routes of delivery, with most *in vivo* work administering P188 via intravenous or intraperitoneal routes, rather than an intrinsic inability of P188 to beneficially stabilize dystrophic skeletal muscle.

This hypothesis is supported by a study that found that intravenous infusion of P188 was protective against skeletal muscle electroporation injury *in vivo* in an animal model where impaired perfusion is not a factor[165,191] . This notion is furthermore strongly supported by a recent study showing that chronic dosing of P188 using subcutaneous delivery improves diaphragm function in *mdx* and *mdx:utr*$^{-/-}$ as well as improved both systolic and diastolic function in *mdx* hearts[195]. As the diaphragm is arguably one of the most affected skeletal muscles in DMD, these results are encouraging that similar protective effects could be observed in limb skeletal muscles via optimization of P188 delivery.

1.6.3 Pharmacokinetics of Poloxamer 188

A distribution, metabolism and excretion study has been performed for purified P188 in rats, dogs, and healthy humans[196]. P188 has been shown to be widely distributed throughout all organs following intravenous (IV) injections in various animal models with higher concentration in tissues with high blood flow, such as the heart[196,197]. P188 is primarily excreted by the kidneys without modification with a half-life of about 5 hours in small mammals and about 18 hours in humans[196,197]. Adverse reactions including

muscle soreness, proteinuria and elevated liver enzymes have been reported following high concentrations perfusions of P188 in healthy human volunteers[198]. These have since been determined to be due to the presence of small molecular weight contaminants resulting from side reactions occurring during synthesis of the P188 batch used in the studies[199,200]. Removal of these contaminants allowed high doses to be well tolerated in sickle cell patients[176].

To date, most safety and pharmacokinetic studies have been performed in order to examine acute intravenous P188 administrations in the context of phase I and II clinical trials for sickle cell anemia but there is a paucity of information on the pharmacokinetics of chronic P188 administration as well as little information on the pharmacodynamics of P188 following different delivery routes. It is also unclear if the pharmacokinetics and pharmacodynamics of P188 could differ in DMD. A small study performed in normal C56BL/6 mice comparing the plasma pharmacokinetics of a single low dose intravenous (4.6 mg/kg) or subcutaneous (3.0 mg/kg) dose revealed markedly different plasma level profiles, with plasma exposure to P188 greater in the subcutaneous dose than in the intravenous dose[195]. These data indicate that the pharmacokinetics of P188 vary significantly depending on routes of delivery.

1.6.4 Biophysical investigations of P188 - membrane interactions

Comprehending how P188 interacts with biological membranes is important to understand the basic mechanism of membrane stabilization by copolymers. The interaction of P188 with membranes of various compositions has been the subject of numerous studies. Systems using Langmuir troughs to modulate the surface area and therefore lipid packing density of supported phospholipid monolayers at the air/water interface have been used to model damage the outer leaflet of the lipid bilayer.

Langmuir isotherms and fluorescence microscopy have been used to analyze the ability of P188 and other poloxamers to interact with lipid membranes. Maskarinec et al.

focused on P188 insertion as a function of surface pressure, which directly correlates to lipid packing density, for both anionic dipalmitoylphosphatidylglycerol (DPPG) and zwitterionic dipalmitoylphosphatidylcholine (DPPC) monolayers and observed that P188 inserts into both lipid types at a surface pressure (π) $\leq$ 22 mN/m, which is lower than the equivalent surface pressure of a normal healthy cell membrane, and remains inserted until the surface pressure is increased back to a threshold surface pressure equivalent to that of a normal healthy membrane[201,202].

X-ray reflectivity results show that at high surface pressure, lipid films with and without P188 exhibit similar electron density profiles[168,203]. This inability to remain inserted at this threshold surface pressure suggests that P188 may be naturally "squeezed out" from the cell bilayer once it has repaired itself. These results indicate that P188 will only adsorb onto localized areas of the membrane where the local lipid density is reduced. Moreover, similar results observed in DPPC and DPPG monolayers, which have different lipid head group charge, suggest that P188 interactions are not influenced by electrostatics. Morphologically, P188 insertion was found to tighten lipid packing via physical occupation of surface area[168,201]. P188 was found to rapidly "insert" into the membrane in a reversible manner, that is, P188 was promptly ejected out of the membrane once the surface pressure and lipid density were re-established back to normal[201,202].

Based on these results, P188 therefore does not appear to interact with membranes when the phospholipid packing is normal. This led to the hypothesis that only when lipid packing density is low enough that the hydrophobic core of the monolayer is exposed that P188 partitions into the membrane via hydrophobic interactions. Moreover, P188 partitions into the monolayer in localized patches rather than uniformly across the membrane[168]. However, supported monolayers are a very simplistic approximation of biological bilayer membranes. While artificial lipid monolayers are simple models to experimentally control and observe, the results obtained on those model systems cannot

be fully extended to biological membrane systems, which are structurally heterogeneous and complex.

Giant unilamellar vesicles (GUVs) with diameters of 10-50 um have been widely used as a three dimensional mimic of a cell bilayer due to their large size allowing for ease of observation with optical microscopy and ability to be loaded with components such as fluorescent dyes. One study monitored the loss of structural integrity of single fluorescent dye-loaded GUVs undergoing a membrane swelling hypo-osmotic stress in the presence of 50 uM P188[169]. GUVs undergoing hypo-osmotic stress show swelling and formation of transient pores through which leakage of fluorescent dye was monitored. The authors observed an incubation time-dependent two state mechanism to P188 interaction with the GUV: an adsorption state where P188 slows down GUV swelling and retards leakage of the intravesicular fluorescent dye, in time followed by an insertion state where very long incubation (~several days) leads to P188 inserting into the GUV membrane and induced lipid packing disruption and increased membrane permeability.

To more closely investigate the physical nature of P188-membrane interactions, ^{1}H Overhauser dynamic nuclear polarization NMR spectroscopy was employed to closely examine the local hydration dynamics at the P188-lipid membrane interface[170]. The resolution permissible by this technique allowed for probing of the local water diffusivity in lipid bilayer systems and showed that P188's weak adsorption on the membrane surface was effective to retard membrane hydration dynamics and intrabilayer water diffusivity without transposing in the bilayer interior nor affective lipid packing[204].

1.6.5 Block copolymer structure-function

Block copolymers are comprised of two or more distinct polymer moieties (blocks A,B,C…) covalently bonded together that exist in a variety of molecular sizes, relative degree of polymerization of each block (composition), chemical moieties, and

architectures, from di-block (A-B), to tri-block (A-B-A, B-A-B, A-B-C…) to multi-blocks (A-B-A-B-A) (**Figure 4**). There are therefore almost infinite possible distinct chemical configurations of block copolymers that can be synthesized by varying the lengths of A and B segments, and not much is known on the structure-function relationships of these block copolymers in the context of both material and biological applications. There is considerable interest on block copolymers due to their overall surface active and solvent-selective characteristics which are directly dictated by the specific blocks inherent thermodynamic properties[205,206].

Figure 4: Schematic drawing of two-component copolymers. Variation in PEO and PPO chain lengths leads to changes in physicochemical properties

Studies of the effects of poloxamers on lipid membranes showed that the hydrophobicity of the copolymer had a leading role in copolymer-membrane interactions, with more hydrophobic copolymers decreasing membrane microviscosity[164,207], increasing the rate of lipids flip-flopping across the membrane outer and inner leaflets of vesicular membranes[164], and increasing membrane leakiness[162,208]. Studies have investigated whether the size of the hydrophobic PPO subunit regulates insertion capabilities of the copolymer into lipid films by testing poloxamers of 80% PEO composition but different molecular weights (P108, P238, P188 and P338) for their ability to insert with lipid monolayers[202]. All were found to insert into lipid monolayers and while the copolymers with larger hydrophobic PPO subunits needed lower surface pressure for insertion, presumably due to the bulkiness of the hydrophobic core hindering their insertion compared to the copolymers with a smaller PPO core, they seemed to

maintain their positions more strongly once inserted, with P238 and P338 able to retain their positions at the monolayer at much higher surface pressures than the smaller P108 and P188. The length of the PPO subunit also influences the solubility of the copolymer in the lipid bilayer, with longer PPO subunits having stronger association constant. Moreover, copolymers with longer PPO subunits hinder lateral lipid diffusion more significantly than copolymers with shorter PPO subunits, indicating that longer PPO blocks allows for deeper insertion into the bilayer[209].

Monte Carlo simulations run using a coarse-grained model to capture the main interactions between lipids and poloxamers show that changing poloxamer structure leads to differences in subphase solubility that is also reflected in the degree of lipid corralling, with more hydrophobic and therefore less soluble copolymers having higher adsorption at the membrane and causing lipid domains to be more ordered[167]. Data presented from an isothermal titration calorimetry (ITC) study of poloxamer P338 interaction with liposomes confirm that lipid packing density indeed regulates how poloxamers associate with membranes, with poloxamers observed to not partition into ordered gel-phase bilayers but to partition with relative ease into fluid-phase disordered bilayers[210]. Moreover, results from that study show the existence of a saturation limit at which the lipid membrane can accommodate a maximum number of poloxamer molecules at a point beyond which the liposome integrity is disrupted. This observed outcome indicates that whether a poloxamer acts as a membrane stabilizer or a destabilizer depends in large part on the saturation limit of the membrane and poloxamer/lipid ratio.

Polyethylene glycol (PEO or PEG) is the hydrophilic constituent of poloxamers and has been well investigated in the fusion of model membranes and for its ability to lower water molecule activity at the membrane-solvent interface[211]. While PEG-mediated membrane stabilization has been shown to be effective, the millimolar to molar concentrations required for effectiveness compared to P188 indicate that a central hydrophobic component plays an essential role in driving P188 to effectively interact with and increase membrane stabilization potency[204].

Additionally, the incorporation of poloxamers into the lipid membrane was shown to be endothermic and therefore dominated by entropy, with a gain of entropy significantly contributing to the free energy of partitioning, due to the release of ordered water molecules surrounding the PPO chain upon its partitioning into the bilayer[169,170]. Furthermore, the favorable hydrophobic interactions between the PPO chains and the acyl chain of the lipid additionally contribute to the enthalpy-entropy balance. Importantly, a poloxamer of equivalent PPO/PEO as P188 was found to predominantly incorporate into the outer leaflet of the liposome and only slowly migrated through the bilayer after incubation for an extended period of time[210], indicating that there is a strong impediment to passive diffusion of copolymer across the cell membrane. This asymmetric distribution strongly suggests that it is energetically unfavorable for a poloxamer to adopt a bilayer spanning conformation.

In a study using GUVs undergoing hypo-osmotic stress in the presence of copolymers of varying hydrophobicity, incubation with the hydrophilic PEG, which is believed to only adsorb at the membrane interface, led to prolongation of the swelling process[169], suggesting that the adsorption state of the copolymer is the membrane stabilizing state under hypo-osmotic conditions.

Further experiments examining other poloxamers of varying PPO subunit lengths indicate that the insertion rates of poloxamers correlates well with their hydrophobicity[164,167]. They concluded that while adsorption of poloxamers to the membrane interface is somewhat independent of architecture, insertion is however mainly dictated by their hydrophobicity[169]. This was further confirmed by another study using isothermal calorimetry and small molecule directed lipid peroxidation of liposomes revealing that hydrophilic copolymers at uM concentrations such as P188 and PEG8000 did not exhibit appreciable heat exchange indicative of insertion within their experimental time scale (4 hours) whereas hydrophobic poloxamers P335, P333 and P181 displayed significant heat of partitioning indicative of insertion into the liposomal membrane[212]. They hypothesized that the disruptive effect of copolymer insertion is due

to mismatch in size and hydrophobicity between the PPO block and the lipid hydrocarbon tails. This was further demonstrated in the increased instability of lipid-P188 mixed GUVs that was dependent on the concentration of P188 inserted at the membrane[169].

These findings underlie the hydrophobicity dependence of differential kinetics of insertion between poloxamers, with more hydrophobic copolymers inserting at faster rates by initially embedding below the lipid head group region, opening up the packing of acyl chains, and accelerating the passage of molecules such as water across the membrane[170,204].

1.6.6 Micellization/Aggregation behavior of block copolymers

One parameter of biological importance is the critical micelle concentration (CMC), which is defined as the isothermal copolymer concentration at which micelles of an amphiphilic copolymer start to self-assemble and at which equilibrium between unimeric copolymers and micelles is established[213,214]. The main driving force for self-assembly is the solubility differences between blocks. Also, while not a linear rule, as molecular size and specifically, the size of the hydrophobic chain increases, the free energy to keep the molecule solvated increases, and CMC therefore decreases.

Temperature also plays a crucial role in micelle formation with CMC of block copolymers tending to decrease with rising temperature[178]. This phenomenon is at least in part attributed to the dehydration of PEO blocks at higher temperature and consequently a lower solubility of the PEO chains in water. A list of reported CMCs for P188 and other poloxamers are presented in **Table 1**. Experimental determination of CMC can be conducted using various techniques where a break in the curve of a measured signal against concentration signifies the start of micellization[178,215–217].

The most common methods of CMC determinations are surface tension measurements, scattering, viscosity, and fluorescent dye solubilization. The latter is the most widely used, typically involving measuring the emission or absorbance of insoluble

fluorescent probes such as DPH or pyrene that fluoresce when solubilized in micelles[178,218]. There is however significantly variable sensitivity and accuracy across methods complicated by the fact that micellization of block copolymers is significantly more complex than for small molecules species.

Reported CMC (mM)	Temperature (C°)	Reference
1.4	25	[219]
0.125	30	[201]
0.5	37	[220]
5	37	[221]
8.3	40	[178]

Table 1: Reported CMCs for P188 using various detection methods.

Nevertheless, CMC is a critical parameter to consider when thinking about biological applications. The behavior of the monolayer differed above and below the CMC of P188, suggesting the unimeric form of the block copolymer is suggested to be the active agent. While it remains unclear whether or not *in vivo* micellization would occur at certain concentrations and how that would affect *in vivo* pharmacokinetics and pharmacodynamics once injected, it is important to keep in mind the potential physiological implications of poloxamer self-aggregation and dissociation.

1.7 Thesis overview and major objectives

1.7.1 Membrane-stabilizing copolymer efficacy in dystrophic skeletal muscle

The principal objective of **Chapter 2** was to assess copolymer P188 efficacy in preserving dystrophic skeletal muscle function and sarcolemmal integrity *in vivo*. Despite wide usage of P188 in pre-clinical studies to stabilize membranes from various injury modalities, it is surprising that basic elements of P188 pharmacodynamics have not been examined in the context of DMD skeletal muscle. It is well established that drugs and molecules exhibit a wide range of pharmacokinetic and pharmacodynamics properties *in vivo* depending on covariants such as size of the drug or molecule, its chemical composition, and importantly, the route of delivery[222,223]. Thus, the pharmacodynamics of P188 was investigated by directly comparing the functional effects between three parenteral delivery routes: intravenous, subcutaneous and intraperitoneal. A hindlimb skeletal muscle lengthening contraction protocol was employed as a well-established quantitative measure of the consequences of dystrophin-deficiency *in vivo*[36,46,102,224,225] to test whether P188 can prevent the force loss and membrane instability associated with lengthening contractions in *mdx* mice. Results indicate that pharmacodynamics optimization of P188 delivery is critical to conferring protection against force loss to dystrophic skeletal muscle undergoing physiological stress. Moreover, another triblock copolymer of equivalent composition as P188 but larger size also demonstrates membrane stabilization *in vitro* and *in vivo*. These findings establish proof-of-principle that support synthetic membrane stabilizers as a first-in-class therapeutic strategy for prevention of injury in dystrophic skeletal muscle *in vivo*.

1.7.2 Structure-function relationship of membrane stabilizing diblock copolymers

The principal objective of this aim was to seek a deeper understanding of block copolymer structure-function to provide insights into the membrane stabilizer mechanism of action. It is currently unclear how the structural properties of P188 confer its membrane stabilizing functionality. Biophysical studies investigating the mechanism of interaction for P188 and other poloxamer formulations with phospholipid monolayers suggest that the PPO/PEO ratio is a critical variable for membrane interaction[169,202,212]. Investigations up to now have focused on the triblock architecture of the poloxamer family, which are constrained to those that have been synthesized and made commercially available by the chemical company BASF. For a more effective structure-function approach, it is necessary to explore the role of architecture i.e., whether a triblock architecture is necessary for membrane stabilization. To do so, the diblock architecture (A-B) is explored in **Chapter 3**. Diblocks are an attractive alternative option to triblocks because they have a simpler synthetic process which allows for methodical alterations to PPO/PEO and block lengths. Furthermore, removal of one of the PEO chains allows for customization of the PPO block functional end group with different chemical moieties to strategically and more minutely modulate block hydrophobicity in order to fine tune copolymer-bilayer interactions. Results from the work in this chapter are the first to establish the efficacy of the diblock architecture for membrane stabilization. Moreover, as exciting proof-of-principle, addition of a small hydrophobic end group to the PPO block significantly enhances membrane protection in vivo, leading to an "anchor and chain" hypothesis of bilayer interaction. The ability to more easily customize diblock chemical properties eases access to a vast chemical landscape to be further explored.

1.7.3 Atomistic level investigation of block copolymers interaction with lipid membranes using Molecular Dynamics simulations

Despite previous investigations on poloxamers, and specifically their interactions with lipid membranes, it remains unclear what is the mechanism of interaction and the driving force behind these interactions. In this regard, molecular dynamics (MD) simulations have been well established as a method of choice to probe both location and dynamics of membrane active molecules that cannot easily be observed with experimental techniques. As of today, there are few reports detailing MD simulations to study poloxamer-membrane interactions[167,208,226,227] and most use a computationally less intensive and partial model that lack atomistic level insight.

The principal objective of **Chapter 4** of this work was to use all-atomistic MD simulations to provide molecular insight on the effect of lipid bilayer surface tension changes on P188-bilayer interactions. Increases in surface tension applied to the lipid bilayer revealed an area-per-lipid dependence of adsorption vs. insertion of P188, which supports monolayer studies that demonstrated that P188 inserts into areas of decreased lipid density and gets "squeezed-out" once membrane integrity is restored[202]. Another new finding that resulted from this study is the observation that one or both PEO chains of the triblock initiate insertion of the copolymer, hypothetically as a priming step to lower solvent accessible area on the hydrophobic PPO block.

CHAPTER 2

MEMBRANE-STABILIZING COPOLYMERS CONFER MARKED PROTECTION TO DYSTROPHIC SKELETAL MUSCLE *IN VIVO* (PAPER 1)

Evelyne M Houang[1], Karen J Haman[2], Antonio Filareto[3], Rita C Perlingeiro[3], Frank S Bates[2], Dawn A Lowe[4] and Joseph M Metzger[1].

[1]Integrative Biology and Physiology, University of Minnesota, United States; [2]Department of Chemical Engineering and Material Science, University of Minnesota, United States; [3]Department of Medicine, Lillehei Heart Institute, University of Minnesota, United States and [4]Rehabilitation Science and Program in Physical Therapy, University of Minnesota, United States.

Published in Molecular Therapy - Methods & Clinical Development (2015) 2, 15042; doi:10.1038/mtm.2015.42

2.1 Summary

Duchenne muscular dystrophy (DMD) is a fatal disease of striated muscle deterioration. A unique therapeutic approach for DMD is the use of synthetic membrane stabilizers to protect the fragile dystrophic sarcolemma against contraction-induced mechanical stress. Block copolymer-based membrane stabilizer poloxamer 188 (P188) has been shown to protect the dystrophic myocardium. In comparison, the ability of synthetic membrane stabilizers to protect fragile DMD skeletal muscles has been less clear. Because cardiac and skeletal muscles have distinct structural and functional features, including differences in the mechanism of activation, variance in sarcolemma phospholipid composition, and differences in the magnitude and types of forces generated, we speculated that optimized membrane stabilization could be inherently different. Our objective here is to use principles of pharmacodynamics to evaluate membrane stabilization therapy for DMD skeletal muscles. Results show a dramatic differential effect of membrane stabilization by optimization of pharmacodynamic-guided route of poloxamer delivery. Data show that subcutaneous P188 delivery, but not intravascular or intraperitoneal routes, conferred significant protection to dystrophic limb skeletal muscles undergoing mechanical stress *in vivo.* In addition, structure-function examination of synthetic membrane stabilizers further underscores the importance of copolymer composition, molecular weight, and dosage in optimization of poloxamer pharmacodynamics *in vivo*.

2.2 Introduction

Duchenne muscular dystrophy (DMD) is an X-linked recessive disease of marked striated muscle deterioration affecting 1 in 3500-5000 boys[10]. DMD results from the lack of the cytoskeletal protein dystrophin, which is essential for maintaining the structural

integrity of the muscle cell membrane[1]. DMD patients develop severe skeletal muscle degeneration, along with clinically significant cardiomyopathy[19,228,229]. There is no cure for DMD patients, or any effective treatment to halt, prevent or reverse DMD striated muscle deterioration. Symptomatic clinical management includes glucocorticoids that show positive improvements in muscle strength and cardiac function[98,104] but also have significant negative side effects[101,103]. Current experimental DMD therapeutics are novel gene and cell-based strategies,[230,231] including exon-skipping strategies to restore dystrophin production which have shown some promise in pre-clinical studies[124,126,127,232]. To date, however, these approaches have not yet been translated successfully in human patients[129,130]. In this context, it is essential to consider additional approaches that target the primary defect of DMD: severe muscle membrane fragility.

DMD is a particularly daunting disease because striated muscle represents ~40% of body mass, and includes all skeletal, respiratory and cardiac muscles. This point is important, as leading experimental therapeutic efforts to date appear to preferentially target dystrophic skeletal muscles, leaving the diseased heart untreated[12]. Skeletal muscle-centric strategies to improve ambulation for DMD patients could lead to increased stress on the untreated dystrophic myocardium as a result of increased cardiac demands[12,153]. This interplay between the progression of DMD cardiomyopathy and the skeletal myopathy as a pathophysiological load on the heart underscores the importance of a therapeutic strategy that can simultaneously treat all striated muscles.

The primary pathophysiological defect in DMD is the marked susceptibility to contraction-induced membrane stress[34,233] and the subsequent muscle damage and degeneration that occurs due to loss of muscle membrane barrier function. In this context, a unique therapeutic approach is the use of synthetic membrane stabilizers. This strategy aims to prevent muscle degeneration by directly stabilizing the dystrophin-deficient sarcolemma during muscle contraction. The triblock copolymer poloxamer 188 (P188) has numerous features that make it an attractive synthetic membrane stabilizer candidate for DMD treatment. P188 (8.4 kDa) is a nonionic block copolymer belonging

to a family of triblock copolymers comprised of a hydrophobic polypropylene oxide (PPO) core flanked on either side by hydrophilic chains of polyethylene oxide (PEO) (**Table 1**). We and others have shown that both acute and chronic delivery of membrane stabilizer P188 confers protection to the dystrophic myocardium and in both small and large animal models of DMD[37,187,195,234]. However, P188 has so far shown little to no efficacy in protecting dystrophic limb skeletal muscle function *in vivo*[187,189,190]. This apparent non-efficacious effect is interesting considering that P188 is effective in protecting hindlimb skeletal muscle in a range of other conditions, including electroporation injury[165], hindlimb ischemia-reperfusion injury[180], and in a model of dysferlin-deficiency[193] in vivo. Furthermore, P188 does confer protection to dystrophic skeletal muscle *in vitro*[194]. These examples raise the possibility that the ineffective protection exhibited by P188 in dystrophic skeletal muscle *in vivo* in past work[189] is due to sub-optimal pharmacodynamics, rather than an intrinsic inability of P188 to beneficially stabilize dystrophic skeletal muscle. We therefore hypothesize that optimization of pharmacodynamics of P188 is crucial in conferring protective efficacy to dystrophic skeletal muscle *in vivo*.

Polymer	Pluronic®	Average MW (Da)	2(PEOa)	PPOb	PPO/PEO
P188	**F68**	8400	160	27	0.17
Ext-P188	**F108**	14600	280	44	0.16
P331	**L101**	3800	14	54	3.86
PEG8000	**-**	8000	-	-	-

Table 1: Summary of triblock copolymers. Pluronic®: BASF trademark designation; PEO: Polyethylene oxide; PPO: Polypropylene oxide**;** HLB: hydrophile-lipophile balance where a high HLB value indicates a relatively more hydrophilic polymer.

The objective of this study was three-fold. First, we tested whether block copolymers can stabilize dystrophic skeletal muscle membranes *in vitro*, thereby

bypassing any potential *in vivo* pharmacodynamic/kinetic barrier to the molecule. Second, we sought a deeper understanding of block copolymer P188 structure-function to provide insights into the membrane stabilizer mechanism of action. P188 belongs to a family of block copolymers called Poloxamers (or Pluronics) that are available in varying molecular weights and PPO/PEO (hydrophobic/ hydrophilic) ratios. It is currently unclear how the structural properties of P188 confer its membrane stabilizing functionality. Biophysical studies investigating the mechanism of interaction for P188 and other poloxamer formulations with phospholipid monolayers suggest that the PPO/PEO ratio is a critical variable for membrane interaction[169,202,212]. Accordingly, we investigated triblock copolymer composition and mass to gain insight into the role of these structural features on skeletal muscle membrane stabilization function *in vitro*.

The third and principal objective of this work was to assess copolymer P188 efficacy in preserving dystrophic skeletal muscle function and sarcolemmal integrity *in vivo*. Despite wide usage of P188 in pre-clinical studies to stabilize membranes from various injury modalities, it is surprising that basic elements of P188 pharmacodynamics have not been examined in the context of DMD skeletal muscle models *in vivo*. It is well established that drugs and molecules exhibit a wide range of bioavailability and pharmacokinetic/pharmacodynamic properties *in vivo* depending on covariants such as size of the drug or molecule, its chemical composition, and importantly, the route of delivery[222,223]. Thus, we investigated the pharmacodynamics of P188 by directly comparing the *in vivo* functional effects between three parenteral delivery routes: intravenous, subcutaneous and intraperitoneal. We employed a hindlimb skeletal muscle lengthening contraction protocol as a well-established quantitative measure of the consequences of dystrophin-deficiency *in vivo*[36,46,102,224,225]. We tested whether P188 can prevent the force loss and membrane instability associated with lengthening contractions in *mdx* mice, the mouse model of DMD. Results indicate that pharmacodynamic optimization of P188 delivery is critical to conferring protection against force loss to dystrophic skeletal muscle undergoing physiological stress. These new findings support

synthetic membrane stabilizers as a first-in-class therapeutic strategy for prevention of injury in dystrophic skeletal muscle *in vivo*.

2.3 Results

Membrane stabilization prevents membrane stress-induced leakage of LDH from dystrophin-deficient skeletal muscle cells in vitro

We used a hypo-osmotic stress as a structure-function screening tool to assess membrane stabilizer effects on skeletal muscle cells *in vitro*[235,236]. Hypo-osmotic stress involves sarcolemmal swelling and stretching and can serve as an *in vitro* mechanical stress model. We used this model to evaluate the membrane stabilizing capacity of P188 by its ability to prevent the release of an intracellular enzyme, lactate dehydrogenase (LDH), from normal and dystrophic muscle cells. Because myotubes derived from satellite cells can be grown to high density and maintained in culture more efficiently than isolated myofibers, we used control (dystrophin and utrophin replete) myotubes derived from an *ex vivo* expansion of satellite cells using conditional expression of Pax3 as an initial test bed for membrane stabilization screening. Furthermore, in order to examine the structure-function relationship between the PPO/PEO ratio, molecular weight, and membrane stabilization, we examined the LDH release blocking efficacy of several other triblock copolymers (**Figure 1A, Table 1).**

In control satellite cell-derived myotubes exposed to hypo-osmotic stress, P188 treatment decreased LDH release in a dose-dependent manner (~20% decrease in LDH release at 1 μM and ~50% decrease at 150 μM, $^{\#}P = 0.017$) **(Figure 1B)**. Moreover, extended-P188 (ext-P188), a triblock copolymer featuring an equivalent PPO/PEO ratio to P188 at a larger molecular weight, was as effective as P188 at lower concentrations (~70% decrease in LDH release at 1 μM), suggesting that membrane stabilization

capacity *in vitro* is linked to molecular size and that the original P188 characteristics can be optimized for increased potency. In contrast, the completely PEO based PEG8000 decreased LDH release to a much lesser extent than P188 (~35% decrease in LDH release at 150 μM), indicating that a hydrophobic component is required for optimal block copolymer-based membrane stabilization. Because the addition of copolymers at μM concentrations did not affect total solution osmolarity (data not shown), membrane stabilizing effects can be attributed to direct stabilization at the membrane rather than osmotic factors. Conversely, the small and highly hydrophobic block copolymer P331 (**Table 1**) induced lysis of the myotubes and exacerbated the release of intracellular LDH, indicating that highly hydrophobic polymers destabilize membranes, which is in agreement with previous reports[169,170].

We next examined whether the membrane stabilizers P188 and ext-P188 were also effective in protecting dystrophic skeletal muscle membranes. To do so, we used isolated FDB (Flexor Digitorum Brevis) myofibers from *mdx* mice, as well as iPSC-derived skeletal myotubes from *mdx:utrn*$^{-/-}$ mice as they provide an *in vitro* model where both dystrophin and its compensatory homolog utrophin are absent, making it a closer functional mimic to DMD. The iPSC-derived model was used for procuring *mdx:utrn*$^{-/-}$ myotubes as isolation of myofibers from these mice is technically challenging. Acutely isolated single FDB fibers from *mdx* mice, and iPSC-derived myotubes from *mdx:utrn*$^{-/-}$ mice were thus subjected to hypo-osmotic stress and assessed for LDH release **(Figure 2A,B)**. P188 (150 μM) significantly decreased the release of LDH (~65% decrease compared to non-treated,*$P < 0.05$). Moreover, ext-P188 was again highly protective at a lower dosage, with 1 μM ext-P188 showing a similar extent of protection as 150 μM P188 ($P = 0.49$) and protection extending even to a lower 0.1 μM concentration.

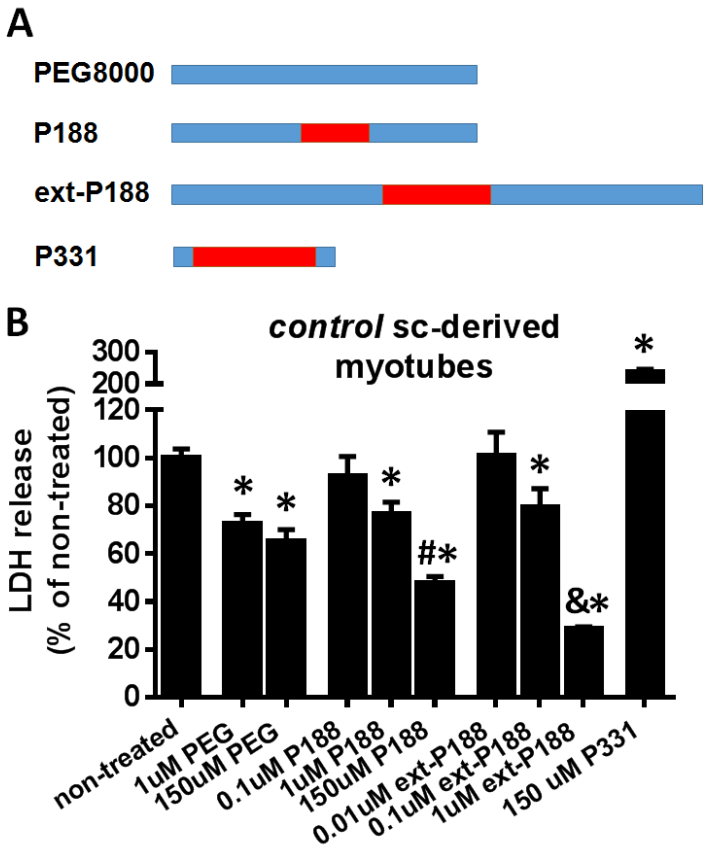

Figure 1: *In vitro* hypo-osmotic stress assay to screen block copolymers for membrane stabilization. (A) Schematic representation of the tested triblock copolymers and the exclusively PEO-based polymer PEG8000, showing relative PPO (red) and PEO composition (blue). (**B**) Satellite cell-derived myotubes from normal muscle were exposed to hypo-osmotic stress media and lactate dehydrogenase (LDH) enzyme release into the media was measured as a marker of membrane breach. The ability of P188 and other copolymers to decrease LDH leakage from stressed myotubes was assessed as a parameter of membrane stabilization. Data are presented as % LDH release normalized to total LDH release (*$P < 0.05$, via one-way ANOVA compared to non-treated group, $^{\#}P < 0.05$ indicates 150 µM P188 is significantly different from 1 µM P188, $^{\&}P < 0.05$ indicates 1 µM ext-P188 is significantly different from 0.1 µM ext-P188). Mean values are derived from at least 3 independent experiments with 3-4 wells of densely cultured myotubes per experiment. Error bars shown as mean +/- S.E.M.

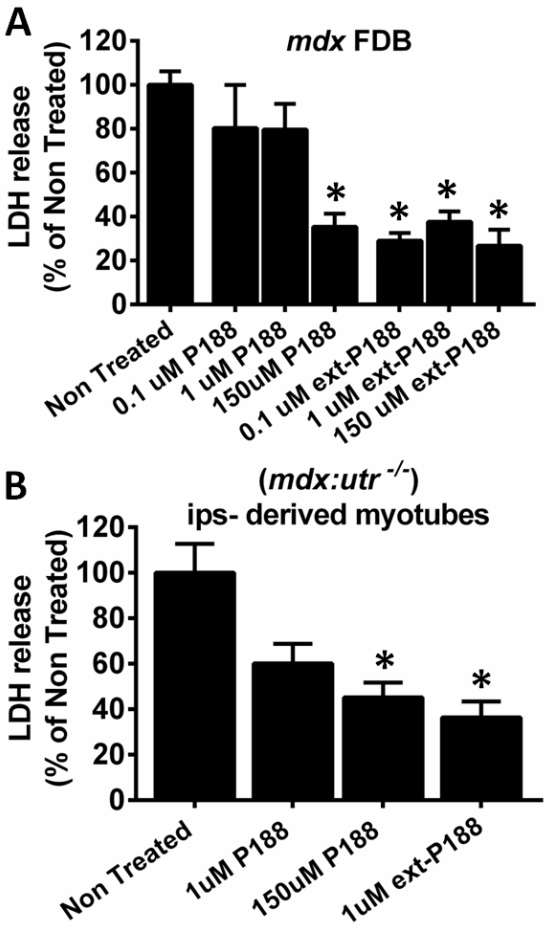

Figure 2: Membrane stabilizers P188 and ext-P188 decrease hypo-osmotic stress-induced release of LDH in dystrophic myotubes and myofibers *in vitro*. (A) Isolated *mdx* Flexor Digitorum Brevis (FDB) myofibers and **(B)** double knockout (*dys/utr* $^{-/-}$) myotubes were subjected to hypo-osmotic stress and lactate dehydrogenase (LDH) release was assessed in the absence (non treated) or presence of increasing concentrations of P188 and ext-P188. Data presented as % LDH release normalized to total LDH release from non-treated. *$P < 0.05$ via one-way ANOVA compared to non-treated group. Mean values are derived from at least 3 independent experiments with 3-4 wells of 20-30 isolated *mdx* FDB myofibers or densely cultured *dys/utr* $^{-/-}$ myotubes per experiment. Error bars shown as mean +/- S.E.M.

Membrane stabilization markedly protects against lengthening contraction-induced force loss and membrane instability in mdx skeletal muscles in vivo.

The *mdx* mouse exhibits significant susceptibility to lengthening contraction injury, as evidenced by a marked force loss after successive lengthening contractions[34,224]. Lengthening contraction injury protocols have been well used as an outstanding preclinical assessment assay for evaluating potential therapeutic strategies in mdx mice[102,115,116,123,232,237–239]. Force loss during contraction-induced muscle injury is a definitive quantitative functional marker of the disease in animal studies, making it a gold-standard physiological benchmark. We therefore evaluated the impact of P188 treatment on *in vivo* physiological function of the hindlimb anterior crural muscle group (dorsiflexors) of *mdx* mice undergoing a lengthening injury protocol. The *in vivo* hindlimb assay is informative as it allows for a maximal, reproducible, and non-invasive torque measurement of the entire anterior crural muscle compartment (including the TA and EDL muscles) via stimulation of the common peroneal nerve, and has been utilized by us and others to assess the efficacy of treatment modalities in the skeletal muscles of dystrophic mice [66,239–242]. Specifically, we investigated whether different parenteral routes of drug delivery (intraperitoneal, intravenous and subcutaneous) could lead to P188 efficacy *in vivo*. First-in-class membrane stabilizer P188 was evaluated at a dosage (460 mg/kg) that was previously shown to be effective in protecting the *mdx* heart *in vivo* as well as in mitigating electropermeabilization damage in rat skeletal muscle[165,37]. Lengthening contraction-induced force loss was markedly higher in *mdx* mice compared to *C57/BL10* mice, with most of the force loss in *mdx* mice occurring within the first 15 contractions (**Figure 3**). Intraperitoneal (IP) and intravenous (IV) delivery of P188 showed no significant effect on muscle function (**Figure 3A, B**), nor improvement in post-injury isometric force (**Figure 6A, B**).

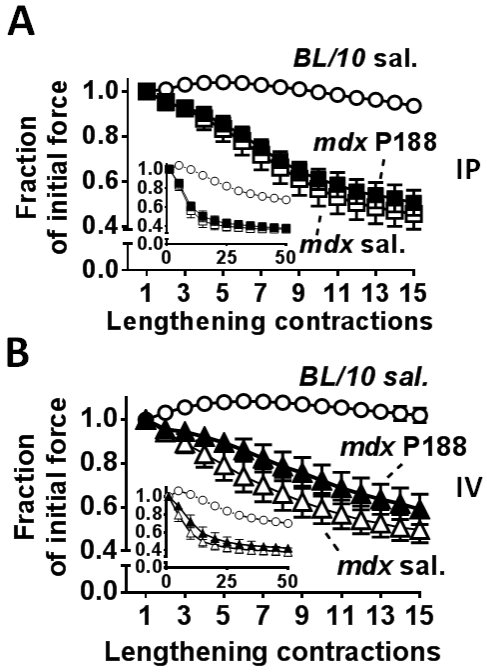

Figure 3: Intraperitoneal and intravenous delivery of P188 have no effect to protect against lengthening contraction-induced force loss in mdx mice *in vivo*. Force loss by the anterior crural muscles in adult *mdx* mice (n = 5-8 per group) treated with 460 mg/kg P188 or saline vehicle either (**A**) intraperitoneally (IP) or (**B**) intravenously (IV), at least 30 min before the injury protocol was assessed over the course of 50 lengthening contractions**.** Force loss is presented as a fraction of the initial maximal force +/- S.E.M. Contractions #1-15 show the marked force deficit in *mdx* mice. Results from BL/10 control mice injected saline via each delivery route are also shown. Inset (**A,B**) shows all 50 contractions. Both IP and IV delivery of P188 had no significant effect to decrease force loss over the course of the protocol**.** Error bars shown as mean +/- S.E.M.

In marked contrast, subcutaneous (subQ) delivery of P188 led to dramatic improvement in *mdx* hindlimb muscle function. Here, force loss was not statistically different from *C57BL/10* over 25 lengthening contractions ($P > 0.10$), and resulted in significantly higher force production than saline treated *mdx* mice over the entire injury protocol (*$P < 0.05$ for contractions #5-50 vs. *mdx* subQ saline) (**Figure 4**). P188 treatment also significantly decreased baseline and lengthening contraction-induced

increased Evans Blue dye uptake in mdx TA muscle (**Figure 5**). Additionally, post-injury isometric force in the subQ P188 treated group was significantly higher than saline treated *mdx* (*$P < 0.05$), and not significantly different from the C57BL/10 saline group ($P = 0.45$) (**Figure 6C**). In contrast, subQ delivery of a PEO homopolymer of similar molecular weight (PEG8000, 8 kDa) showed no improvement in muscle function (**Supplemental Figure 1**).

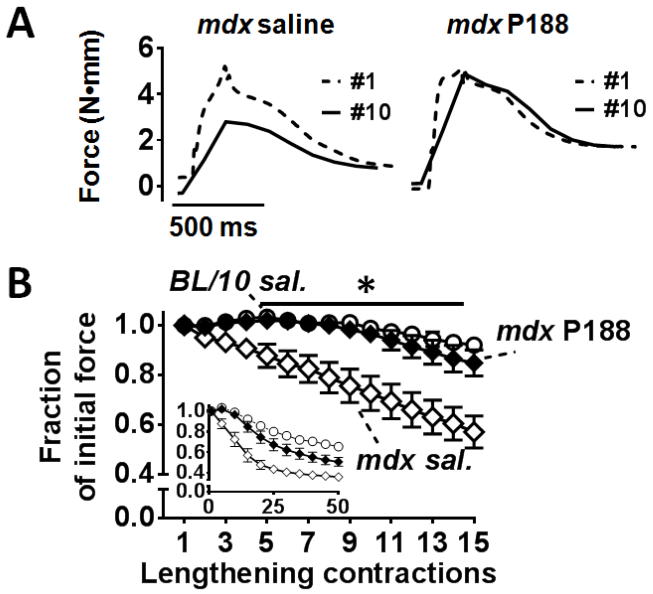

Figure 4: Subcutaneous delivery of P188 markedly protects against lengthening contraction-induced force loss in mdx mice *in vivo*. (**A**) Representative individual force tracings during lengthening contractions #1 vs #10 for subQ saline and subQ P188 treated *mdx* mice. (**B**) SubQ P188 delivery confers significant protection against force loss from contractions #5-50 (*$P < 0.05$ via two-way ANOVA compared to the *mdx* saline group. Contractions #1-15 are highlighted with the entire protocol shown in inset. Error bars shown as mean +/- S.E.M (in some cases symbol size was larger than error bar).

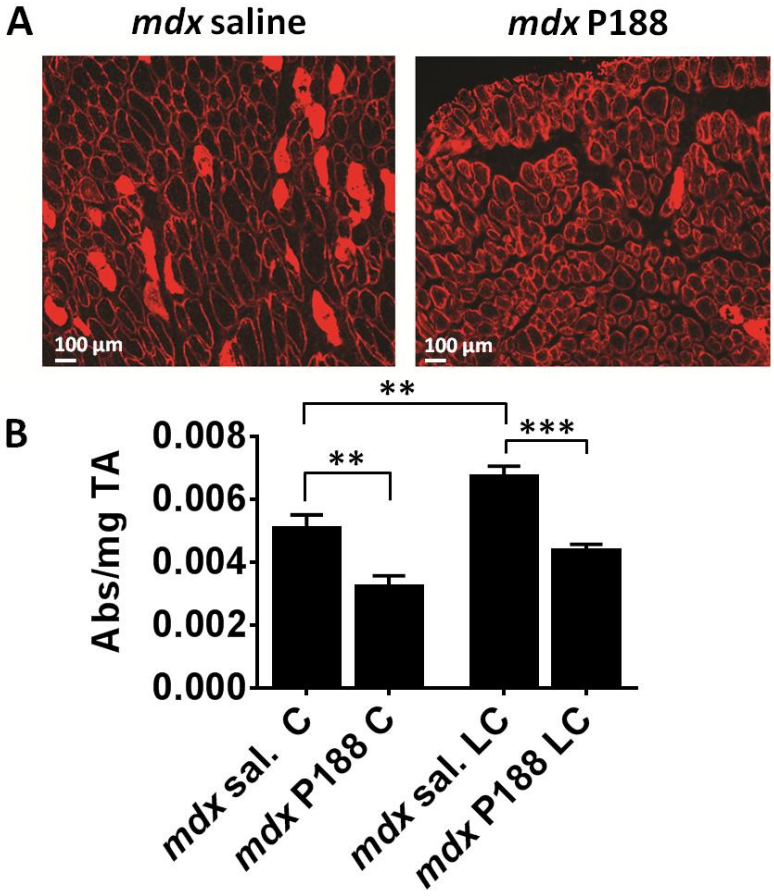

Figure 5: P188 significantly decreases baseline and lengthening contraction-induced sarcolemmal instability. (A) Example images of Evans Blue dye uptake into TA myofibers 2 h post injury in *mdx* mice treated subQ with saline or P188. **(B)** Quantification of total Evans Blue Dye extracted from whole TA muscles. Evans Blue dye was extracted by incubating the whole TA muscle in 1 mL of formamide. "C" denotes the contralateral non-injured TA, "LC" denotes lengthening contraction. Data is shown as absorbance at 620 nm divided by mg of tissue. $^{**}P < 0.01$, $^{***}P < 0.001$ via one-way ANOVA. Error bars shown as mean +/- S.E.M.

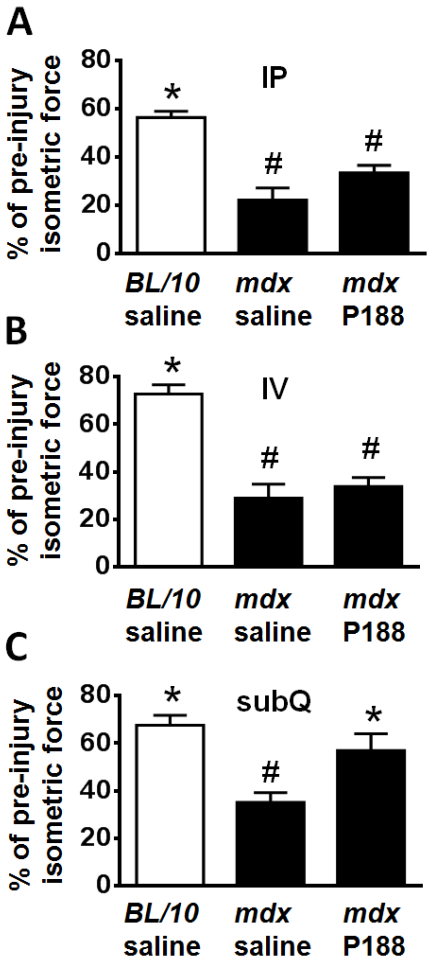

Figure 6: Isometric force measurements in P188 treated mdx mice immediately post-injury. IP **(A)** and IV **(B)** P188 delivery had no significant effect on peak isometric force immediately after injury whereas subQ P188 treatment (**C**) significantly enhanced immediate post-injury isometric force compared to *mdx* saline, and was not significantly different from BL/10 saline group. $^{*}P < 0.05$ one-way ANOVA compared to *mdx* saline, $^{\#}P < 0.05$ one-way ANOVA compared to *BL/10* saline. Error bars shown as mean +/- S.E.M.

The *in vitro* results showed that ext-P188, a block copolymer of identical PPO/PEO ratio but of increased molecular weight than P188, can also stabilize dystrophic skeletal muscle membranes (**Figure 2A, B)**. To further the structure-function understanding of how block copolymer size and PPO/PEO ratio affects *in vivo* efficacy and pharmacodynamics, we next examined whether ext-P188 could confer protection from lengthening contraction-induced force loss. Because ext-P188 showed efficacy at low μM concentrations *in vitro*, we tested ext-P188 at low (60 mg/kg) and high (160 mg/kg) dosages. Interestingly, and in contrast to P188, ext-P188 delivered IP at the low dosage significantly decreased force loss in *mdx* mice undergoing the lengthening injury protocol (*$P < 0.05$ for contractions #8-50) (**Figure 7A**). The post-injury isometric force loss was also not different from the *C57/BL10* saline group ($P = 0.42$) (**Figure 8**). This protective effect was not observed with either IV or subQ delivery and was lost at the high dosage (**Figure 7B, C and Figure 8**). Because a lower volume of the stock ext-P188 was needed to achieve a 60 mg/kg dose, we also tested whether intramuscular (IM) delivery directly into the TA muscle would optimize its pharmacodynamics. Similarly to the IP injection, IM injection of ext-P188 significantly decreased force loss during the lengthening injury protocol (**Figure 7D**) (*$P < 0.05$ for contractions #6-50) and isometric peak force recovery was comparable to control mice given saline IM ($P = 0.86$). These results indicate that a larger triblock copolymer of equivalent PPO/PEO ratio to P188 is capable of conferring protection to dystrophic skeletal muscle during physiological stress and that molecule size, dosage and route of delivery are all critical parameters for optimal pharmacodynamics.

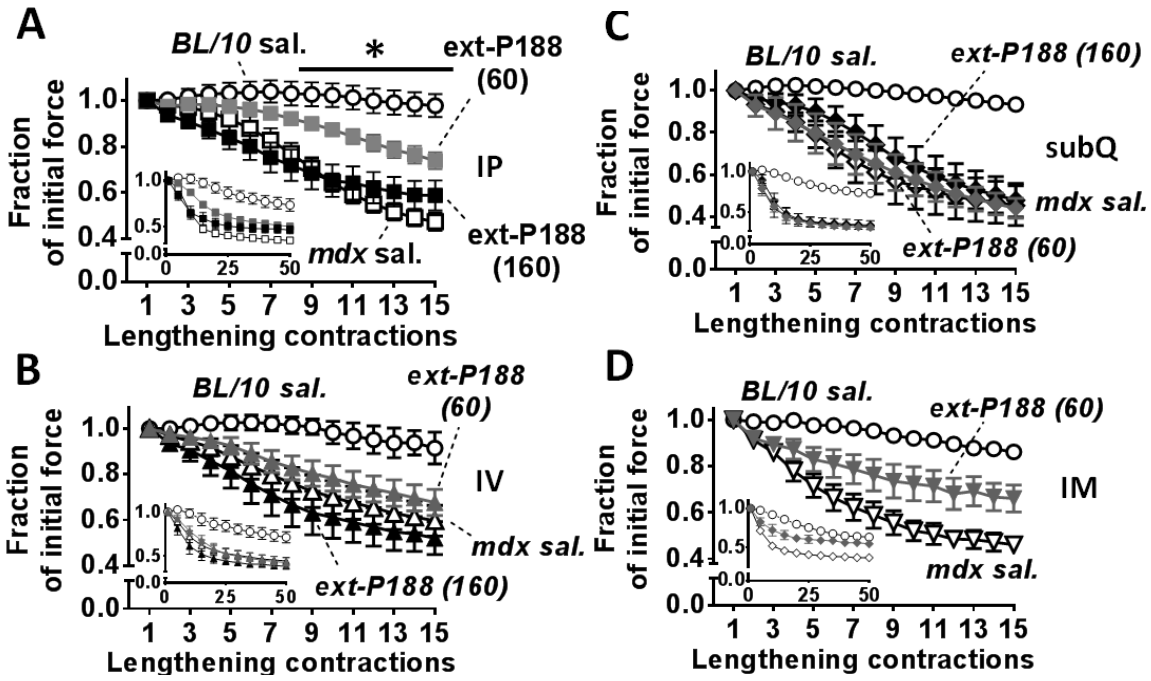

Figure 7*:* Dose and delivery route dependence of ext-P188 in protecting *mdx* mice skeletal muscle from lengthening contraction-induced force loss *in vivo*. *Mdx* mice were administered either low dose (60 mg/kg) or high dose (160 mg/kg) ext-P188 via intraperitoneal (**A**) (IP), (**B**) intravenous (IV)) or (**C**) subcutaneous (subQ) injection at least 30 minutes prior to the protocol and the anterior crural muscle group tested for lengthening contraction-induced force loss over the course of 50 contractions. Force loss is presented as a fraction of the initial maximal force +/- S.E.M. Contractions #1-15 are graphically emphasized. **(A)** High dose ext-P188 (160 mg/kg) had no protective effect against lengthening contraction-induced force loss. However, low dose ext-P188 (60 mg/kg) significantly improved resistance to injury from contraction #8 through #50 (**P* < 0.05 via two-way ANOVA compared to mdx saline). (**B-C**) Neither low dose nor high dose ext-P188 administered IV or subQ had any significant effects on force deficit. (**D**) Low dosage 60 mg/kg ext-P188 was injected into the Tibialis Anterior (TA) muscle of *mdx* mice directly prior to the protocol. Ext-P188 treated mice had a highly significant and sustained resistance to lengthening contraction injury loss (contractions 6-50, **P* < 0.05 two-way ANOVA compared to *mdx saline*). Contractions #1-15 are graphically emphasized, entire protocol shown in inset. Error bars shown as mean +/- S.E.M (in some cases symbol size was larger than error bar).

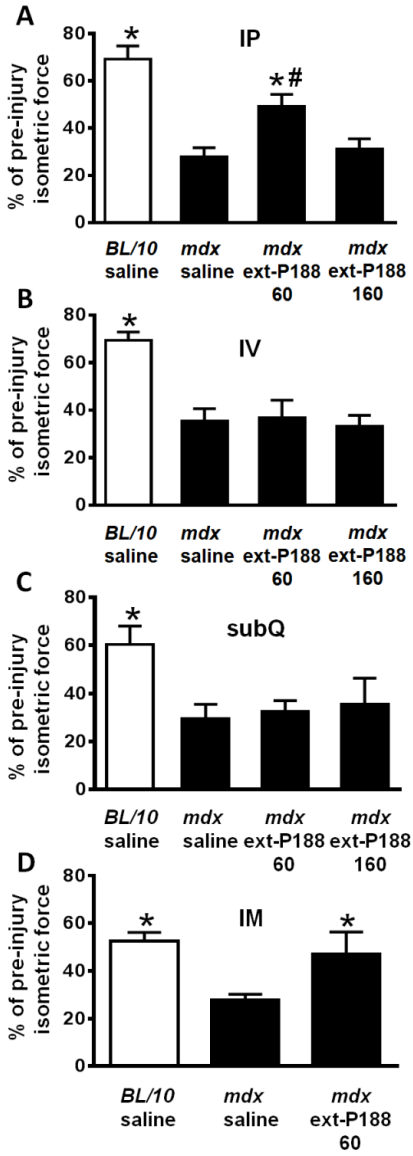

Figure 8: Isometric force measurements in ext-P188 treated mdx immediately post-injury. **(A)** Low dose (60 mg/kg) ext-P188 delivered IP significantly prevented post lengthening protocol isometric force loss (*$P < 0.05$ one-way ANOVA compared to *mdx saline*) although was significantly different from the *BL/10* saline group loss ($^{\#}P < 0.05$ one-way ANOVA compared to *BL/10* saline). (**B-C**) No significant effect obtained for IV or subQ ext-P188 treated mice. (**D**) Post-injury isometric force of mdx mice treated with direct injection of 60 mg/kg ext-P188 into the TA muscle was not significantly different from *BL/10* saline ($^{\#}P = 0.74$, one-way ANOVA compared to *BL/10* saline). Error bars shown as mean +/- S.E.M.

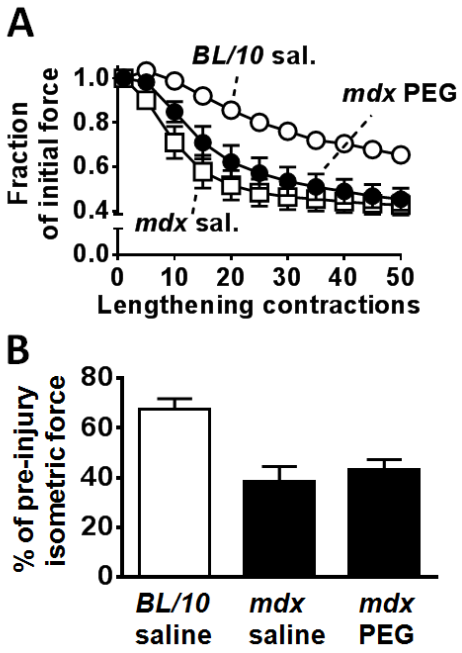

Supplementary Figure S1: Hydrophilic PEG8000 does not protect against force loss *in vivo*. Adult *mdx* mice with either with saline vehicle or 460 mg/kg PEG8000 subcutaneously (subQ) at least 30 min prior to the injury protocol were assessed for anterior crural muscle force loss over the course of 50 lengthening contractions (**A**) and for immediately post injury isometric force assessment (**B**)**.** PEG8000 had no significant effect on the force loss. Force loss is presented as a fraction of the initial maximal force +/- S.E.M.

2.4 Discussion

Our results provide the first evidence, to our knowledge, that synthetic membrane stabilizers significantly protect dystrophic limb skeletal muscles during physiologically relevant mechanical stress *in vivo.* A striking feature of this protective effect is that it is critically dependent upon route of delivery. We report that pretreatment of *mdx* mice with subcutaneous injection of P188 confers marked protection from lengthening contraction-induced force loss *in vivo*. The degree of protection from repetitive

lengthening contractions enabled *mdx* skeletal muscle to function similarly to control *C57Bl/10* mice, with the protection achieved being comparable to transgenic animal studies using highly functional dystrophin molecules[115,118,123,128]. In contrast, two other widely used parenteral means of drug delivery, intraperitoneal and intravenous, showed no beneficial effects. This is direct evidence that the lack of skeletal muscle efficacy reported in previous studies using P188[189,190] can be attributed to suboptimal mode of delivery of P188, rather than a fundamental limitation in the mechanism by which the block copolymer stabilizes fragile skeletal muscle membranes. These new findings underscore the importance of pharmacodynamic optimization, which is essential for drugs to reach clinical efficacy[222,223]. These findings, taken together with previous findings in dystrophic myocardium[37,187,234] along with a recent study demonstrating the efficacy of chronic delivery of P188 in improving both cardiac and respiratory function in dystrophin-deficient mice[195], are evidence that synthetic membrane stabilizers provide a unique first-in-class drug strategy for treating all affected striated muscles in DMD. The use of block copolymer-based membrane stabilizers as systemically delivered functional surrogates for dystrophin is further attractive, in that the mechanism of action is not limited by the specific DMD genetic lesion. Thus, in principle, synthetic membrane stabilizers could be applicable to all DMD patients, regardless of genetic mutation.

Pharmacodynamics is defined as the functional effects of a drug on the body, and incorporates optimization of route of delivery[222,243]. To date, no other study has tested P188 pharmacodynamics in the context of dystrophic skeletal muscle disease. It is well established that delivery route significantly affects pharmacodynamics and bioavailability of molecules injected into the body[222,243]. Differential effects of delivery could serve to explain why previous studies using intraperitoneal injections showed no efficacy of P188 to prevent *mdx* mice skeletal muscle injury *in vivo*[189,190]. Pharmacokinetics (PK) of P188 (the effects of the body on the disposition of P188 once it is injected) have recently been reported in mdx mice. Blood concentrations and clearance of P188 were assessed comparing IV and subQ routes of P188 administration in *mdx* mice and results showed

enhanced plasma exposure over time via subQ administration compared to IV dosing[195]. These findings of differential pharmacodynamics based on route of P188 delivery may help explain the skeletal muscle protection we found by subQ but not IV administration.

The marked differences in protective effects observed between the parenteral delivery routes suggest a differential systemic distribution of P188 to the hindlimb muscle tissues. It is widely supported that subcutaneous delivery leads to the slowest rate of absorption among the parenteral routes of delivery, which may come as a result of a subcutaneous drug depot promoting a sustained release effect[244,245]. Although intraperitoneal injection is the most common and easiest method to administer a high volume of drug to mice in pre-clinical studies, the rate of absorption from the repository site also can be quite slow, due to its main absorption route being the mesenteric vessels. In addition, intraperitoneal delivery is subjected to hepatic metabolism before reaching systemic circulation, which can lead to drug/molecule modifications[245]. On the other hand, intravenous injection has a rapid dispersion profile into the systemic circulation[243]. Thus, differential rates of P188 delivery across the varying routes could help to explain the striking differences in functional outcomes observed here.

Besides the differential effects shown for the parenteral delivery routes, block copolymer molecular weight appears to have a dramatic effect on pharmacodynamics and membrane stabilization efficacy. We speculate that differences arising between P188 and ext-P188 may be attributable to the propensity of the higher molecular weight ext-P188 to aggregate. While numerous reports have investigated the relationships of PPO/PEO ratio, molecular weight, concentration, and temperature to the aggregation behavior of poloxamers in solution[178,217,246,247], we posit that *in vivo* aggregation is prohibitively difficult to measure and likely complicated by the multi-component nature and space constraints of physiological conditions. For ext-P188, the higher dosage (160 mg/kg) corresponds to a total blood volume concentration above a reported aqueous critical micelle concentration at physiological temperature[246]. If aggregation occurs at the higher dosage *in vivo*, it could explain why ext-P188 was protective at the low dosage (i.e. less

likely to aggregate) but not at the high dosage. It is currently unclear how block copolymer pharmacodynamics and excretion would be affected by *in vivo* aggregation but these results indicate that molecular weight and concentration are critical components of membrane stabilizers to consider for *in vivo* application.

Another interesting outcome of this work centers on the apparent differential effect of block copolymer delivery routes to dystrophic cardiac and skeletal muscle. Previous work has shown marked efficacy for P188 to confer protection to dystrophic myocardium in small and large animal models of DMD *in vivo*[37,187,234]. These previous studies used both IP and IV delivery of P188 to confer protection, which appears significantly different from results of this present study where neither of these delivery routes were effective to protect dystrophic limb skeletal muscle from contraction-induced force loss *in vivo*. The basis for these differing results is unknown. Possibilities include the marked differences between skeletal and cardiac muscles in terms of physiological activation, forces borne, cell size, and in sarcolemma lipid composition. For example, extracellular Ca^{2+} is required for activation of cardiac muscle, but not so for skeletal muscles[65]. Also, lengthening contractions are physiologically relevant for skeletal muscle, but not for cardiac muscle. In addition, skeletal and cardiac muscle membranes differ dramatically in terms of neutral lipid composition, and dystrophic muscle is known to have alterations in membrane phospholipid content[248,249]. Collectively, these striated muscle lineage-based differences could help explain the different outcomes observed, in terms of route of block copolymer delivery. Moreover, dystrophic hindlimb tissues have markedly lowered microcirculation due, at least in part, to impaired nNOS modulation of adrenergic vasoconstriction during contractile activity[40,250]. Thus, these issues may ultimately explain why IV delivery of P188 and ext-P188 is ineffective in protecting dystrophic limb muscle against mechanical stress. It is also possible that the minimum effective block copolymer content required at the membrane could be fundamentally different between cardiac and skeletal muscles.

P188 is a triblock copolymer and member of the family of homologous amphiphilic compounds known as Poloxamers (and Pluronics). P188 has been reported for wide use in drug delivery and other biological applications, but virtually nothing is known regarding how P188 serves to stabilize fragile dystrophin-deficient muscle membranes. Biophysical studies examining triblock copolymer interactions with synthetic lipid membranes propose a two-state mechanism of block copolymer interaction: initial adsorption followed by insertion into the lipid membrane[169]. Membrane insertion appears to be highly dependent on the PPO/PEO ratio of the block copolymer, with hydrophobic dominant poloxamers (PPO/PEO > 1) capable of inserting and subsequently permeabilizing the cell membrane[167,169]. In contrast, evidence is emerging that the relatively hydrophilic P188 adsorbs onto the lipid membrane and exerts membrane stabilization by dampening surface and intra-bilayer hydration dynamics, rather than by direct corralling of lipids[212]. This critical dependence on the PPO/PEO ratio is supported by our results showing that the ext-P188, which has the equivalent PPO/PEO ratio to P188 at increased molecular weight, significantly stabilizes membranes *in vitro* and also *in vivo* in a manner dependent on both dosage and delivery route. Because efficacy of ext-P188 shows a clear dosage dependence which may be related to *in vivo* aggregation, it is particularly important to keep molecular weight effects in mind when considering other polymer species as potential membrane stabilizers. Moreover, the completely hydrophilic PEG8000 lacks efficacy *in vivo*, indicating that the hydrophobic PPO block of the copolymer is required for effective targeting of the membrane stabilizer to the damaged membrane. These results provide new mechanistic insights into optimal structural design of a potential next-in-class line of block copolymers for membrane stabilization therapy which are the target of future studies.

2.5 Perspective

The evidence here that membrane stabilizers can significantly protect dystrophic skeletal muscles from contraction-induced injury *in vivo* may have future clinical ramifications. Presently there are no treatments in clinical practice to prevent, halt or reverse disease in DMD patients, including recent drug and gene-based strategies[129,130,251]. This underscores the urgency to investigate alternative strategies aimed at directly targeting the primary defect of membrane fragility in DMD muscles. Synthetic membrane stabilizers have a number of features that make them attractive candidates for DMD treatment. First, the mechanism of action is non-specific to the DMD gene mutation, making this applicable to all DMD patients. In addition, systemic distribution of block copolymers makes them ideal for treatment of all the striated muscles in the body. Immunogenicity concerns of gene-based DMD treatments[252] are also obviated by the use of synthetic sarcolemma stabilizers.

Having established proof-of-principle for membrane stabilizers to protect dystrophic skeletal muscles *in vivo*, future studies are needed to ultimately guide their full potential clinical application. These include establishing minimum effective dose, duration of action, and assessment of long-term protection in small and large animal models of DMD. Importantly, it is the goal to incorporate these current findings with recent works in heart and respiratory function, as well as other dystrophic muscle groups. In addition, as block copolymers have been in use as vehicles for enhanced gene delivery in other applications[246,253], the prospect of bundled therapies with block copolymers and gene-directed strategies is of interest. P188 offers the additional advantage of being previously administered for human use for other conditions, which have been accompanied by extensive pharmacokinetics and ADME studies to validate clinical safety[176,198]. Our results support P188 as a unique first-in-class membrane stabilizer, as any effective DMD treatment must ultimately target all striated muscles: skeletal, respiratory and cardiac.

As DMD is a chronic progressive disease, we envision that membrane stabilizer therapy would likely require life-long treatment in DMD patients, initiated early in the course of disease to prevent mechanical stress-induced muscle damage. In the best case scenario, this clinical treatment would effectively manage disease, analogous, for example, to the effective life-long disease management strategy demonstrated by Type I diabetes patients. Other approaches could be considered as well, including acute treatments. For example, for DMD patients that undergo surgical orthopedic procedures, synthetic membrane stabilizers might also have significant clinical impact in the setting of the anticipated stress induced by general anesthesia[187]. Owing to the proposed membrane stabilizer mechanism of action, this class of therapeutics has a great advantage of potential application to all DMD patients regardless of specific genetic lesion and may extend to other inherited and acquired diseases in which sarcolemma integrity is compromised[179].

2.6 Methods

*Animal*s**.** Adult male and female *mdx* mice (C57Bl/10ScSn-DMD*mdx*) and wildtype *BL/10* mice (C57Bl/10ScSn) aged 2-6 months old were obtained from Jackson Labs (Bar Harbor, ME) and housed locally. The procedures used in this study were approved by the University of Minnesota's Institutional Animal Care and Use Committee (IACUC).

Generation of control iPax3 satellite cells-derived myotubes. Satellite cells were isolated from 6-8 week-old Pax7-ZsGreen mice as described previously[254]. Cell sorting was performed on a BD FACSAria cell sorter. Freshly isolated satellite cells were immediately transduced with the doxycycline inducible iPax3/IRES mCherry lentiviral vector[148] to generate the iPax3-SCs. Pax3 induction prevented the satellite cells from differentiation as soon as they are plated in culture, allowing better expansion of

undifferentiated cells in vitro. When iPax3-SCs were subjected to differentiation conditions (5% horse serum and withdrawal of dox and bFGF), culture gave rise to multinucleated myotubes.

Generation of mdx:utrn$^{-/-}$ iPS cells-derived myotubes. mdx:utrn$^{-/-}$myotubes were generated following a previously published method [148]. Briefly, dystrophic iPS cells were generated from tail tip fibroblasts of mdx:utrn$^{-/-}$ donors and reprogrammed using via retroviral transduction with Oct4, Klf-4 and Sox2. The iPS cells were then modified for doxycycline-regulated Pax3 conditional expression. Pax3 was induced via 0.8 µg/mL of doxycycline from day 3 of embryoid bodies differentiation and paraxial mesoderm progenitors were isolated based on PDGFαR expression and lack of Flk-1[255]. Sorted cells were plated and allowed to proliferate in proliferation myogenic medium (IMDM, 15% FBS, 1% chicken embryo extract, 10% horse serum, 1 µg/mL doxycycline and 5 ng/mL of bFGF). The myogenic precursors were then terminally differentiated by switching to low glucose DMEM and 5% horse serum in the absence of both doxycycline and bFGF.

Flexor Digitorum Brevis single myofiber isolation. The Flexor Digitorum Brevis (FDB) muscles were surgically removed from both hind paws of adult *mdx* mice and enzymatically digested via incubation in M199 containing 0.2% collagenase type II plus 10% fetal bovine serum at 37 °C. Myofiber bundles were dissociated with gentle trituration using Pasteur pipettes and myofibers were plated on 20 µg/mL laminin-coated coverslips and left to adhere overnight at 37°C in 5% CO_2). The myofibers were cultured in M199 media (Sigma, St.Louis, MO) supplemented with 10 mmol/L glutathione, 26.2 mmol/L sodium bicarbonate, 0.02% bovine serum albumin, and 50 U/ml penicillin-streptomycin, with pH adjusted to 7.4. Myofibers were used within 24 hours of isolation.

Block Copolymers. National Formulary grade of P188, P338 and P331 were generously provided by BASF. P338 is denoted as "ext-P188" for simpler interpretation. PEG8000 (Polyethylene Glycol 8000) was purchased from Sigma (St Louis, MO).

Hypo-osmotic stress assay. FDB myofibers were transferred from M199 culture media to a 310 mOsm isotonic solution (in mM: 140 NaCl, 5 KCl, 2.5 $CaCl_2$, 2 $MgCl_2$, and 10 HEPES; pH 7.2) in the absence or presence of polymer. After a 3 min of pretreatment equilibration with the polymer, myofibers were subjected to hypo-osmotic stress for 90 seconds by exchanging in a 140 mOsm solution (composition equivalent to 310 mOsm solution but with NaCl reduced to 50 mM) +/- polymer. The myofibers were subsequently re-equilibrated in an isotonic solution +/- opolymer for a total of 7 min. The remaining myofibers were lysed with 0.01% Triton. Every media change was collected to assess enzyme release throughout the protocol. Enzyme release was assessed as a total release during the course of the protocol over total enzyme content.

Enzyme release assays. Lactate Dehydrogenase (LDH) release was assessed at the end of the hypo-osmotic stress protocol. LDH release was assayed by incubating samples aliquots in 100mM NaPO4, 120µM NADH, 2.3mM pyruvate, and 0.033% bovine serum albumin at 37°C degrees. Absolute LDH release was calculated indirectly from the conversion of NADH to NAD+, which was determined by reading absorbance at 340 nm over time.

Block copolymer treatment and delivery for in vivo injury protocol. Block copolymers were dissolved in sterile saline to final stock solutions of 150 mg/ml. At least 30 min before the start of the *in vivo* injury protocol, mice received specific dosages of Poloxamer or equivalent saline volume intraperitoneally (IP), intravenously (IV), subcutaneously (subQ - beneath the scruff on the back of the neck) or intramuscularly (IM) into the TA muscle.

In vivo lengthening contraction force loss protocol. In vivo force measurements of the anterior crural muscle compartment (tibialis anterior, extensor digitorum longus and extensor hallucis longus) were performed as described previously [102,237]. Mice were anesthetized with a combination of fentanyl citrate (0.2mg/kg), droperidol (10mg/kg) and diazepam (5 mg/kg) and the left hindlimb was depilated. The left foot was then secured to an aluminum foot-plate coupled to a servomotor (Model 300B-LR;Aurora Scientific, Aurora, Ontario, Canada). Contractions were induced via stimulation of the peroneal nerve via percutaneously inserted Pt-Ir electrode wires (Model E2-12; Grass Technologies, West Warwick, RI, USA) connected to a stimulator and stimulus isolation unit (Models S48 and SIU5, Grass Technologies). This system allows for a non-invasive evaluation of skeletal muscle contractile properties *in vivo* [224]. An initial pre-injury maximal isometric force was determined (250 Hz and 150 ms duration), followed by an injury protocol consisting of 50 lengthening contractions. For the lengthening contractions, the foot underwent 19 degrees passive dorsiflexion at which a pre-lengthening 100 ms isometric contraction was initiated followed by another 50 ms of stimulation as the foot was actively moved to 19 degrees of plantarflexion (for a total ankle rotation of 38 degrees). Each lengthening contraction was separated by 10 seconds to prevent fatigue. Maximal force was measured for each lengthening contraction during the course of the injury protocol and presented initialized to the first lengthening contraction force. A final isometric force was measured at the end of the lengthening protocol. $n \geq 5$ mice (both males and females) for each treatment group of each experiment.

Evans blue dye uptake assay. To assess the integrity of the muscle fiber membrane pre- and post-lengthening contractions, *mdx* mice (n = 6-8 per experimental group) received an intraperitoneal injection of 3% Evans blue dye (EBD; Sigma, St. Louis, MO) (wt/vol) in phosphate-buffered saline (PBS, pH 7.4) at a volume of 1% body mass. This solution

was sterilized by passage through a Millex-GP 0.22 μm filter (Millipore, Bedford, MA) and administered 2h before initiation of the lengthening injury protocol. Both the injured and contralateral TA muscles were collected and weighed 2h after injury and dye uptake was measured by absorbance reading at 620 nm after dye extraction from the minced tissue by incubation in 1 ml formamide at 55°C[63,256]. A subgroup of injured TA muscles was snap-frozen in isopentane cooled with liquid nitrogen, cryosectioned, and visualized for red fluorescence as a signal of dye uptake in myofibers.

Statistics. All results are expressed as mean ± SEM. Multi-group comparisons for *in vitro* LDH release experiments were assessed using one way analysis of variance (ANOVA) with Tukey post-hoc test and $P < 0.05$ considered statistically different. A two-way ANOVA followed by a Bonferroni-post hoc test was used to assess the effect of lengthening contraction numbers and treatment routes across the 50 contractions protocol with $P < 0.05$ considered statistically different. All statistical analysis was carried out using Prism (GraphPad Software).

CHAPTER 3

STRUCTURE-FUNCTION RELATIONSHIP OF MEMBRANE STABILIZING DIBLOCK COPOLYMERS

Evelyne M Houang[1], Karen J Haman[2], Mihee Kim[2], Benjamin J Hackel[2], Dawn A Lowe[3], Frank S Bates[2] and Joseph M Metzger[1].

[1]Integrative Biology and Physiology, University of Minnesota, United States; [2]Department of Chemical Engineering and Materials Science, University of Minnesota, United States; and [3]Rehabilitation Science and Program in Physical Therapy, University of Minnesota, United States.

Manuscript in preparation

3.1 Introduction

The investigation of poloxamers as membrane stabilizing agents has been ongoing for decades[165,166,257]. Poloxamers are triblock copolymers composed of a polypropylene oxide (PPO) core flanked on each side by polyethylene oxide (PEO) chains. We and others have established that one such poloxamer, P188, has biological membrane stabilizing capacity in the context of various muscle diseases, including as described in Chapter 2, the degenerative disease Duchenne Muscular Dystrophy (DMD)[258].

In addition to P188, these copolymers come in various molecular weights and PPO/PEO ratios and are constrained, in terms of ease of acquisition, to those made available commercially by the chemical company BASF. This limitation is an impetus for pushing our exploration of the copolymer chemical landscape beyond that of the triblock architecture. In order to intelligently design an optimal membrane stabilizer for DMD, it is necessary to increase our understanding of the parameters that control copolymer association with muscle membrane bilayers.

Studies have reported that membrane stabilizing triblock copolymers such as P188 are weakly adsorbed to the lipid bilayer[170,212]. It is hypothesized that this weak association is due to poor integration of the PPO unit inside the bilayer due to steric constraints imposed by the flanking PEO chains[203]. Removal of one of the flanking PEO chains to form a diblock PEO-PPO architecture (**Figure 1**) allows for assessment of the association of the hydrophobic PPO core with the lipid bilayer due to reduction in the steric constraints that prevent PPO incorporation amongst the hydrophobic acyl chains.

A recent study employing small- and wide-angle X-ray scattering examined the structure of a lipid bilayer and the phase produced by either the triblock P188 or a PEO-PPO with an equivalent PPO block length[259]. They observed that P188 interaction with a synthetic lipid bilayer produced an aggregate phase structure suggesting inadequate insertion of the polymer in the lipid bilayer. On the other hand, the PEO-PPO diblock produced a well-ordered lamellar phase indicative of being well-anchored in the

bilayer[259]. This suggests that removing one of the flanking PEO chains facilitates PPO block anchoring into the hydrophobic acyl chain region of the lipid bilayer and strengthens copolymer-bilayer interaction.

In addition to decreasing steric constraints to increased PPO interaction with the hydrophobic region of the bilayer, removal of one of the flanking PEO chains allows for more straightforward additions of end-group moieties to the PPO block. This capability allows us to investigate in greater depth, the role of the PPO block in interacting with the bilayer. Specifically, we can now strategically modulate PPO block hydrophobicity by addition of relatively hydrophobic small end groups as a means to fine tune diblock-bilayer interactions.

There is currently little known on the physio-chemical basis of PEO-PPO diblock copolymer interaction with lipid bilayers *in vitro*, and even less so under physiological conditions. The objectives of this work were to demonstrate, for the first time to our knowledge, that diblock PEO-PPO architectures are effective membrane stabilizers for DMD, and that both PPO/PEO composition and PPO end group chemistry play crucial roles in optimizing membrane stabilization.

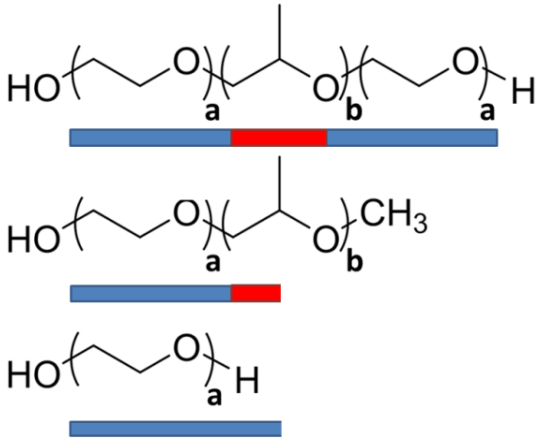

Figure 1: Copolymer structures for PEO-PPO-PEO triblocks, PEO-PPO diblocks and PEO homopolymer. The hydrophilic PEO chain is represented in blue and hydrophobic PPO core is represented in red.

A PEO-PPO diblock architecture became a focus of investigation due to 1) a simpler synthesis process that allows for methodical changes to composition and molecular weight, 2) gaining insight into whether a triblock architecture is required for membrane stabilization, and 3) allowing for addition of end groups moieties to either PEO and/or PPO blocks to alter overall diblock chemistry and membrane interaction.

This work is the result of collaboration with Professor Frank Bates' group in the department of chemical engineering and materials science (CEMS) at the University of Minnesota. Diblock copolymers were designed and synthesized by Dr. Karen Haman and graduate student Wenjia Zhang. Dr. Mihee Kim helped collect and analyze part of the *in vitro* data.

3.2 Role of architecture in membrane stabilization: triblock vs. diblock comparison

Little is known, to our knowledge, about whether or not diblock architectures can stabilize biological membranes *in vitro* or *in vivo*. Due to the established membrane stabilization activity of Poloxamer 188[165,37,187,234,258], direct comparison was first made with its composition analog diblock (di-80%), which was purchased from Polymer Source (Montreal, Quebec). In this case, the two copolymers share the same PPO/PEO composition ratio and hydrophilic PEO chain length (**Table 1)**. Of note, the terminal PPO end group on the di-80% is a methoxy group (-mE) (**Figure 1**), which role will be addressed in a later part of the study. We also tested PEG8000 as a negative control as we have demonstrated previously in Chapter 2 that PEO alone is not sufficient for optimal membrane stabilization.

Copolymer	*Average MW (Da)*	*Total PEO*	*PPO*	*PPO/PEO*
P188	8400	2 x 75	30	0.19
di-80%	4200	75	16	0.20
PEO8000	8000	-	-	-

Table 1: Polymer characteristics for P188, the diblock of P188 (di-80%) and PEG8000

First, we tested whether di-80% can stabilize muscle membranes *in vitro*, bypassing any potential pharmacokinetics/dynamics effects on the molecule, which we established in Chapter 2 are important factors affecting *in vivo* efficacy. The principal objective of this work was to then assess and compare di-80% and its triblock analog P188 in terms of efficacy in preserving dystrophic skeletal muscle function and sarcolemmal integrity *in vivo*.

Di-80% has in vitro membrane stabilizing efficacy comparable to P188

We used our established membrane injuring hypo-osmotic stress assay[258] to compare the efficacy of di-80% and P188 in preventing stress-induced lactate dehydrogenase (LDH) release from cardiac myocytes and skeletal myoblasts (**Figure 2**). In rat cardiac myocytes exposed to hypo-osmotic stress, 150 uM P188 decreased LDH release (~40% decrease, *P < 0.0001) (**Figure 2B**). Similarly, P188 significantly decreased LDH in control skeletal myoblasts release (~80% decrease, *P < 0.0001), as expected[258] (**Figure 2C**). Di-80% at 150 uM shows comparable membrane stabilization as P188 in cardiomyocytes (~40% decrease in cardiomyocytes, *P = 0.0002). In contrast, di-80% was significantly less effective than P188 in stabilizing skeletal myoblasts (~65% decrease compared to ~85% for P188, P = 0.0009). Interestingly, the completely PEO based PEG8000 decreased LDH release in rat cardiomyocytes to the same extent as P188 and di-80% (~40% decrease, *P = 0.0024) but was not as effective in blocking LDH release from skeletal myoblasts. These results indicate that di-80% is not as effective a

membrane stabilizer as P188 in skeletal myoblasts, at least in the context of hypo-osmotic stress.

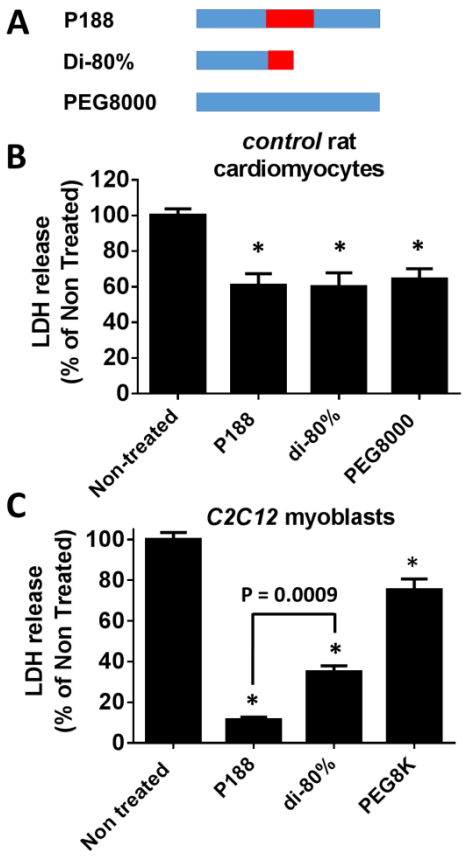

Figure 2: ***In vitro*** **hypo-osmotic stress assay to compare P188 and its analog diblock di-80% for membrane stabilization. (A)** Schematic of P188, di-80%, and the exclusively PEO-based polymer PEG8000, showing relative PPO (red) and PEO composition (blue). (**B**) Rat adult cardiomyocytes were exposed to hypo-osmotic stress media in the presence of 150 uM copolymers and LDH release was measured as a marker of membrane permeability. (**P* < 0.05, via one-way ANOVA compared to non-treated). (**C**) LDH release from *C2C12* myoblasts exposed to hypo-osmotic stress in the presence of 150 uM copolymers (**P* < 0.0001, via one-way ANOVA compared to non-treated group). Mean values are derived from at least 3 independent experiments. Error bars shown as mean +/- S.E.M. The myoblasts data were collected and analyzed by Dr. Mihee Kim, from the Department of Chemical Engineering and Material Sciences at the University of Minnesota.

Effects of *Di-80% as a muscle membrane stabilizer in vivo*

The *mdx* mouse exhibits significant susceptibility to lengthening contraction injury, as evidenced by a marked force loss after successive lengthening contractions[36,258]. We have established in **Chapter 2** that it is an outstanding physiological assay to evaluate the impact of membrane stabilizers *in vivo*. In brief, the hind paw of each mouse was secured to a foot plate connected to a servomotor which allowed for controlled plantarflexion and dorsiflexion of the hind limb about the ankle joint. Lengthening contractions of the anterior crural muscle compartment were induced via electrical stimulation of the common peroneal nerve and the resulting torque from each lengthening contraction was measured. We therefore used this assay to evaluate the impact of di-80% treatment on physiological muscle function of the hindlimb anterior crural muscle group (dorsiflexors) in comparison against its established membrane stabilizing triblock analog, P188.

As demonstrated in **Chapter 2**, subcutaneously (subQ) delivery of P188 results in significant protection against force loss during the lengthening contraction injury protocol. In contrast, di-80% delivered subcutaneously shows no improvement in force maintenance (**Figure 3A**). Di-80% showed a trend of improvement as compared to P188 using intraperitoneal delivery (**Figure 3B**) but not to a significant extent. Considering di-80% appears as efficacious as P188 *in vitro*, it is surprising that a lack of efficacy is observed *in vivo*. While it remains unclear why a differential effect is seen, the pharmacodynamics of both molecules appear different and either not enough or no di-80% copolymer at all reaches the injured muscle tissues following subQ or IP injection. As previously demonstrated in chapter 2, when comparing P188 to its PEO homopolymer analog PEG8000, the PPO core seems to drive membrane stabilizing efficacy *in vivo*. We speculate that PPO core length drives copolymer targeting to the injured membrane, which could explain why di-80% is as efficacious as P188 *in vitro* where there are no impediment to membrane interaction but lacks efficacy once injected into the body.

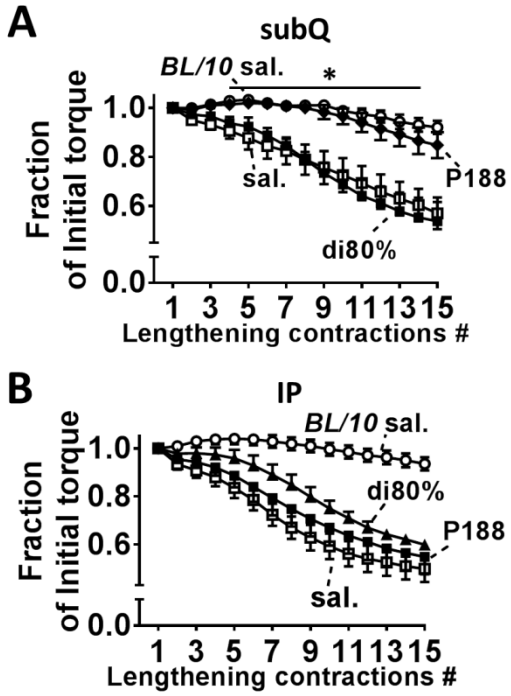

Figure 3: Comparison of intraperitoneal delivery of di-80% vs. P188 against lengthening contraction-induced force loss in *mdx* mice *in vivo*. Force loss by the anterior crural muscles, in adult *mdx* mice (*n* = 3-8 per group) treated with (**A**) 460 mg/kg P188 or di-80% subcutaneously (subQ) and (**B**) 1000 mg/kg P188, di-80% intraperitoneally (IP) at least 30 min before the injury protocol, was assessed over the course of 50 lengthening contractions**.** Force loss is presented as a fraction of the initial maximal force +/- S.E.M. Contractions #1-15 show the marked force deficit in *mdx* mice. Results from *BL/10* control mice injected with saline are also shown. Inset shows all 50 contractions.

3.3 Role of PPO end groups in diblock membrane stabilization efficacy

The elimination of one of the PPO flanking PEO chains allows for end group modification of the PPO core itself. As the PPO hydrophobicity is speculated to drive membrane efficacy, we wanted to study the impact of adding small end groups of varying hydrophobicity on membrane stabilization.

Diblocks with two different end group moieties on the PPO block were synthesized: tert-butoxy- and hydroxyl- functional blocks (Schematic 1, Figure 4). A third end group was also evaluated, as the commercially available diblock of P188 features a methoxy functional group on the PPO block, which is relatively less hydrophobic than a tert-butoxy group but more hydrophobic than a hydroxyl group (tert-butoxy > methoxy > hydroxyl).

To generate a tert-butoxy functionalized diblock (PEO_a-PPO_b-t), PPO was grown from a tert-butoxide initiator and its attached PEO was terminated with a hydroxyl group (**scheme 1, A, B**). Another diblock with a hydroxyl functionalized diblock (PEO_a-PPO_b-OH) was generated from commercially from mono-methoxy PEO (**scheme 1, A, B**). While a methoxy group is present in the initial PEO starting block rather than an hydroxyl group, its low hydrophobicity relative to the size and hydrophilicity of the PEO group makes it relatively inert and it is therefore not expected to affect membrane interactions. Representative structures of the tested diblocks are shown in **Figure 4.**

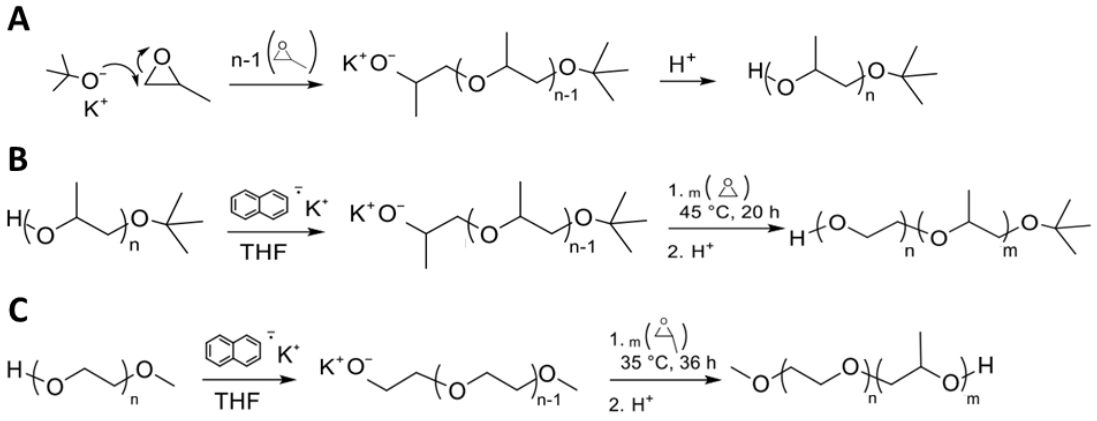

Schematic 1: Synthesis of diblock PPO-PEO copolymers. (**A**) Initiation, propagation and termination of PPO. (**B**) Re-initiation of tert-butoxy terminated PPO and living anionic polymerization of ethylene oxide (EO) to form a PEO-PPO-t-butoxy diblock. (**C**) Formation of a PEO-PPO-OH diblock. Adapted from schematic by Dr. Karen Haman.

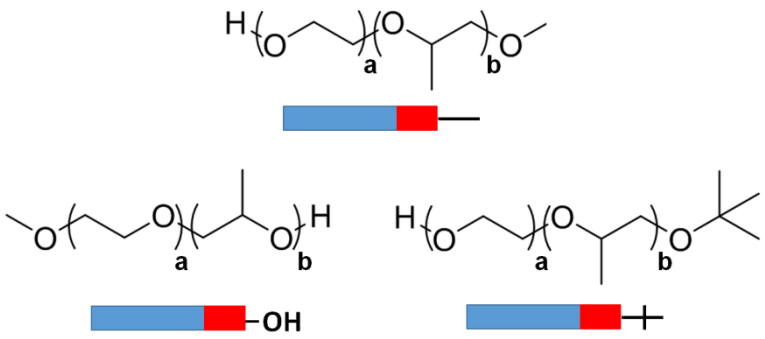

Figure 4: Schematic of diblock PEO-PPO copolymers with hydroxyl (OH), methoxy (mE) and t-butyl (tert) terminated end groups on the hydrophobic PPO (red).

Two pairs of diblocks were evaluated. The first pair includes the P188 diblock analog, di-80%, which we previously mentioned was obtained commercially. The industrial synthesis scheme resulted in a methoxy terminated di-80%, which adds a slightly higher hydrophobic character to the PPO core compared to the normally hydroxyl terminated PEO end blocks of P188. To compare and contrast the effect of additionally increasing the relative hydrophobicity of the PPO core, a tert-butoxy di-80% diblock was generated. In addition, to determine whether a PPO/PEO ratio of ~0.20 (or 80% PEO composition) was absolutely critical to optimal membrane stabilization, a diblock containing the same PPO core length (N = 16) as di-80% but of smaller PEO chain was synthesized, resulting in a PPO/PEO ratio of 0.33. This diblock (di-70%) was then terminated with either a hydroxyl or a tert-butoxy end group. The tested diblocks are listed in **Table 2**.

Copolymer	***Average MW (Da)***	***PEO$_b$***	***PPO$_a$***	***PPO/PEO***
di-80%-methoxy	4200	75	16	0.21
di-80%-t-butoxy	4350	75	16	0.21
di-70%-OH	2900	48	16	0.33
di-70%-t-butoxy	3000	48	16	0.33

Table 2. Summary of polymer structures of tert-butoxide (t), methoxy (mE), and hydroxyl (OH) terminated PEO-PPO diblocks.

Effects of PPO end groups and PPO/PEO ratio on membrane stabilization in vitro

Once again, to assess membrane stabilization efficacy independently of any pharmacokinetics/dynamics effects, the capability of diblock copolymers, with either tert-butoxy (tert), methoxy (mE), or hydroxyl (OH) end groups to protect muscle cells from hypo-osmotic stress *in vitro*, was investigated (**Figure 5**).

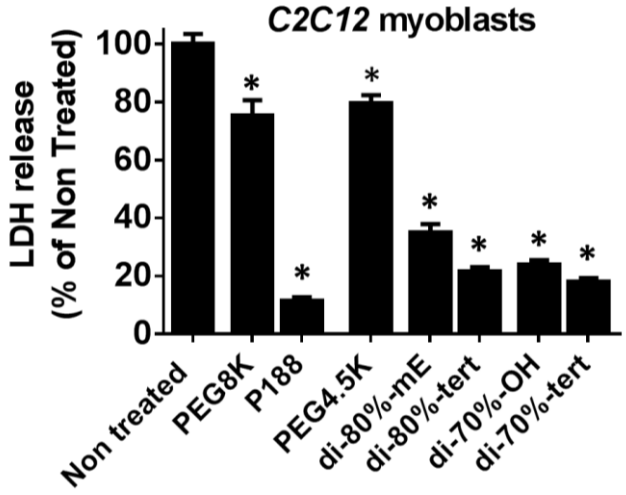

Figure 5. ***In vitro*** **hypo-osmotic stress assay to screen diblock copolymers for membrane stabilization.** LDH release from C2C12 myoblasts exposed to hypo-osmotic stress (*$P < 0.0001$, via one-way ANOVA compared to non-treated group) in the presence of 150 uM copolymers. Mean values are derived from at least 3 independent experiments. Error bars shown as mean +/- S.E.M. These data were collected and analyzed by Dr. Mihee Kim, from the Department of Chemical Engineering and Material Sciences at the University of Minnesota.

As expected and as observed in skeletal myoblasts (**Figure 2**), enzyme release was significantly blocked by the presence of P188, whereas the PEO homopolymer PEG8000 had no significant membrane stabilization effect. As demonstrated in skeletal myoblasts earlier in this study, the commercial di-80%-mE at 150 uM also had significant protection against hypo-osmotic stress induced released of LDH (~60% decrease) but it was not as protective as P188 (P= 0.013). Interestingly, replacement of the methoxy

group by a more hydrophobic tert-butoxy trends towards improving enzyme blocking efficacy, although it was not significant.

On the other hand, both hydroxyl and tert-butoxy di-70% diblocks were significantly protective, with no difference in efficacy observed between the two different end groups. Also, membrane stabilizing efficacy observed with a diblock of 0.33 PPO/PEO ratio is evidence that a ~0.20 PPO/PEO ratio of the well-established membrane stabilizer P188, is not necessarily the "sweet spot" for membrane stabilization efficacy and that diblock hydrophobicity can be modulated for increased membrane stabilization.

The tert-butoxy PPO end group significantly potentiates membrane stabilization during lengthening contraction injury in vivo

We next assessed the impact of the PPO functional end group on membrane stabilization *in vivo*. Due to preliminary experiments showing efficacy of intraperitoneal (IP) delivery of 1000 mg/kg of the tert-butoxy diblocks, this delivery route and dosage was used for PPO end group comparison purposes.

When comparing composition analog diblocks that differ only on terminal end group chemistry, the t-butoxy functional diblock copolymers exhibited marked protection against lengthening contraction injury (**Figure 6**). In stark contrast, their hydroxyl- and methoxy-terminated analogs, which showed significant membrane stabilization efficacy *in vitro* (**Figure 5**), had no significant protective effect *in vivo*. Relative to the hydroxyl- and methoxy-terminated end groups, the tert-butoxy group imparts considerably more hydrophobicity to the PPO core of the diblock. These data suggest that the overall hydrophobic strength of the hydroxyl and methoxy-terminated PPO group is not substantial enough to improve membrane stabilization *in vivo*, but that further increase in hydrophobic character via substitution of a t-butoxide group significantly changes the membrane stabilization property of the copolymer.

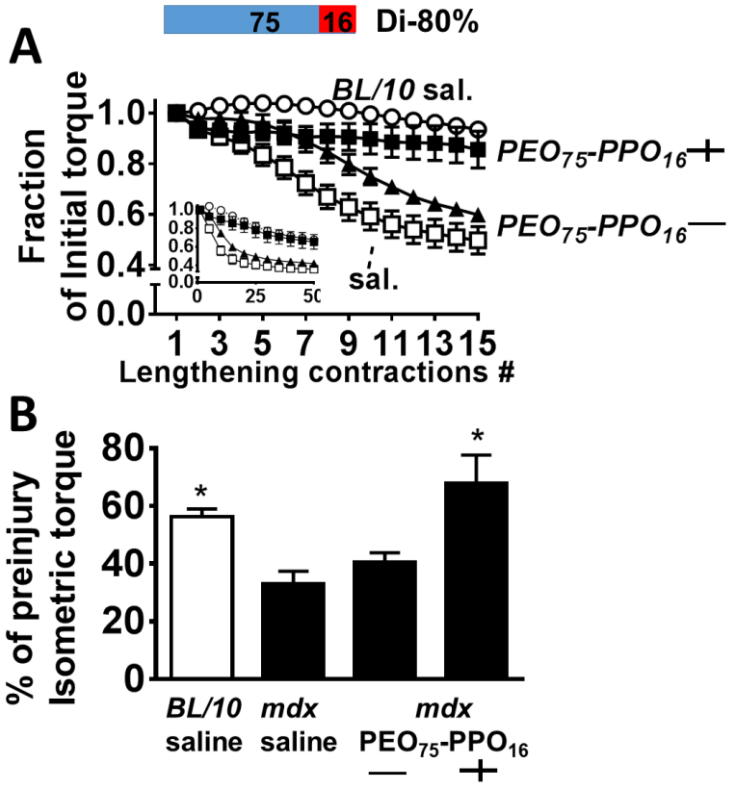

Figure 6: Comparison of methoxy vs t-butoxy end groups of di-80% against lengthening contraction-induced force loss in *mdx* mice *in vivo*. (**A**) Force loss by the anterior crural muscles, in adult *mdx* mice (*n* = 4-7 per group) treated with 1000 mg/kg of each di-80% diblock or saline vehicle intraperitoneally at least 30 min before the injury protocol, was assessed over the course of 50 lengthening contractions**.** Force loss is presented as a fraction of the initial maximal force +/- S.E.M. Contractions #1-15 show the marked force deficit in *mdx* mice. Results from BL/10 control mice injected with saline are also shown. Inset shows all 50 contractions**.** (**B**) The methoxy-terminated di-80% had no significant effect on peak isometric force immediately after injury whereas the t-butoxide terminated di-80% treatment significantly enhanced immediate postinjury isometric force recovery compared to *mdx* saline, and was not significantly different from *BL/10* saline group.

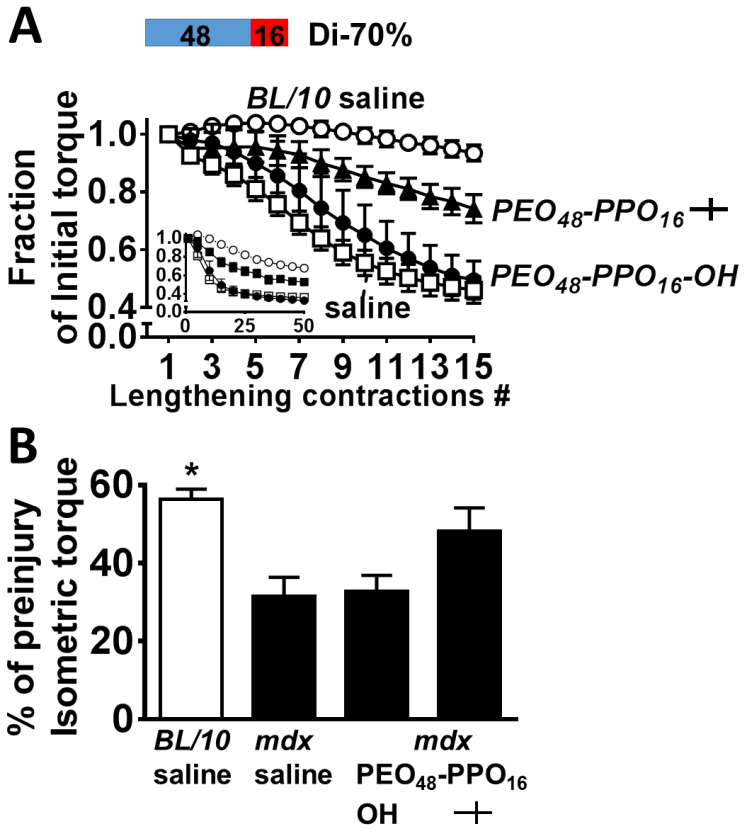

Figure 7: Comparison of hydroxyl vs t-butoxy end groups of di-70% against lengthening contraction-induced force loss in *mdx* mice *in vivo*. (**A**) Force loss by the anterior crural muscles, in adult *mdx* mice (*n* = 4-7 per group) treated with 1000 mg/kg of each di-70% or saline vehicle intraperitoneally at least 30 min before the injury protocol, was assessed over the course of 50 lengthening contractions**.** Force loss is presented as a fraction of the initial maximal force +/- S.E.M. Contractions #1-15 show the marked force deficit in *mdx* mice. Results from *BL/10* control mice injected with saline are also shown. Inset shows all 50 contractions**.** (**B**) The hydroxyl-terminated di-70% had no significant effect on peak isometric force immediately after injury while the t-butoxide terminated di-70% treatment trended towards enhanced immediate postinjury isometric force recovery compared to *mdx* saline, and was not significantly different from *BL/10* saline group. *P < 0.05 one-way analysis of variance compared to mdx saline, #P < 0.05 one-way analysis of variance compared to *BL/10* saline. Error bars shown as mean ± standard error of the mean.

3.4 Discussion

This study is the first mechanistic investigation into the structure-function relationship of block copolymer architecture in terms of defining the basis of copolymer-based membrane stabilization in live cells under physiological conditions. Our results provide new evidence that synthetic diblock PEO-PPO copolymers have biological membrane stabilization efficacy both *in vitro* and *in vivo*. First, we provide new insight into block copolymer architecture in terms of membrane stabilization properties. We show for the first time that a triblock architecture is not required for effective membrane stabilization. This result is important as it opens a new structure-function avenue featuring smaller and easier to synthesize membrane stabilizing diblock copolymers. In addition, the PEO-PPO diblock architecture allows ready access to PPO block end group modifications. We demonstrate that membrane stabilization *in vivo* can be optimized via modulation of the PPO block end group chemistry. Our results underscore the striking effect of the hydrophobic PPO core terminal end group to membrane interaction and stabilization *in vivo*. To account for these new findings, we propose an "anchor and chain" working model of copolymer-membrane interaction (**Figure 8**), as detailed below.

We report here that the addition of a hydrophobic tert-butoxy end group to the PPO core confers significantly improved membrane protection to dystrophic limb skeletal muscles during *in vivo* mechanical stress. In stark contrast, while substitution of either the relatively less hydrophobic methoxy terminal end group or the hydrophilic hydroxyl end group to the PPO core still imparts membrane stabilization efficacy *in vitro*, efficacy is completely lost *in vivo*. It remains unclear why the relative strength of hydrophobicity of the PPO end group induces the diblock copolymer to exhibit markedly differential effects *in vivo*. Nevertheless, these findings underscore the importance of modulating the hydrophobicity of the PPO block to enhance interaction with the membrane bilayer and indicate that the PPO block is the driving component for membrane interaction and stabilization *in vivo*.

Compared to the hydrophobicity of the alkyl tails of a phospholipid membrane bilayer, PPO itself is relatively mildly hydrophobic. This mismatch in hydrophobicity is hypothesized to lead to arrangement of the PPO at the polar lipid heads and hydrophobic alkyl chain tails border rather than full insertion into the alkyl chain region of the bilayer[259,260]. Further penetration at significantly increased overall copolymer hydrophobicity would lead to disruption of the lipids and membrane lysis, such as observed with copolymers with high PPO/PEO ratios[208,261]. We propose an "anchor and chain" model (**Figure 8**) whereby the addition of a relatively hydrophobic but small end group "anchor", as demonstrated by tert-butoxy, increases the hydrophobic character of the PPO core without significantly increasing its overall hydrophobicity of the copolymer, leading to an "anchoring" of the PPO core at the alkyl tail region of the bilayer. On the other hand, the PEO chain is required to preserve the amphiphilic behavior of the copolymer to maintain it at the solvent-membrane interface (**Figure 8**).

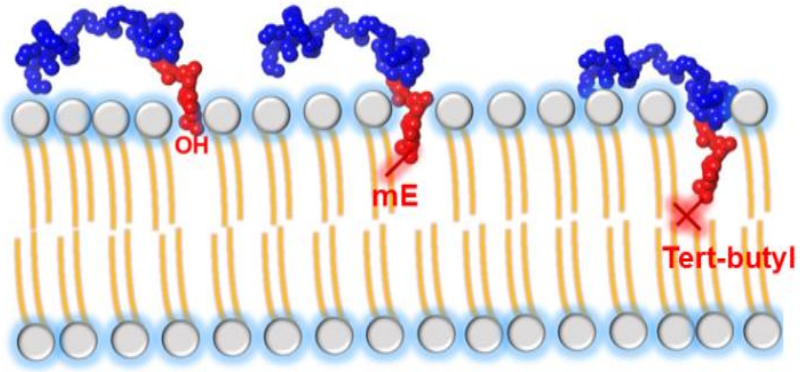

Figure 8: Schematic of triblock vs diblock copolymer interactions with a lipid bilayer. In this "anchor and chain" hypothesis, the t-butyl terminated end group on the hydrophobic PPO block (red) anchors the diblock copolymer within the hydrophobic region of the bilayer. The PEO block (blue) is the chain required to prevent further penetration and subsequent lysis of the bilayer.

Moreover, these results suggest that the length of the PEO block is not a critical factor beyond imparting enough hydrophilicity to the copolymer to maintain its

PPO/PEO ratio below a critical point above which complete insertion and membrane lysis would occur. In contrast, related studies demonstrated that the length of the PPO block determines the nature of copolymer association with the membrane[203,260], with longer PPO block inducing insertion into damaged lipid membranes at lower surface pressures[167]. This suggests that for effective membrane stabilization, the second PEO chain in the triblock architecture is redundant as long as a minimum PEO length is maintained to keep the molecule at the head group/acyl chains interface, and that the extra flanking PEO chain in the triblock architecture imposes steric constraints that weakens copolymer-bilayer interactions and increases water solubility of the PPO block[259]. This indicates that effective membrane stabilizing diblock copolymers can be synthesized with both smaller PPO and PEO block sizes, resulting in a smaller overall molecule.

We demonstrated in Chapter 2 that pharmacokinetics and pharmacodynamics of copolymers appear to vary depending on route of delivery, copolymer molecular weight, and PPO/PEO ratio. In this study, we chose to deliver the diblock copolymers using intraperitoneal delivery due to observed protective effects of all the tested tert-butoxy diblocks via this route. Keeping the delivery and dosage constant, the role of the PPO end group could be teased apart independently of delivery. Nonetheless, it is unclear whether varying delivery routes would influence the results obtained and further work is under consideration to reconcile pharmacokinetics/dynamics to copolymer structure and composition.

3.5 Perspective

Very little is known in the copolymer based membrane stabilization literature beyond studies of commercially available PEO-PPO-PEO triblocks. We demonstrate here for the first time the efficacy of a diblock architecture in stabilizing injured biological

membranes. The diblock architecture offers several advantages, including an easier and more controlled chemical synthetic process allowing to more precisely control PPO and PEO block sizes, as well as the ability to substitute various functional end groups to the hydrophobic PPO core for membrane interaction. This latter benefit allows for sensitive manipulation of the diblock PPO block hydrophobicity for optimal membrane interaction and stabilization. In addition, substitution of a PPO block with other chemistries could be considered, such as a relatively more hydrophobic polybutylene oxide block (PBO). These exciting proof-of-principle results establish physiological relevance to diblock copolymers and support further investigation of the copolymer chemical space.

3.6 Methods

*Animal*s**.** Adult male and female *mdx* mice (C57Bl/10ScSn-DMD*mdx*) and wildtype *BL/10* mice (C57Bl/10ScSn) aged 2-8 months old were obtained from Jackson Labs (Bar Harbor, ME) and housed locally. The procedures used in this study were approved by the University of Minnesota's Institutional Animal Care and Use Committee (IACUC).

Ventricular rat cardiomyocytes isolation.
Adult rat ventricular myocyte isolation was performed as previously described[262,263]. Briefly, adult female rats were anaesthetized by inhalation of isoflurane followed by i.p. injection of heparin (1500 U/kg) and Nembutal (162.5 U/kg). Following enzymatic digestion by retro-grade perfusion with collagenase and gentle trituration of the cardiac ventricles, cardiac myocytes were plated on laminin-coated glass coverslips ($2x10^4$ myocytes/coverslip) and cultured in M199 media (Sigma, supplemented with 10 mmol/L glutathione, 26.2 mmol/L sodium bicarbonate, 0.02% bovine serum albumin, and 50 U/ml penicillin-streptomycin, with pH adjusted to 7.4, additionally insulin (5μg/ml),

transferrin (5μg/ml) and selenite (5ng/ml) (ITS) were added (Sigma I1884)). Myofibers were used within 24 hours of isolation.

Myoblast cell culture

Mouse muscle myoblasts (C2C12; American Type Culture Collection, Manassas, VA) were grown in cell growth media consisting of high glucose DMEM (Gibco Invitrogen, Grand Island, NY), 20% fetal bovine serum (Gibco Invitrogen, Grand Island, NY) and 1% Penicillin/Streptomycin (Gibco Invitrogen, Grand Island, NY) at 37^{o}C humidified atmosphere of 5% CO_2. At 70% confluency, cells were split in order to prevent partial differentiation due to cell-cell contact. The cell culture media was replaced every two days.

Block Copolymers.

National Formulary grade of Poloxamer 188 was generously provided by BASF (Pluronic F68, Wyandotte, MI),and its diblock analog (Di-80%) was purchased from Polymer Source (P1862-EOPO, Montreal, Quebec). PEO-8k was purchased from Sigma, St.Louis, MO).

Diblock copolymer synthesis. Synthetic methods for PEO-PPO diblocks using sequential anionic polymerization are well established (refs). In brief, PPO was first initiated and propagated using tert-butoxide (from potassium tert-butoxide) as the reaction initiator (**scheme 1**). The use of 18-crown-6 ether to complex with potassium counter ions resulting from the tert-butoxide initiation has been shown to be a catalyst for the propagation step of PPO thereby limiting the polydispersity of the resulting copolymer (refs). Following a purification and characterization step, the polyethylene oxide chain was grown from the propylene oxide block by living anionic polymerization of ethylene oxide after reinitiating the monohydroxyl terminated PPO starting block with potassium naphthalenide. The reaction was then terminated with excess acidic methanol solution

and the resulting diblock copolymer recovered by solvent removal. Following filtration, dialysis and drying, the resulting purified copolymers were characterized and confirmed by size exclusion chromatography and H^1 NMR.

*Polymer Characterization***.** Polymers were characterized by size exclusion chromatography (SEC, Waters) equipped with a refractive index detector and tetrahydrofuran as the solvent to determine dispersity (Đ), and 1H NMR (Bruker AV-500 in deuterated chloroform, CDCl3) was used to determine block compositions.

Hypo-osmotic stress assay. Rat cardiomyocytes were transferred from M199 culture media to a 310 mOsm isotonic solution (in mM: 140 NaCl, 5 KCl, 2.5 $CaCl_2$, 2 $MgCl_2$, and 10 HEPES; pH 7.2) in the absence or presence of 150 uM copolymer. After a 3 min of pretreatment equilibration with the polymer, cardiomyocytes were subjected to hypo-osmotic stress for 90 seconds by exchanging in a 170 mOsm solution (composition equivalent to 310 mOsm solution but with NaCl reduced) +/- copolymer. The cardiomyocytes were subsequently re-equilibrated in an isotonic solution +/- copolymer for a total of 7 min. The remaining cardiomyocytes were lysed with 0.01% Triton X-100. For myoblasts screening, around 10^4 cells were inoculated into a 96 well plate and grown to cover enough well plate surface. When ready to use, the cells were transferred from the growth media to a 310 mOsm isotonic buffer +/- copolymer. After incubating for 30 min, the cells were subjected to hypo-osmotic stress by exchanging the isotonic buffer to 133.5 mOsm hypotonic buffer +/- copolymer for 50 min. The cells were subsequently re-equilibrated in an isotonic buffer +/- copolymer for 30 min. Finally, the cells were lysed with 0.01% Triton X-100. In every buffer exchange step, the buffer pulled out of the well was collected and stored at 4 ^oC before being used for enzyme release assay.

Enzyme release assays. Lactate Dehydrogenase (LDH) release was assessed at the end of the hypo-osmotic stress protocol. LDH release was assayed using a kit from Pointe Scientific (Canton, MI).

Block copolymer treatment and delivery for in vivo injury protocol. Block copolymers were dissolved in sterile saline to final stock solutions of 150 mg/ml. At least 30 min before the start of the *in vivo* injury protocol, mice received specific dosages of Poloxamer or equivalent saline volume intraperitoneally (IP) or subcutaneously (subQ - beneath the scruff on the back of the neck).

In vivo lengthening contraction force loss protocol. In vivo force measurements of the anterior crural muscle compartment (tibialis anterior, extensor digitorum longus and extensor hallucis longus) were performed as described previously [102,237]. Mice were anesthetized with a combination of fentanyl citrate (0.2mg/kg), droperidol (10mg/kg) and diazepam (5 mg/kg) and the left hindlimb was depilated. The left foot was then secured to an aluminum foot-plate coupled to a servomotor (Model 300B-LR;Aurora Scientific, Aurora, Ontario, Canada). Contractions were induced via stimulation of the peroneal nerve via percutaneously inserted Pt-Ir electrode wires (Model E2-12; Grass Technologies, West Warwick, RI, USA) connected to a stimulator and stimulus isolation unit (Models S48 and SIU5, Grass Technologies). This system allows for a non-invasive evaluation of skeletal muscle contractile properties *in vivo* [224]. An initial pre-injury maximal isometric force was determined (250 Hz and 150 ms duration), followed by an injury protocol consisting of 50 lengthening contractions. For the lengthening contractions, the foot underwent 19 degrees passive dorsiflexion at which a pre-lengthening 100 ms isometric contraction was initiated followed by another 50 ms of stimulation as the foot was actively moved to 19 degrees of plantarflexion (for a total ankle rotation of 38 degrees). Each lengthening contraction was separated by 10 seconds to prevent fatigue. Maximal force was measured for each lengthening contraction during

the course of the injury protocol and presented initialized to the first lengthening contraction force. A final isometric force was measured at the end of the lengthening protocol. $n \geq 5$ mice (both males and females) for each treatment group of each experiment.

Statistics. All results are expressed as mean ± SEM. Multi-group comparisons for *in vitro* LDH release experiments were assessed using one way analysis of variance (ANOVA) with Tukey post-hoc test and $P < 0.05$ considered statistically different. A two-way ANOVA followed by a Bonferroni-post hoc test was used to assess the effect of lengthening contraction numbers and treatment routes across the 50 contractions protocol with $P < 0.05$ considered statistically different. All statistical analysis was carried out using Prism (GraphPad Software).

CHAPTER 4

ALL-ATOMISTIC MOLECULAR DYNAMICS INVESTIGATION OF BLOCK COPOLYMER-LIPID MEMBRANE INTERACTIONS

Evelyne M Houang[1], Yuk Y Sham[2] and Joseph M Metzger[1].

[1]Integrative Biology and Physiology, University of Minnesota, United States; [2]Center for Drug Design, Academic Health Center, University of Minnesota, United States.

Manuscript in preparation

4.1 Introduction

The investigation of the triblock copolymer poloxamers has generated significant attention as they have been demonstrated to be of use in a broad range of biomedical applications, including as biological membrane interacting molecules[166,169,201]. Poloxamers are a class of amphiphilic triblock copolymers composed of a polyethylene oxide (PPO) core flanked on both sides by linear chains of polyethylene oxide (PEO). Poloxamers have been designed with specific modifications in overall molecular weight and in the relative PPO/PEO ratio. These two parameters are hypothesized to be critical elements underlying how copolymers modulate membrane interactions, as well as affecting poloxamer solubility[167,209]. These features make poloxamers highly customizable for specific industrial uses or for potential biomedical applications.

Poloxamer 188 (P188) is of particular biomedical interest as a membrane stabilizer.P188 has been found beneficial in an extensive range of clinical conditions of membrane injury, including electrical shock[191], irradiation[182,183], thermal burns[181], and other diseases that affect cell membrane integrity[264,176,193,257,265,266]. Of particular interest to us, we have established in Chapter 2 and 3 that P188 acts as membrane stabilizer in the context of muscle membrane mechanical disruptions such as in Duchenne muscular dystrophy[37,187,195,234,258].

Biological membranes function as the boundary between the cellular cytoplasm and the cell's extracellular environment to maintain cellular homeostasis. The membrane to extracellular fluid interface plays an important role in many biological and pharmacological phenomena. Membrane bilayers are composed of amphiphilic lipid molecules held together via hydrophobic bonds between their acyl chains and hydrophilic interactions between their head groups. These relatively weak intermolecular interactions influence the fluidity and packing of the whole membrane.

When considering a triblock copolymer such as P188 interacting at the membrane interface, there are three types of copolymer/lipid interactions: 1) interaction of the

copolymer with the lipid head groups; 2) interaction with the hydrophobic alkyl chains; or 3) interactions with both head groups and acyl chains. The latter two types of interactions require the copolymer to penetrate past the head group region to access the hydrophobic region of the bilayer. In addition, the copolymer hydrophobic and hydrophilic chains can interact with themselves considering the relatively hydrophobic PPO core would in theory minimize its own solvent accessible area.

Despite previous investigations on poloxamers, and specifically their interactions with lipid membranes, it remains unclear what is the mechanism of interaction and the driving force behind these interactions. Studies using lipid monolayers spread on a Langmuir trough demonstrate that copolymers insert into areas of low lipid density at low surface pressures and disorders the lipid packing[201,202]. Another study found that adsorption of copolymers to liposome-based lipid bilayers induce considerable disordering of the lipid packing and enhanced membrane permeability[164] whereas another study posited that insertion and not adsorption disorders lipid packing[212].

More recent studies demonstrate that copolymer interaction with a lipid bilayer involves initial adsorption at the polar head group level, followed by insertion inside the bilayer[170,210,212], and that insertion is dependent on temperature, copolymer solubility, and PPO block length[209]. Moreover, several studies provide evidence that adsorption of the copolymer does not affect lipid diffusion, whereas insertion hinders lipid diffusion[209] and increases lipid packing[210]. These inconsistencies likely arise from experimental studies employing different models of lipid membranes (monolayers[202], bilayers[267] or unilamellar vesicles[169]) and different experimental methods of measurement (Langmuir isotherms[201,202], X-ray scattering[168] methods, isothermal calorimetric measurements[210], and fluorescence microscopy[169,201]).

Understanding the fundamental interactions of block copolymers with the biological membrane interface has critical implications in designing and optimizing membrane stabilizing copolymers structure. In this regard, molecular dynamics (MD)

simulations have been well established as a method of choice to probe both location and dynamics of membrane active molecules such as small molecule drugs[268] and fluorophores[269] that cannot readily be observed with experimental techniques.

As of today, there are few reports detailing molecular dynamic simulations to study poloxamer-membrane interactions[167,208,226,227]. Growing efforts directed to the computational study of copolymer-lipid interactions have mostly applied Monte Carlo and coarse-grained molecular dynamics. These allow for larger timescale simulation, but give only a partial and representative view of the membrane structural properties with loss of atomic resolution information, reduced number of degrees of freedom, and inaccuracy in describing the subtle dynamics of the system. Other studies using all-atomistic resolution simulations have so far only investigated small and highly hydrophobic triblock copolymers[208].

Here we use all-atomistic MD simulations to provide new molecular insights into how membrane stabilizing copolymers, principally P188, interact with the membrane bilayer in the context of increased membrane permeability. All-atomistic MD simulations are superior to coarse-grained models as they give atomistic level resolution and more detailed mechanistic insight. We use here a 1,2-dipalmitoyl-sn-glycero-3-phosphocholine (DPPC) bilayer as a model lipid bilayer as it is one of the most extensively studied phospholipids, both experimentally[168,201,261] and computationally[270–273]. Model synthetic membranes lack the typical structural complexity of native membranes, as they do not precisely replicate all aspects of a living biological cell membrane. Nonetheless, they have been demonstrated and recognized as an invaluable tool for understanding molecular-level biophysical interactions of polymer-lipid bilayer systems.

We evaluated in a first system, the effect of lipid bilayer surface tension changes on P188-bilayer interactions. The rationale for using increases in surface tension to induce altered membrane fluidity/permeability is based on a study using coarse-grained MD to simulate the effects of surface tension on the structure and properties of the DPPC bilayer by evaluating its area-per-lipid, lipid-order parameters, membrane thickness, and

lipid-molecule planar diffusion[274]. In that study, an increase in the applied surface tension of the bilayer resulted in a significant increase in the area-per-lipid, and therefore an increased fluidity of the bilayer, as well as increased lipid lateral diffusion and decreased lipid-tail order. Similar results showing the effect of increasing surface tension on the bilayer area-per-lipid have been demonstrated before[272,275]. Further underscoring the role of membrane tension in lipid bilayer integrity, P188 has been demonstrated to significantly lower apparent membrane tension and aid restore membrane resealing in tetanus toxin-treated cells[84]. As P188 is presumed to only associate with damaged membranes[168,201,202], we hypothesize that increased membrane permeability via increased surface tension will lead to increase P188-bilayer interaction.

Additionally, hydrophilic pore formation and DPPC membrane rupture have been observed to occur under mechanical stress, as reported in an atomic level MD simulation study where systematic variation of the bilayer lateral pressure was exerted[276].Hydrophilic pore formation also occurs when a strong transmembrane voltage is applied to the membrane, as happens during electrical trauma[277], leading to loss of intracellular homeostasis and eventual cell death. As P188 has been shown in numerous studies to prevent the transmembrane passage of enzymes[258] and various extracellular dyes and large molecules by sealing the porated membrane[165,37,181] , we simulated in a second system the interaction of P188 with a bilayer containing a hydrophilic pore to evaluate P188's ability to prevent water molecules to translocate through the membrane.

4.2 Systems setup

System 1: Constant surface tension (NPγT ensemble) simulations.

A single P188 molecule was simulated atop a lipid bilayer containing 280 lipids (140 per leaflet) DPPC lipids (**Figure 1**) with the system solvated with TIP3P to explicitly simulate water molecules The final unit cell size for the copolymer/DPPC bilayer system was 96 x 92 x 70 angstroms, for a total of 55911 atoms, from which 6028 were TIP3P water molecules and 17 molecules each of Na^+ and Cl^- to neutralize the system. Due to the use of periodic boundary conditions and current all-atom membrane potential models not being able to maintain appropriate surface areas on long time scales in simulations of pure membranes, a baseline surface tension of ~2000-3000 bar/Å is recommended for DPPC bilayers to retain normal bilayer structure[275,278]. Surface tension (γ) was held constant at 1000, 2000, 3000, 3250 and 3500 bar/Å to simulate the surface tension ranges that would induce bilayer compression (< 2500 bar/Å) or lengthening (> 2500 bar/Å).

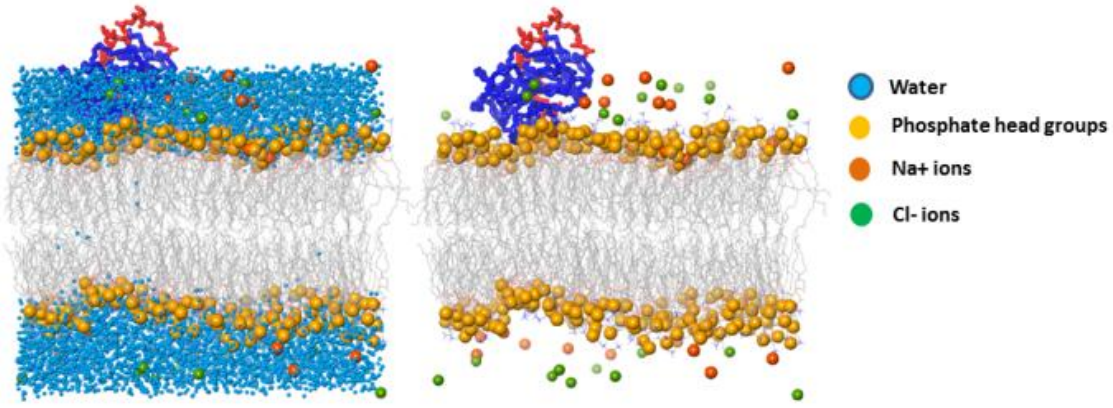

Figure 1: Setup of P188-DPPC bilayer system with P188 initial starting position atop the bilayer. (Right) Water molecules and salt ions are not shown for clarity.

The temperature was maintained at 310K and 1 atm. In terms of simulations timescale for model lipid bilayers, it was determined that long simulation times (larger than 50 ns) are necessary to distinguish differences in surfaces tensions or equilibrium areas and proper sampling of membrane undulations[279]. Simulations for each system were therefore run for 150 ns to ensure convergence or until the system became unstable due to bilayer collapse.

System 2: Simulations of P188 – DPPC lipid bilayer with and without pore induction (NPAT ensemble).

A system of P188-DPPC bilayer was generated for simulation at NPAT (constant pressure, area and temperature) conditions. The NPAT ensemble is required to prevent spontaneous bilayer resealing and to maintain the hydrophilic pore over the course of the entire simulation. A DPPC bilayer constituted of 280 lipids (140 per leaflet) was generated and a single molecule of P188 was placed atop the bilayer. The system was solvated with 7774 TIP3 molecules and neutralized with 22 Na and Cl ions, for a total of 61159 atoms. For the hydrophilic pore containing bilayer, the system generated above was used and 21 individual lipid molecules were deleted using Schrodinger Maestro software to create a pore of diameter ~20 Å (**Figure 2**). The system was solvated with 8533 TIP3 molecules and neutralized with 24 Na and Cl ions, molecules with a final unit cell size for the copolymer/DPPC bilayer system of 92 x 90 x 70 angstroms for a total of 60710 atoms. Both systems were run for 75 ns at temperature of 310K.

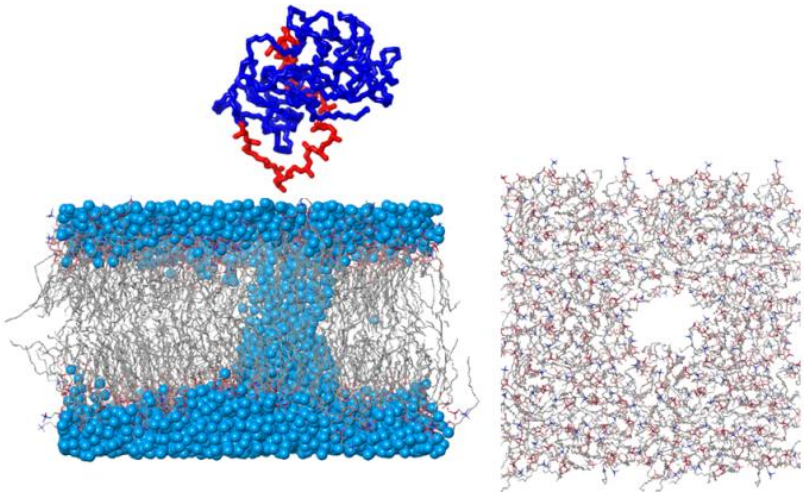

Figure 2: Setup of P188-DPPC bilayer with a pore system with (**left**) P188 initial position atop the bilayer and water molecules colored in blue, and (**right**) top view of the pore containing bilayer with water molecules not shown for clarity. The pore diameter is ~20 Å. NPAT conditions were used to maintain the pore over the course of the simulation.

4.3 Results

System 1: Surface tension of the lipid bilayer dictates adsorption or insertion of P188

The objective of this system was to obtain atomistic-level mechanistic insights on how surface tension affects P188-DPPC bilayer interactions. We first examined the effects of surface tension on the structure and property of the DPPC bilayer by observing the area-per-lipid perturbations induced by step-wise modification of surface tension (γ). The area-per-lipid reflects the density of lipid molecules in each leaflet of the bilayer and is an important parameter to validate simulations against experimentally measured values. Here, we used the Visual Molecular Dynamics (VMD) plugin MEMPLUGIN[280] to compute the area per lipid over the course of each simulation at various surface tensions (γ) (**Figure 3**). In each case, the initial starting area per lipid was ~58 $Å^2$, which is in agreement with values reported in previous studies of DPPC bilayers[274,279].

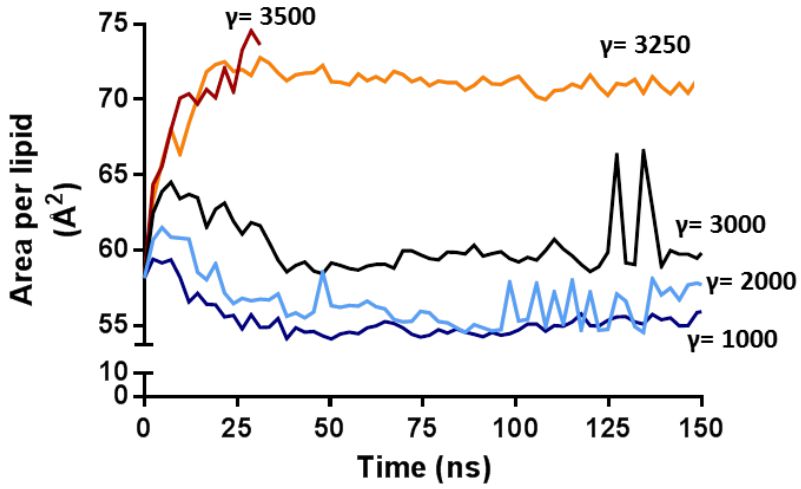

Figure 3: Area per lipid of DPPC bilayers at various surface tensions (γ). The simulation run at γ = 3250 (red) became unstable and crashed at 34 ns.

(γ) (bar/Å)	**Area per lipid +/- S.D. (Å²)**
1000	54.94 ± 0.48
2000	56.05 ± 1.15
3000	59.90 ± 1.62
3250	70.99 ± 0.45

Table 1: Mean area per lipid over the last 100 ns of simulation at various surface tensions (γ).

For each surface tension, the mean area-per-lipid of each simulation is summarized in **Table 1**. These values are comparable to those reported in previous studies[272,274,275]. As expected, an increase in γ above 2000 bar/Å led to an increase in the area-per-lipid of the bilayer, i.e., increased fluidity and permeability of the bilayer. Simulations run at γ= 3500 bar/Å and above became unstable within the first 40 ns and could not be continued. These results suggest that there is a critical area per lipid value

(~74 $Å^2$) at which the DPPC bilayer starts to collapse. On the other hand, a γ value below 2000 bar/Å induces bilayer compression and decreases bilayer fluidity.

Next, we examined whether the DPPC bilayer's surface tension influenced P188 interaction. For both the γ = 3250 (**Figure 4**) and γ = 3500 (data not shown) simulations, the bilayer lengthened in the x-y phase (as shown by an increase in area per lipid) and visual inspection shows that bilayer thickness (z) also decreases with increasing area per lipid, indicating increased membrane fluidity. Both the PPO core and the PEO chains of P188 start inserting within the first 40 ns of both simulations, with the full copolymer residing in the hydrophobic part of the bilayer by 33 ns at γ = 3500 (prior to membrane collapse) and 70 ns at γ = 3250.

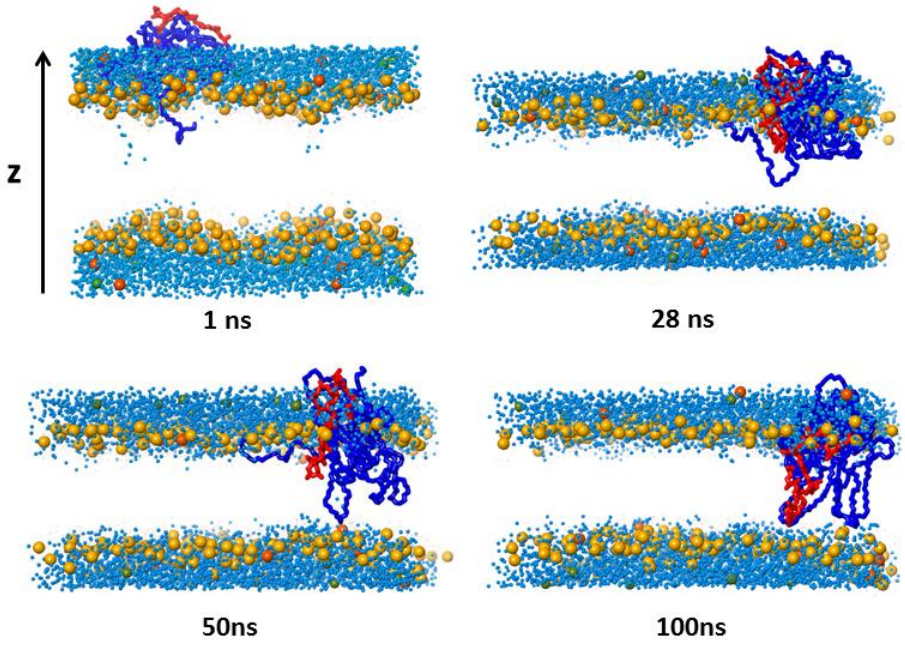

Figure 4: Snapshots taken over the course of the P188-DPPC simulation run at γ = 3250 showing insertion of P188 starting at ~40 ns as well as increased area per lipid (x*y) and decreased bilayer thickness (z). The PPO core is colored red and the PEO chains are colored in blue. Lipid tails are not shown for clarity.

On the other hand, at $\gamma = 3000$, the lipid bilayer dimensions do not change significantly and it takes a longer time for P188 to start inserting. Initially, only one of the PEO chains inserts and PPO core interaction initial interaction and insertion doesn't start until ~55 ns. The full copolymer does not insert until ~80 ns (**Figure 5**).

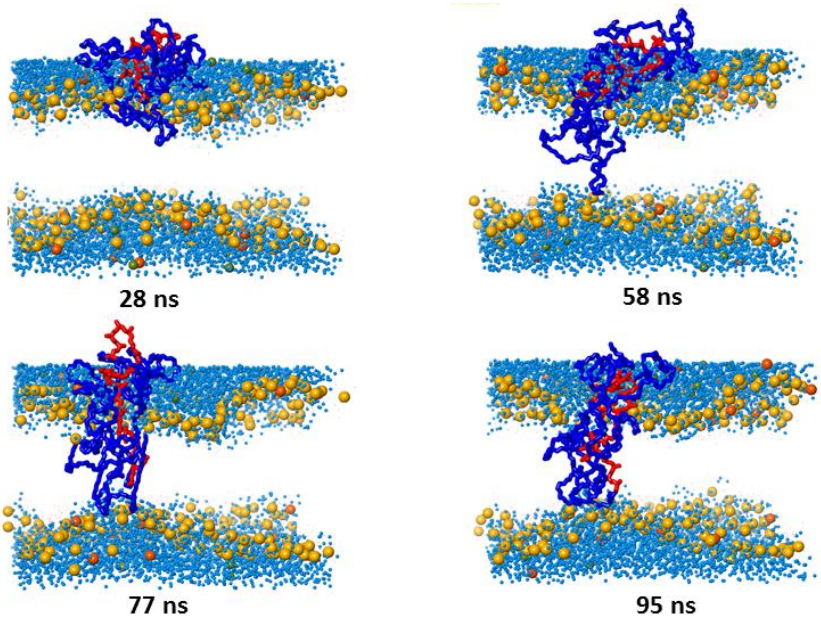

Figure 5: Snapshots taken over the course of the P188-DPPC simulation run at $\gamma = 3000$ showing beginning of insertion of P188 at ~58 ns as well as increased area per lipid and decreased bilayer thickness. The PPO core is colored red while the PEO chains are colored in blue. Lipid tails are not shown for clarity.

In contrast, at $\gamma = 2000$, the lipid bilayer compresses slightly over time in accord with the observed decreased in area per lipid and increased bilayer thickness (**Figure 6**). While part of the PEO chain inserts over the course of the simulation, the rest of the P188 molecule remains at the water-bilayer interface at $\gamma = 2000$. This suggests that the fluidity and permeability of the bilayer is too low and presents a steric barrier to copolymer insertion. This is further demonstrated at $\gamma = 1000$ where the bilayer is even further

compressed, keeping PEO interaction at the lipid head group level and preventing further interaction with the acyl chains of the bilayer (**Figure 7**).

Taken together, these simulations show that the surface tension and its effect on the lipid packing of the bilayer is an important factor to P188 adsorption and/or depth of insertion within the membrane bilayer. Moreover, these data indicate that there is a minimum area-per-lipid at which P188 insertion occurs. This aligns well with the conclusion of a previous study using lipid monolayers in the Langmuir trough whereby P188 is "squeezed" out once membrane integrity and normal surface pressure are restored[201].

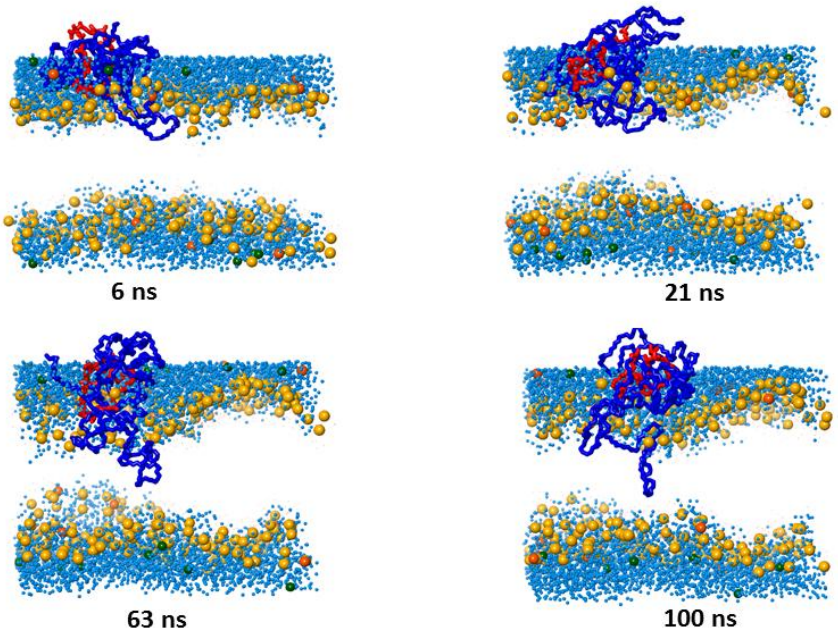

Figure 6: Snapshots taken over the course of the P188-DPPC simulation run at $\gamma = 2000$ showing insertion of the PEO chain and slight compression of the bilayer over time. P188 does not fully insert. The PPO core is colored red while the PEO chains are colored in blue. Lipid tails are not shown for clarity.

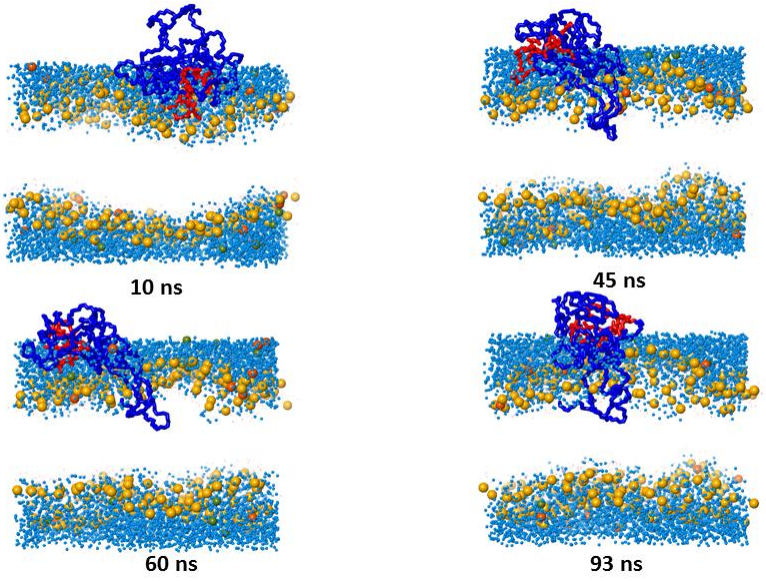

Figure 7: Snapshots taken over the course of the P188-DPPC simulation run at $\gamma = 1000$ showing slight insertion of the PEO chain and compression of the bilayer over time. P188 does not fully insert. The PPO core is colored red while the PEO chains are colored in blue. Lipid tails are not shown for clarity.

Interestingly, and in contrast to what has been previously reported in molecular dynamics simulations of copolymers and bilayers[227,281], the PEO chains do insert into the hydrophobic acyl chain region of the bilayer along with the PPO core. This is not surprising as PEO is not purely hydrophilic and is itself considered an amphiphiles[282].

System 2:

In this system, the P188-DPPC bilayer was run at NPAT (constant pressure, area and temperature) without and with a hydrophilic pore to investigate P188 interactions with a healthy bilayer and one that is damaged and leaky.

In the first scenario, P188's PEO chains intermittently make contacts with the polar lipid head groups of the DPPC bilayer but do not insert. The P188 copolymer remains in close proximity at the water-lipid interface, with its PPO core consistently

shielded from the solvent by its flanking PEO chains (**Figure 8**). This latter shape is in contradiction with coarse-grained models depicting free flowing and seemingly solvated PPO and PEO chains[274,281].

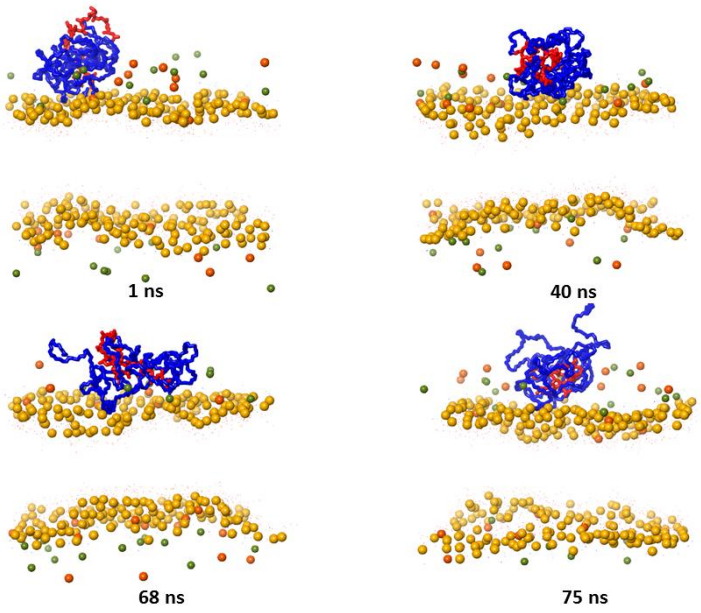

Figure 8: Snapshots of P188-DPPC bilayer simulation run at NPAT conditions without a pore. The PPO core is colored red while the PEO chains are colored in blue. Water and lipid tails are not shown for clarity.

However, in the presence of a ~20 Å pore through the DPPC bilayer, P188 inserts into the hydrophilic pore at approximately 35 ns into the simulation run (**Figure 9**). Once again as observed in System 1, the PEO chains, not the PPO core, initially inserts into the pore before insertion of the entire copolymer. The initial insertion of the PEO chain into a water filled pore makes sense considering the hydrophobicity of the PPO core. We hypothesize that the PEO insertion is a "priming" step to allow the hydrophobic PPO to remain unexposed to the aqueous solvent before and during insertion into the bilayer. In addition to inserting into the lipid bilayer, P188 prevents water molecules from translocating through the pore (**Figure 10**) thereby effectively acting as a membrane sealant.

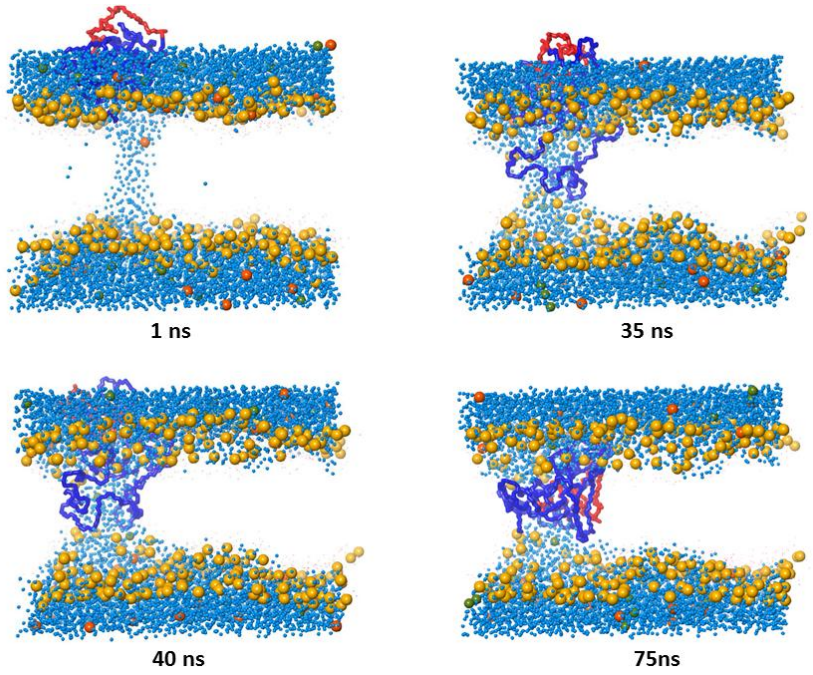

Figure 9: Snapshots of P188-DPPC bilayer simulation run at NPAT conditions in the presence of a pore. The PPO core is colored red while the PEO chains are colored in blue.

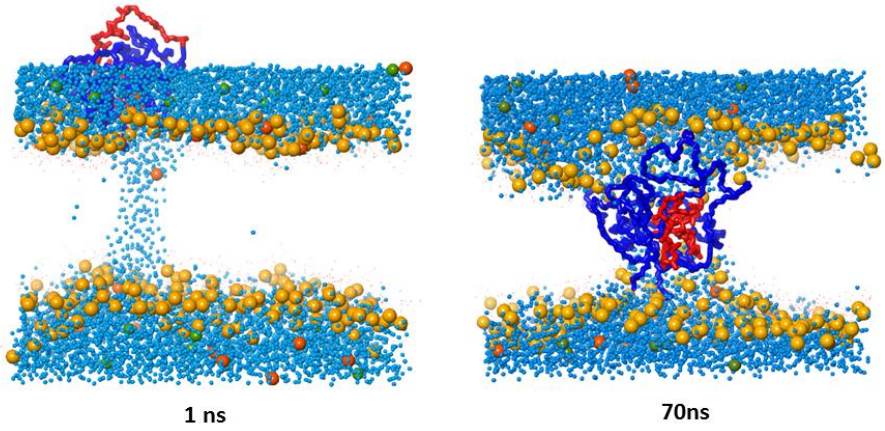

Figure 10: Snapshots of P188-DPPC bilayer simulation run at NPAT conditions in the presence of a pore. Water molecules are shown in light blue. The PPO core is colored red while the PEO chains are colored in blue.

4.4 Discussion

This study is, to our knowledge, the first all-atomistic MD simulation investigation of P188-bilayer mechanism of interaction. Our main new findings show that P188 adsorption at the lipid-head group region, compared to insertion inside the hydrophobic tail region of the bilayer, depends on the area-per-lipid, i.e. the permeability, of the membrane. Increases in the area-per-lipid via increases in applied surface tension, or induction of a hydrophilic pore, lead to an increased rate of insertion of P188. In contrast, reduction of area -per -lipid prevents P188 insertion, with the closely packed lipids maintaining P188 in an adsorption state. Moreover, we observed that the generally considered "hydrophilic" PEO chain, also inserts at high membrane permeability, in contrast to earlier studies reporting that the flanking PEO chains remain at the lipid head group level[227,281].

Experimental biophysically-based studies examining P188 interactions with synthetic lipid membranes propose a two-state mechanism of block copolymer interaction: initial adsorption followed by insertion into the lipid membrane[169]. Our simulations show that adsorption vs. insertion is dependent on the integrity of the membrane, with area-per-lipid affecting the rate at which P188 inserts into the bilayer, rather than adsorb at the head-group region.

Increases in surface tension of the DPPC bilayer induces changes in the structural properties of the bilayer, such as increases in its area per lipid and lateral diffusion coefficients of its lipid molecules, and decreases in lipid order parameter and thickness of the bilayer[274]. Altogether, these changes increase the fluidity and permeability of the bilayer. We therefore used an increase applied surface tension on a DPPC bilayer as a molecular mimic of membrane stretching and damage. Our study was based in part on seminal biophysical studies that demonstrated using synthetic lipid monolayers that P188 and other membrane stabilizing copolymers insert into injured regions of membranes

when surface pressure is reduced and gets "squeezed-out" when membrane integrity is restored[201,202].

At optimal surface tension γ (in the case of a DPPC bilayer simulated using Desmond force field parameters, optimal γ = ~2000 bar/Å), the membrane is in a state in which attractive interactions between its lipids hydrocarbon chains and the repulsive interactions between their head groups are in balance, resulting in optimal lipid packing density and a free energy minimum with respect to its surface area[283]. As observed in our results, while the PEO chains of P188 make contact and interact with the lipid head groups of the bilayer and even insert into the hydrophobic region of the bilayer, the PPO core is sterically hindered from entering the bilayer

However, as γ deviates from this optimal value, the bilayer will either shrink or expand, altering the structural properties of the bilayer in response[272,274]. As expected, further compression of the bilayer at γ = 1000 prevents further PEO insertion into the bilayer, limiting its interaction at the polar head group level. In contrast, expansion of the bilayer at γ = 3000 or above leads to spreading of the lipids and eventual insertion of P188, with the time of insertion occurring earlier at higher γ. These results underscore the dependence of copolymer insertion on area per lipid, with increased area per lipid of the bilayer lowering the penetration barrier. This is further demonstrated in system 2 when comparing a healthy membrane run with its area kept constant using the NPAT ensemble to a membrane with a hydrophilic pore. While the PEO chains of P188 make contacts with the head group region of the healthy lipid bilayer, insertion does not occur in the timeframe of the simulation. In contrast, presence of a pore drives the copolymer to insert and block translocation of water molecules from one side of the bilayer to the other, effectively sealing the bilayer pore.

Our findings that the PEO chains insert along with the PPO core at increased area per-lipid-are in apparent contradiction with previously reported coarse-grained reports of copolymer-bilayer interactions showing that only the PPO core is capable of inserting into the bilayer, with the PEO chains being restrained to the head-group region at the

membrane-water interface[227,281]. However, insertion of PEO into the bilayers should not be surprising as PEO also possesses some hydrophobic character[284]. At high degree of hydration in an aqueous environment such as outside the membrane, PEO is highly hydrophilic. However, at a low degree of hydration such as in the hydrophobic region of the bilayer, PEO becomes relatively more hydrophobic[284]. This has been further demonstrated in a an experimental and computational study showing that addition of NaCl, which is present in our system at physiological concentration, decreases PEO block solubility in aqueous solution[285]. Moreover, a previous study has found that at a lower lipid order, PEO chains can enter the hydrophobic region of a bilayer, whereas they are excluded in higher-order phases[286]. Spontaneous entry of pure PEO into the hydrophobic region of a DMPC bilayer after overcoming the outer leaflet head-group region has also been demonstrated previously using atomistic MD simulations[208,226]. These studies concluded that PEOs interacting with the hydrophobic tails inside the bilayer is a consequence of strong Lennard-Jones interaction energy between the polymer and the tails, and this is also responsible for PEOs contrasting hydration behavior in aqueous media as compared to a hydrophobic environment.

We established in chapter 2 and 3 that along with P188, there are other PEO-PPO-PEO triblocks and PEO-PPO diblocks that interact with membranes in order to either stabilize or destabilize them. Studies using Langmuir isotherm and fluorescence microscopy experiments using a synthetic lipid monolayer spread at the air-water interface in the presence of injected poloxamers of varying architectures showed that a longer hydrophobic block caused the copolymer to be less soluble and in more polymer adsorbed to the interface[167] as well as in stronger penetration. Lateral compression of the monolayer squeezes out copolymers at different pressures depending on the interplay between both PEO:PPO ratio and total size of the copolymer, with lower PPO:PEO ratio and smaller polymer sizes resulting in lower squeeze-out pressure and thereby lower maintenance within the monolayer[167] Membrane insertion appears to be highly dependent on the PPO/PEO ratio of the block copolymer, with hydrophobic dominant poloxamers

(PPO/PEO > 1) capable of inserting and subsequently permeabilizing the cell membrane[167,169]. Another study has shown that copolymers that contain a PPO block length comparable to the bilayer thickness tends to percolate across the lipid bilayer while copolymers with a shorter PPO block length only partially insert into the membrane with the PEO blocks remaining in the solvent[281]. Using all-atomistic MD simulations and varying applied surface tension on the bilayer will allow for further probing of architectural and compositional differences in membrane stabilization efficacy, in particular, how substitution of terminal end groups on a diblock architecture affects its bilayer interaction.

Finally, the constituent of a biological bilayer affects its properties. Biological cell membranes are composed of a complex assortment of lipids and proteins distributed asymmetrically to the outer and inner leaflets. Furthermore, the lipid composition of the dystrophic muscle membrane differs from that of a healthy muscle membrane composition[248]. The goal of future MD studies will be to more closely mimic muscle membrane lipid compositions to determine how they affect copolymer interaction.

4.5 Perspectives

All-atomistic MD simulation is an extremely powerful tool providing molecular level insights into the mechanism of copolymer-bilayer interaction. Moreover, it allows for sensitive modulation of the architectural and compositional parameters of the copolymer, as well as biophysical parameters of the bilayer to mimic in vitro injury systems. Finally, computational simulations allow for relatively quick design and testing of copolymers-bilayer interaction to guide optimal membrane stabilization synthesis. With this approach we have obtained new insights into the fundamental basis of

copolymer-membrane interactions that are key to understanding the membrane stabilization function of poloxamers.

4.6 Methods

Software package and high performance computing. The Schrodinger modeling suite and the Desmond molecular dynamics simulation package were used for the modeling, simulation, and analysis. Each simulation was carried out using 400 or 600 parallel computing cores on the Mesabi supercomputer at the Minnesota Supercomputing Institute, a Hewlett-Packard high-performance supercomputer with a LINUX operating system that consists of 8,728 compute cores and 24 TB of random-access-memory.

Building copolymer systems*:* Using Maestro, the graphical user interface of the Schrodinger modeling suite package, each PEO and PPO subunits was built, duplicated, and linked to generate a P188 molecule (PEO_{75}-PPO_{30}-PEO_{75}). All subunits were numbered and colored by hydrophobicity (red) and hydrophilicity (blue). Each of the built copolymers was then energy minimized using the OPLS 2005 force field run by a truncated Newton algorithm for at least 10,000 steps to allow collapse of the built linear copolymer structure to its more globular-like representative conformation.

Building copolymer-phospholipid membrane systems*:* System Builder in Desmond was used to build the simulation box consisting of the energy-minimized copolymer placed atop a DPPC phospholipid bilayer membrane and solvated using TIP3 water molecules. To create a hydrophilic pore for System 2, individual phospholipid molecules were deleted to form a transmembrane pore of ~20Å diameter.

Setup of molecular dynamics simulations*:* Each simulation was carried out under constant temperature (310 K) and constant pressure of 1 atm at 2 fs timestep using the OPLS 2005 force field. Constant surface tension simulations were performed in the NPγT ensemble (constant pressure, constant surface tension and constant temperature). Simulations of the systems evaluating a membrane pore were run using the NPAT ensemble to maintain the pore and prevent collapse of the system. Simulations were carried out using a default initialization protocol included in the Desmond simulation package with gradual heating to the targeted temperature (*9*). A snapshot at every 1 ps, equivalent to 500 fs timesteps, was collected over the course of the simulation for analysis.

Analysis: The collapse or expansion of the copolymer was monitored by examining changes in area-per-lipid of the DPPC bilayer. Event Analysis module in Desmond was used to area-per-lipid for each simulation. Visual Molecular Dynamics (VMD) MEMBRANEPLUGIN tool was used for bilayer structural analysis[280].

CHAPTER 5
SUMMARY

The central objective of this work was to investigate the mechanisms of copolymer-based membrane stabilization to protect striated muscle membranes in the context of Duchenne Muscular Dystrophy (DMD) using a structure-function approach.

While there have been numerous studies investigating the use of synthetic triblock copolymers as membrane stabilizers for various pathophysiological conditions of cell membrane injury[165,287,179,264,184,175,288,185,289], there has, at the beginning of this project 5 years ago, only been a handful of studies looking at copolymer-based membrane stabilization in the context of DMD[37,187,188,194]. Most of these studies focused on treating the cardiomyopathy of the disease, leaving efficacy on the skeletal muscle pathology unclear. Additionally, these studies focused on the use of one particular copolymer, Poloxamer 188, which is only one of an exponentially large copolymer chemical landscape. This work highlights structure-function studies to fundamentally dissect, for the first time to my knowledge, how the mechanism of membrane interaction and stabilization is impacted by critical molecular properties of copolymers including architecture, composition and chemistry. As such, the overarching theme of this work aimed to investigate the optimization of membrane stabilizing copolymers for DMD using *in vitro*, *in vivo*, and *in silico* methods.

P188 is protective in the context of both DMD cardiomyopathy and skeletal pathology

Prior to this work, the effects of P188 on the DMD skeletal myopathy have been uncertain[187,194,189]. In **Chapter 2**: "Membrane-stabilizing copolymers confer marked protection to dystrophic skeletal muscle *in vivo"*, an *in vitro* membrane-injuring hypo-

osmotic stress assay was developed and optimized to screen for membrane stabilization efficacy of P188 and other triblock copolymers in dystrophic skeletal muscle cells. The results obtained using this assay establish that P188 is efficacious at preventing hypo-osmotic stress-induced enzyme release *in vitro* using a copolymer concentration that was demonstrated to be efficacious in stabilizing the membrane of *mdx* cardiomyocytes. Based on these results, I concluded that P188 can stabilize dystrophic skeletal muscle membranes and that the lack of *in vivo* efficacy observed in previous studies was not due to a differential effect of P188 on skeletal vs cardiac lipid membranes but rather due to the pharmacokinetics and pharmacodynamics of the molecule once injected *in vivo*.

For the first time, this work establishes that P188 efficacy in protecting against lengthening contraction-induced force loss is crucially dependent on route of delivery. Furthermore, a larger triblock copolymer of equivalent PPO/PEO composition also showed efficacy at lower dosage but also showed differential pharmacodynamics. This is another proof-of-principle result that copolymer-based membrane stabilizers can be optimized beyond the P188 structure.

Chapter 2 established proof-of-principle that membrane stabilizing copolymers protect dystrophic skeletal muscles *in vivo*. The long-term goal would be to incorporate these findings with recent studies of P188 preserving cardiac[37,187,188] and respiratory function[195] to ultimately guide potential clinical application to treat all striated muscles in DMD patients. Because P188 has already been administered for human use for other conditions, it has already passed extensive pharmacokinetics and ADME studies to validate clinical safety[176,198]. It will be critical to perform long-term studies in small and large animal models of DMD to establish the pharmacokinetics and optimal pharmacodynamics of P188 and assessing protection following both acute and chronic treatment.

A PEO-PPO diblock architecture is sufficient for membrane stabilization and PPO end group modification significantly affects *in vivo* efficacy

To my knowledge, no work has been performed to assess copolymer based membrane stabilization beyond the PEO-PPO-PEO triblock architecture. The work performed in **Chapter 3**:"Structure-function relationship of membrane stabilizing diblock copolymers" demonstrates for the first time that a PEO-PPO diblock architecture is sufficient in stabilizing injured biological membranes. This result is significant as a diblock architecture allows for easier exploration of the copolymer chemical landscape due to simpler synthesis process and, importantly, the ability to modify the terminal end group of the hydrophobic PPO core for optimized membrane insertion and anchoring.

This latter capability is substantial as it allows for fine-tuning of the PPO interaction at the membrane. As exciting proof-of-principle, substitution of a hydrophobic tert-butoxide group to the PPO block of two compositionally different PEO-PPO diblocks significantly improved their membrane stabilization efficacy *in vivo*. Based on these new findings we propose an "anchor and chain" model whereby the PPO block inserts into the hydrophobic alkyl tail region of the injured membrane and is stabilized or "anchored" there by its terminal tert-butoxide group. A PEO chain of sufficient length to maintain the diblock copolymer relatively hydrophilic is required to prevent complete insertion and permeabilization of the membrane.

The ability to modulate diblock copolymer-membrane interaction via chemical alteration of diblock molecular properties eases access to a vast chemical landscape to design optimized membrane stabilizers that can be first screened *in vitro* using the hypo-osmotic assay optimized in **Chapter 2**. Furthermore, substitution of the actual PPO block with other hydrophobic chemical moieties such as polybutylene oxide (PBO) is another avenue worth exploring in future studies. These are the focus of future studies.

Development of an all-atomistic Molecular Dynamics system to assess copolymer-bilayer interactions *in silico*

Significant advances in the field of computational modeling now allow for investigating complex biological systems at faster speeds and lowered computational cost. MD simulation methods have become a powerful array of tools to investigate the complex structural and dynamical behaviors of polymers and lipid membranes that are difficult to probe experimentally at a molecular level. **Chapter 4**: "All-atomistic Molecular Dynamics investigation of block copolymer-lipid membrane interactions" is the first demonstration of all-atomistic simulations for evaluation of P188-DPPC bilayer interactions. Using increases in surface tension applied to the lipid bilayer, an area-per-lipid dependence of adsorption vs. insertion was uncovered, supporting previous monolayer studies showing that P188 inserts into areas of decreased lipid density and gets "squeezed-out" once membrane integrity is restored[202]. Another new finding that resulted from this study is the observation that one or both PEO chains of the triblock initiate insertion of the copolymer. This is in contrast to previous computational studies and models using coarse-grained models that depict the PEO chains remaining at the lipid head group interface. This is not a surprising finding as PEO hydrophobicity is modulated by its hydration level, which likely differs inside the membrane compared to the bulk solvent[284,285]. This new observation suggests that the copolymer prefers to minimize its solvent accessible area, particularly to its more hydrophobic PPO group, by using its PEO chains to shield the PPO group from water. Testing this hypothesis by calculating the solvent accessible surface areas for the whole copolymer and its individual blocks is a focus of future work. Furthermore, other parameters can be obtained from MD simulations, such as lipid tail order, bilayer thickness, and radii of gyrations, which are key factors to fully understand copolymer, bilayer, and copolymer-bilayer behaviors.

In future studies, these newly developed computational approaches will allow to theoretically assess how copolymers of varying architecture, sizes, and chemical

compositions interact with a bilayer. This is extremely powerful as it allows to more intelligently guide design and synthesis of optimized copolymer molecules for in *vitro* and *in vivo* testing.

CHAPTER 6
THOUGHTS AND PRELIMINARY DATA FOR FUTURE DIRECTIONS

In addition to the corpus of work summarized above, as well as the potential future studies that can stem from each chapter of this thesis, several other endeavors have been started to further our understanding of copolymer membrane stabilizers as potential therapeutics. Some of the very preliminary results and thoughts obtained from these studies are summarized below.

6.1 Cardiac stress-test studies to screen copolymers for cardiac membrane stabilization

P188 has been well-established to be cardioprotective in the context of beta-adrenergic stress in dystrophy[37,187,234] and we demonstrated in **Chapter 2** that it is also protective in the context of skeletal muscle lengthening contraction injury. Because of the interplay between progression of DMD cardiomyopathy and the skeletal myopathy as a "pathophysiological load" on the heart, it is important to evaluate other candidate membrane stabilizers to validate their effectiveness in both cardiac and skeletal muscle. Moreover, due to the differential effects of delivery routes on pharmacodynamics *in vivo*, it is important to determine whether differential routes of delivery can target both the heart and skeletal muscles concurrently.

The efficacy of both intravenous and intraperitoneal delivery in protecting the dystrophic myocardium is known. On the other hand, neither of these delivery routes effectively targets the hind-limb skeletal muscles, which we demonstrated that subcutaneous delivery was optimal for. It was therefore important to determine whether or not subcutaneous delivery would also be as effective for the heart. To test that, we

used an isoproterenol stress in *mdx* mice receiving either saline or 460 mg/kg P188 subQ or IP (**Figure 1**). While the Kaplan-Meier statistics showed no significant difference between the saline and P188 groups over the course of the 60 hours protocol, results indicate that both IP and subQ delivery of P188 appear to be protective over the first 24 hours of the challenge in contrast to the saline treated mdx group which had over 40% mortality within that timeframe. This challenge protocol could be shortened in future studies for faster screening of other copolymer architectures, dosages, and delivery routes.

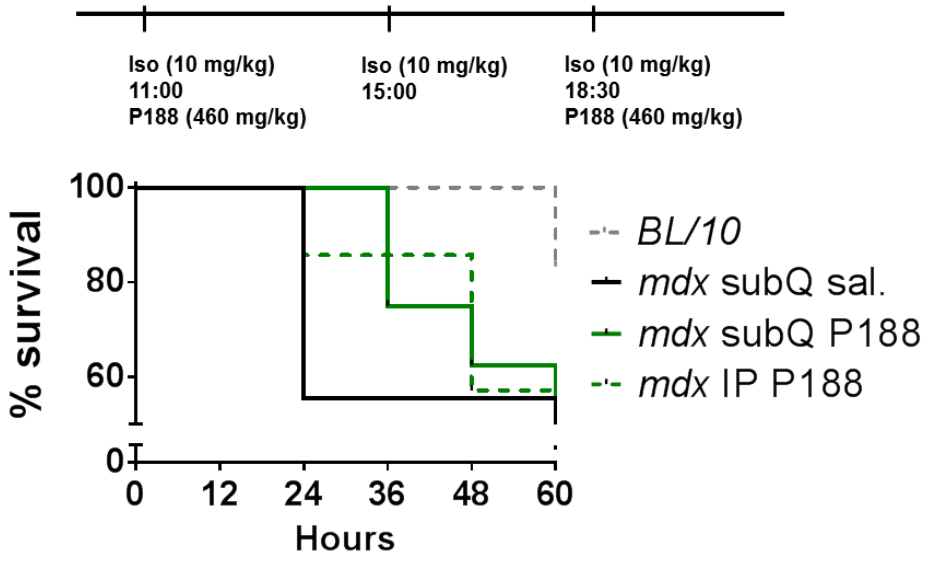

Figure 1: Survival study of mdx mice subjected to isoproterenol stress in the presence or absence of 460 mg/kg P188. *Mdx* mice were injected with 10 mg/kg isoproterenol IP 3x/day and simultaneous P188 treatment was given at the same time as the first and last isoproterenol injections of the day. BL/10 group served as control and were given saline IP. N = 7-8 mice per group.

It will be important in future studies to establish the cardiac efficacy of the tert-butoxide diblocks and other potential membrane stabilizing copolymers that are found to be protective in skeletal muscle to further probe whether routes of delivery *in vivo* would differentially target the heart and the limb muscles. The goal would be to optimize

membrane stabilizers that target both systems and that could be delivered chronically, such as via subcutaneous pumps that are commonly used clinically for diabetic patients.

6.2 Exploration of block lengths, overall hydrophobicity, and block moieties for membrane stabilization

We have demonstrated in **Chapters 2 and 3** that both triblock and diblock architectures can function as membrane stabilizers. As mentioned previously, the synthetic chemical landscape available is incredibly vast. Therefore, an intelligent approach toward structure-function screening needs to be undertaken to discover what the critical chemical parameters for membrane stabilization are. For example, triblock and diblock architectures have been investigated in this work. We determined in **Chapter 3** that a triblock architecture is not necessary for membrane stabilization. Moreover, we discovered that fine-tuning of the functional end group on the PPO block significantly altered membrane stabilization efficacy leading to an "anchor and chain" model of membrane stabilization. We hypothesize that this hydrophobic end-group anchors the copolymer inside the hydrophobic bilayer while the presence of the PEO chain prevents the copolymer from fully inserting through to potentially permeabilizing the membrane. As a focus of future studies, it will be important to determine how the hydrophobicity of this PPO end group and of the hydrophobic block overall affects membrane insertion. Perhaps this terminal end group could be further optimized by making it slightly more hydrophobic by extending it and/or adding extra methyl groups.

We and others have shown that PPO/PEO ratio is important in controlling stabilization vs. lysis of the membrane[164,208,258]. We also demonstrated that the 0.20 PPO/PEO ratio of P188 is not necessarily the "sweet spot" in membrane stabilization, as we observed protective effects of a diblock with 0.30 PPO/PEO ratio in **Chapter 3**. It will be important to determine the PPO/PEO ratio range that is needed for membrane

stabilization, as it will determine the ratio in blocks lengths when designing a copolymer. Furthermore, it is also necessary to determine if there is an optimal PPO block length for membrane stabilization. Synthesis and screening of diblock copolymers of varying PPO block lengths and associated PEO chain lengths to maintain the PPO/PEO ratio within membrane stabilization range could be an exciting and important future step in the structure-function study of diblock copolymers.

Beyond tuning PPO block lengths and functional end groups, it would be interesting to explore substituting the PPO block itself with a different hydrophobic moiety, such as polybutylene oxide. Other architectures, such as reversed triblocks (A-B-A and B-A-B) as well as sequential copolymers (A-B-A-B…) could also be explored. To do so, the hypo-osmotic stress assay used in this work needs to be optimized for higher throughput screening in 96 or more well plates.

6.3 Labeling of P188 for fluorescence imaging

While many biophysical and physiological studies have made P188 interaction at the membrane interface an accepted model, actual experimental observation using microscopy techniques is still lacking. Fluorescent labeling was chosen over alternative labeling strategies, such as radioactive and heavy metal labeling, due to easier handling and conjugation. The hydroxyl end groups on the PEO chains of the P188 are reactive groups that can be chemically substituted for functionality with fluorescent tags. Several different fluorescent labels have been considered so far. A Rhodamine-B derivative was first chosen as a lower-cost alternative for bulk volume infusions necessitated by large animal *in vivo* studies, ease of detection, and known synthetic method. Alternatively, the far-red fluorescent dye Alexa Fluor 647 was chosen as another test label due to its ease of conjugation and low membrane interaction factor[290].

Tagging of P188 with Rhodamine B

The Rhodamine B derivative synthesis and labeling with P188 was performed by Wenjia Zhang, a graduate student in Prof. Frank Bates in CEMS at the University of Minnesota. Briefly, Rhodamine B base (Sigma, St. Louis, MO) was transformed to Rhodamine B acide chloride and reacted with the hydroxyl-terminated PEO chains of P188 to yield RhB-P188 (**Figure 2**). A tagging efficiency of ~1.6 dye molecules per P188 was estimated using calibration curves at Rhodamine absorption wavelength of 556 nm.

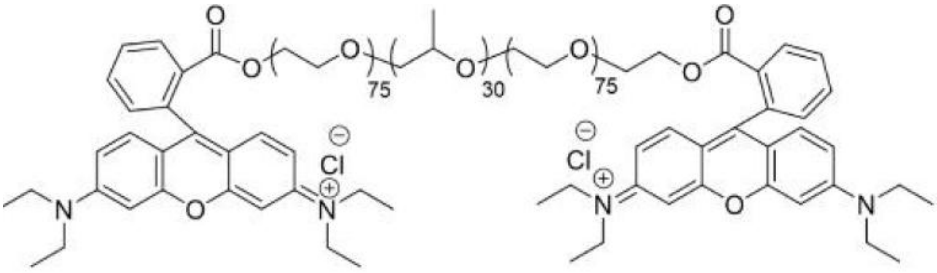

Figure 2: RhB-P188. Poloxamer 188 labelled at both PEO blocks terminal hydroxyls with Rhodamine B. (Figure obtained from Wenjia Zhang).

Preliminary imaging experiments of RhB-P188 using confocal microscopy

The confocal microscopy imaging was performed by D'Anna Nelson, a graduate student, as part of her rotation project under my mentorship. As a first pass experiment, HEK cells were subjected to a 15 second distilled H_2O hypo-osmotic stress in the presence or absence of RhB-P188.

Visualization was performed using confocal microscopy at the University Imaging Center (UIC). As seen on **Figure 3**, the RhB-P188 appears to localize at the periphery of the cells suggesting membrane labeling. However, labeling was observed in both stressed and unstressed conditions, indicating non-specific interaction with the cells. This was further confirmed when addition of pure rhodamine dye to unstressed HEK cells still led to intense labeling signals (data not shown). This result is not surprising

considering the innate hydrophobicity of rhodamine itself. A recent study has demonstrated that hydrophobicity of a dye is the major determinant of non-specific binding[291].

Another study examining non-specific membrane interaction of a range of water-soluble fluorophores exposed to unilamellar lipid vesicles found that another rhodamine derivative, Sulforhodamine B, has a high membrane interaction factor[290]. However, this study also showed that another red shifted fluorophore, Alexa Fluor 647 (640 nm excitation), has a relatively insignificant membrane interaction factor, making it an arguably better label candidate to test.

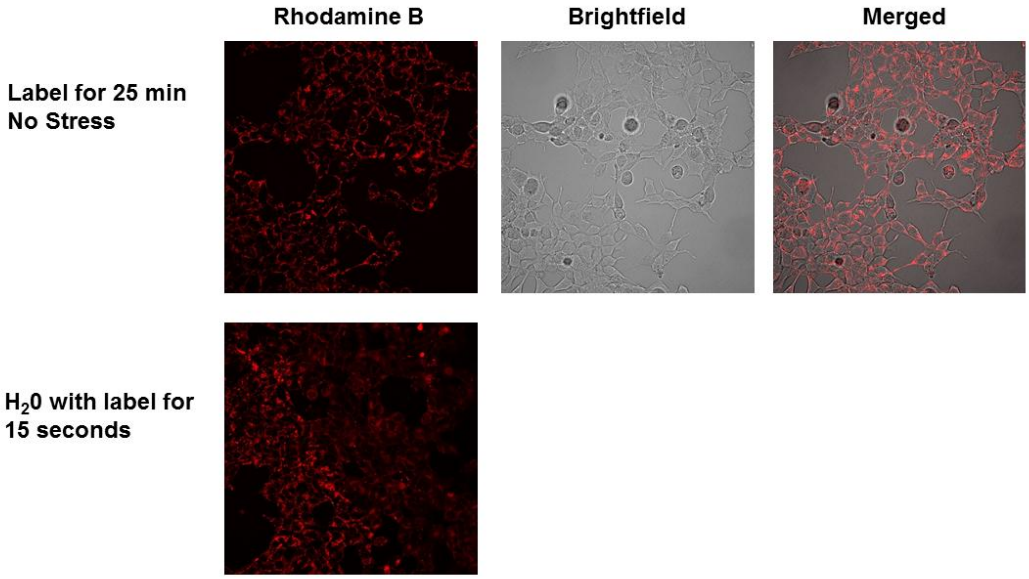

Figure 3: RhB-P188 labels both stressed and unstressed HEK cells. HEK cells were subjected to 25 minute incubation with 150 uM RhB-P188. The label-containing media was then replaced with dye-free media for imaging. Red channel and brightfield images were then taken under normal isotonic conditions (**top panels**) and under hypo-osmotic stress (**bottom panel**). Label-containing media was replaced with dye-free media for imaging.

Tagging of P188 with Alexa Fluor 647 dye

To label P188 with Alexa Fluor 647, a copper-free click chemistry approach was chosen. Conjugation of the Alexa dye necessitated azide-functionalization of the terminal end groups of the copolymer. This synthetic step was designed and performed by Dr. Karen Haman, a collaborating former graduate student in Dr. Frank Bates group in CEMS. Briefly, azide-functionalization of P188 required tosylation of the normally hydroxyl-terminated P188 followed by reaction with sodium azide to substitute the tosylated end groups with azide. The product was characterized with NMR and FTIR to ensure successful azide substitution.

To generate the Alexa Fluor 647-P188, the copper-free click reagent Alexa Fluor 647 DIBO alkyne (Invitrogen, Carlsbad,CA) was reacted in 1.5x molar excess with azide-functionalized P188 at room temperature in the dark, overnight.

Preliminary imaging experiments of AlexaFluor647-P188 using confocal microscopy

The confocal microscopy imaging was performed by D'Anna Nelson, a graduate student, as part of her rotation project under my mentorship. Based on the high non-specific labeling observed using the rhodamine-B tagged, the first control experiment was to determine whether or not incubation of HEK cells with the AlexaFluor 647 probe alone would result in non-specific interaction. As seen on **Figure 4**, the AlexaFluor647 label itself does not appear to non-specifically bind to HEK cells. Labeling of dead rounded cells is observed.

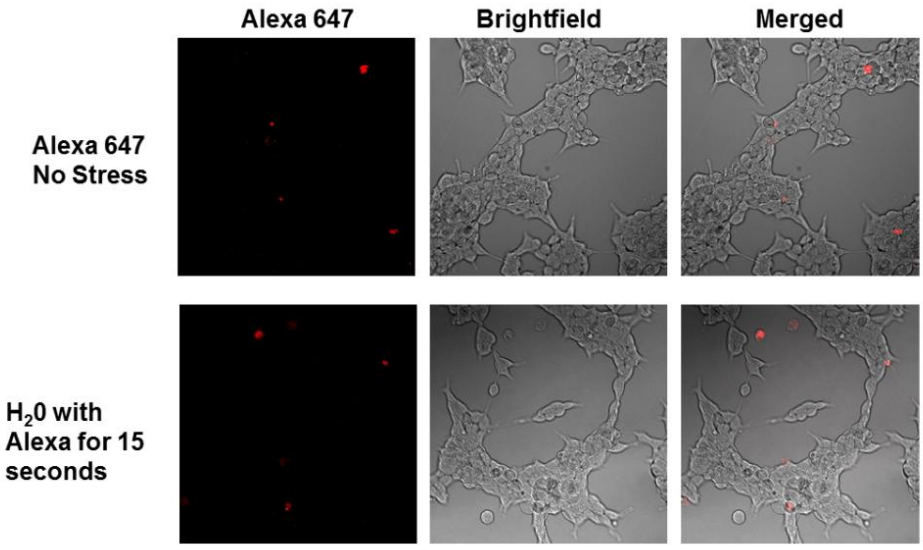

Figure 4: Alexa Fluor 647 label alone does not label HEK cells. Red channel and brightfield images taken after 10 minute incubation with 150 uM Alexa Fluor 647 under normal isotonic conditions (top panels) and under hypo-osmotic stress (bottom panels). Label-containing media was replaced with dye-free media prior to imaging.

We next visualized the Alexa Fluor 647-P188 conjugated molecule in HEK cells undergoing a hypo-osmotic stress (**Figure 5**). Except for dead rounded cells, no labeling signal was observed. These preliminary results raise several hypotheses: 1) it is possible that any membrane-specific interaction is too weak and that any potential tagged P188 is detached and washed away during media replacement; 2) while the Alexa Fluor 647 fluorophore has been determined to have low membrane interaction[290], attachment of the bulky and still relatively hydrophobic Alexa Fluor 647 molecule (MW = 1500 g/mol) on potentially both ends of the P188 copolymer (MW = 8400 g/mol) could certainly affect the copolymer's interaction with lipid bilayers. Our work in **Chapter 3** demonstrate that fine tuning of terminal end-groups of a diblock copolymer can significantly affect membrane interaction capacity, and it would be overly optimistic to think that attaching a large fluorophore at the ends of the copolymer would be completely inconsequential.

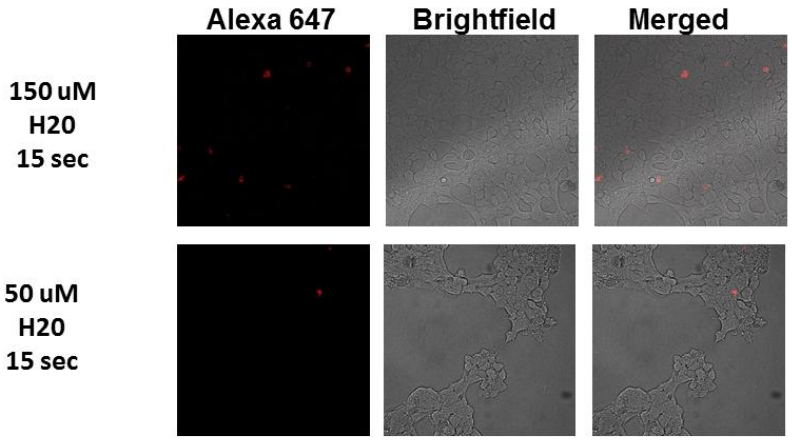

Figure 5: Alexa Fluor 647-P188 labels shows no labeling signal under hypo-osmotic stress in HEK cells. Red channel and brightfield images taken after 25 minute incubation with 150 uM Alexa Fluor 647 -P188 under normal isotonic conditions (top panels) and under hypo-osmotic stress (bottom). Label-containing media was replaced with dye-free media prior to imaging.

In summary, it remains unclear whether there is a fluorophore that combines both ease of synthesis and labelling with low effect on actual copolymer-membrane interaction. Another potential approach and subject of future studies would be to use radiolabeling of the copolymer for *in vivo* tracking purposes, as it has been done in previous pharmacokinetics studies of P188[196].

6.4 Electromyography analysis of membrane stabilizing copolymer treated *mdx* mouse during lengthening injury in vivo

It is well-established that mechanical stress during lengthening contraction disrupts muscle membranes, more notably so in DMD[96]. Along with maintaining cellular homeostasis by acting as a barrier, the cell membrane is also responsible for propagating action potentials from the neuromuscular junction, along the myofibers and down to the transverse-tubules. It has therefore been hypothesized that excitation-contraction

coupling at the level of the muscle membrane would be affected in dystrophic muscle, particularly in the context of the membrane damaging lengthening contraction injury. Studies have shown that dystrophic muscle fibers have depolarized membrane potentials, implicating impaired action potential generation and/or propagation and potentially impaired ion movement homeostasis[292–295]. Electromyography (EMG) analysis of dystrophic *mdx* muscle during lengthening contractions reveal impairment in the generation and conduction of action potentials as observed in significant decrease in M-wave root mean square (RMS)[225]. Furthermore, it was observed that *mdx* muscle fibers are depolarized post-injury, in contrast to post-injury fibers from control mice which retain normal resting membrane potential. These observations were not seen in *mdx* mice performing concentric contractions indicating that impairment in action potential generation and/or propagation is a direct result of lengthening contraction injury rather than other muscle force loss causing factors such as fatigue.

One hypothesis is that lengthening contraction injury impairs maintenance of the electrochemical gradient by disrupting intracellular homeostasis via injury-induced increased membrane permeability. To test this hypothesis, we performed a very preliminary study where we used a membrane stabilizer copolymer to stabilize the membrane during *in vivo* lengthening contractions while simultaneously performing EMG analysis in order to assess whether a stabilized membrane would prevent a loss in M-waves RMS. This study was performed in collaboration with Dr. Dawn Lowe from the Physical Therapy and Rehabilitation Science department at the University of Minnesota. Dr. Lowe performed the surgical implantations of the electrodes necessary for EMG measurements.

The electrodes were implanted in the TA muscles of *mdx* mice as described previously[296]. Briefly, mice were anesthetized using isoflurane and the distal ends of two platinum-iridium electrode wires with de-insulated ends were passed through a 26-gauge needle beneath the superficial fascial sheath of the TA so that the wires lay 2 mm apart. This spacing allows for sampling of the M-wave activity from the entire TA muscle. The

proximal ends of the wires were run subcutaneously to the dorsal cervical region and through the skin to be connected to an EMG amplifier during the actual experiment. Mice were allowed to recover for 10 days before testing.

30 min prior to testing, *mdx* mice were injected intraperitoneally (IP) with either saline vehicle, or 1000 mg/kg copolymer. Because this was a very preliminary study, the copolymer used in this study is a triblock copolymer of equivalent PPO/PEO ratio as P188 but of smaller molecular weight. While not mentioned previously in this work, this copolymer has also demonstrated *in vivo* efficacy using 1000 mg/kg IP injections in a n = 5 *mdx* mice group (data not shown).

Very preliminary results (n = 1 for copolymer treated group) suggest that copolymer based-membrane stabilization reduces M-wave RMS decreases during a lengthening injury protocol (**Figure 6**). If confirmed under rigorous further study, this would support the hypothesis that the impairment in action potential generation/conduction occurs at the membrane level upward of the intracellular contractile machinery. While these are very preliminary results and a larger group of treated animals need to be further tested, we can speculate about the mechanisms underlying this impairment. Previous findings that injured fibers are depolarized post lengthening injury[225] suggest the involvement of ion channels at the membrane, such as stretch and voltage activated Na^+ and Ca^{2+} channels, as well as increased transmembrane influx and outflow of ions due to increased membrane permeability.

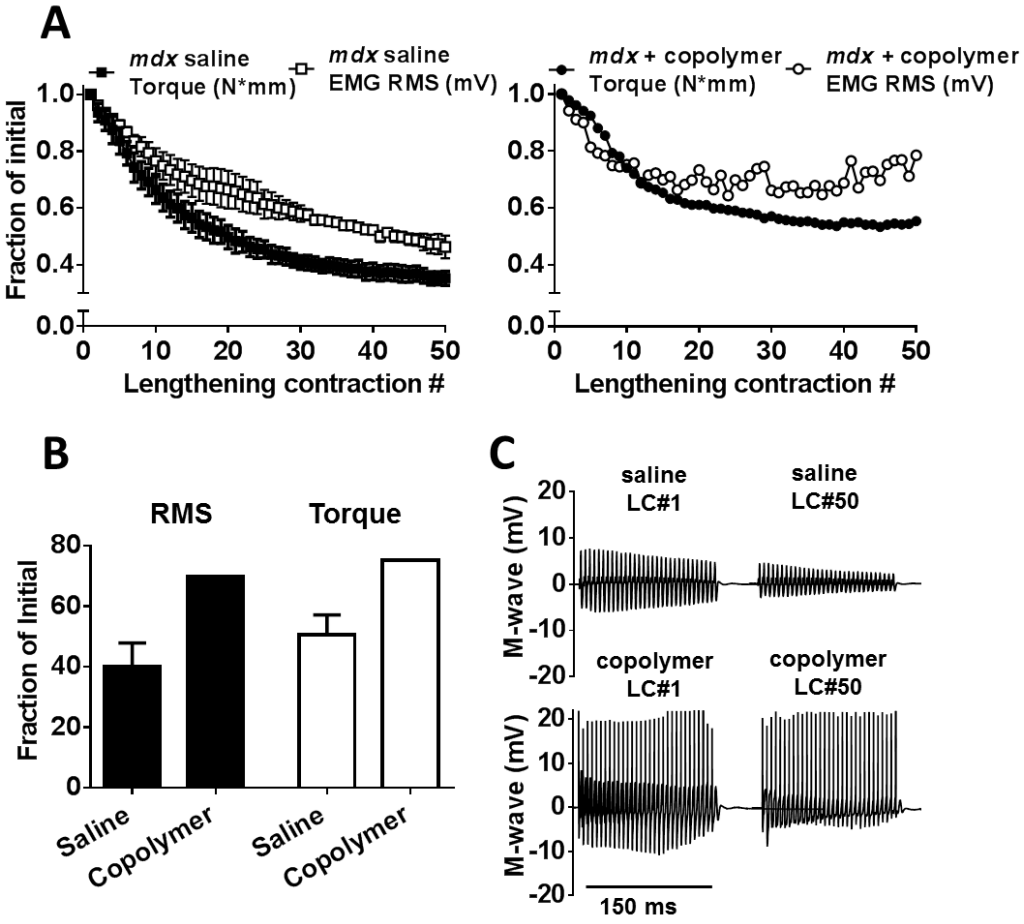

Figure 6: Torque and M-wave in mdx mice treated with saline or membrane stabilizing copolymer. (**A**) Force loss and M-wave RMS of the anterior crural muscles, in adult *mdx* mice treated with saline (n = 4) or 1000 mg/kg copolymer (n =1) intraperitoneally at least 30 min before the injury protocol, was assessed over the course of 50 lengthening contractions**.** Force loss and M-wave RMS is presented as a fraction of the initial maximal force +/- S.E.M. (**B**) Postinjury isometric torque and RMS recovery. (**C**) Representative M-wave tracings at lengthening contraction#1 and #50 for saline and copolymer treated *mdx* mice.

Impairment in the tightly regulated electrical gradient could lead to the reported observed increased Na^+ and Ca^{2+} concentrations inside cells and dysregulation of the activity of channels that are part of that electrochemical cascade. Moreover, sustained depolarization of individual fibers renders them unexcitable and less likely to contribute

to force production. Copolymer-based membrane stabilization could therefore play a role in preventing transmembrane leaking of ions and help maintain normal resting membrane potential. More work could be done to dissect this mechanism of impaired action potential generation/conduction including measuring resting membrane potentials of injured myofibers in the presence of membrane stabilizers and membrane channel blockers to tease apart specific contributions to the deficit. While the total force deficit observed during lengthening contraction injury in DMD is likely the result of multiple factors, the purpose of this study is to tease apart the specific contribution of the impaired electrophysiology and to potentially relate it to the concurrently observed loss of intracellular homeostasis.

FINAL REMARKS

This whole body of work is the final product of an interdisciplinary and collaborative approach to further understanding how to optimize synthetic copolymers for biomedical application in the context of Duchenne Muscular Dystrophy. Collectively, the results obtained in this dissertation work has highlighted and addressed several gaps in knowledge in the field. These include issues of *in vivo* delivery for optimal efficacy, a first mechanistic investigation of block copolymer architecture and chemistry, and finally, the development of a computational tool to probe mechanism of interaction at a biophysical level. It represents a significant advancement to what is a relatively new area of research and discovery and hopefully furthers the potential clinical application of a line of medically-relevant polymer chemistries.

REFERENCES

1. Hoffman, EP, Brown, RH and Kunkel, LM (1987). Dystrophin: the protein product of the Duchenne muscular dystrophy locus. *Cell* **51**: 919–928.
2. Emery, AE (1993). Duchenne muscular dystrophy--Meryon's disease. *Neuromuscul. Disord.* **3**: 263–266.
3. Emery, AEH (1991). Population frequencies of inherited neuromuscular diseases - A world survey. *Neuromuscul. Disord.* **1**: 19–29.
4. Emery, AEH (2002). The muscular dystrophies. *Lancet* **359**: 687–695.
5. Gowers, WR (1895). *A manual of the nervous system*, Philadelphia.
6. Strehle, E-M and Straub, V (2015). Recent developments in the management of Duchenne muscular dystrophy. *Arch Dis Child*doi:10.1016/j.paed.2011.06.007.
7. McDonald, DGM, Kinali, M, Gallagher, AC, Mercuri, E, Muntoni, F, Roper, H, *et al.* (2002). Fracture prevalence in Duchenne muscular dystrophy. *Dev. Med. Child Neurol.* **44**: 695–698.
8. Eagle, M, Baudouin, S V., Chandler, C, Giddings, DR, Bullock, R and Bushby, K (2002). Survival in Duchenne muscular dystrophy: Improvements in life expectancy since 1967 and the impact of home nocturnal ventilation. *Neuromuscul. Disord.* **12**: 926–929.
9. Bushby, K, Finkel, R, Birnkrant, DJ, Case, LE, Clemens, PR, Cripe, L, *et al.* (2010). Diagnosis and management of Duchenne muscular dystrophy, part 2: implementation of multidisciplinary care. *Lancet Neurol.* **9**: 177–189.
10. Emery, A (2002). Duchenne muscular dystrophy. *Motulski AG* **10**: 138–51.
11. Boland, B, Silbert, P and Groover, R (1996). Skeletal, cardiac, and smooth muscle failure in Duchenne muscular dystrophy. *Pediatr. Neurol.* **14**: 7–12.
12. Townsend, D, Yasuda, S and Metzger, J (2007). Cardiomyopathy of Duchenne muscular dystrophy: pathogenesis and prospect of membrane sealants as a new therapeutic approach. *Expert Rev. Cardiovasc. Ther.* **5**: 99–109.

13. Bushby, K, Finkel, R, Birnkrant, DJ, Case, LE, Clemens, PR, Cripe, L, *et al.* (2010). Diagnosis and management of Duchenne muscular dystrophy, part 1: diagnosis, and pharmacological and psychosocial management. *Lancet Neurol.* **9**: 77–93.
14. Cox, GF and Kunkel, LM (1997). Dystrophies and heart disease. *Curr. Opin. Cardiol.* **12**: 329–343.
15. Muntoni, F (2003). Cardiomyopathy in muscular dystrophies. *Curr. Opin. Neurol.* **16**: 577–583.
16. Moxley, RT, Pandya, S, Ciafaloni, E, Fox, DJ and Campbell, K (2010). Change in natural history of Duchenne muscular dystrophy with long-term corticosteroid treatment: implications for management. *J. Child Neurol.* **25**: 1116–1129.
17. Spurney, CF (2011). Cardiomyopathy of Duchenne muscular dystrophy: current understanding and future directions. *Muscle Nerve* **44**: 8–19.
18. Nigro, G, Comi, LI, Politano, L and Bain, RJ (1990). The incidence and evolution of cardiomyopathy in Duchenne muscular dystrophy. *Int. J. Cardiol.* **26**: 271–7.
19. Finsterer, J and Stöllberger, C (2003). The heart in human dystrophinopathies. *Cardiology* **99**: 1–19.
20. Hinton, VJ, De Vivo, DC, Nereo, NE, Goldstein, E and Stern, Y (2000). Poor verbal working memory across intellectual level in boys with Duchenne dystrophy. *Neurology* **54**: 2127–2132.
21. Jagadha, V and Becker, LE (1988). Brain morphology in Duchenne muscular dystrophy: a Golgi study. *Pediatr Neurol* **4**: 87–92.
22. Muntoni, F, Torelli, S and Ferlini, A (2003). Dystrophin and mutations: One gene, several proteins, multiple phenotypes. *Lancet Neurol.* **2**: 731–740.
23. Sadoulet-Puccio, HM and Kunkel, LM (1996). Dystrophin and its isoforms. *Brain Pathol.* **6**: 25–35.
24. Bhasin, N, Law, R, Liao, G, Safer, D, Ellmer, J, Discher, BM, *et al.* (2005). Molecular extensibility of mini-dystrophins and a dystrophin rod construct. *J. Mol.*

Biol. **352**: 795–806.

25. Chamberlain, JS (2002). Gene therapy of muscular dystrophy. *Hum. Mol. Genet.* **11**: 2355–2362.
26. Barnabei, MS, Martindale, JJ, Townsend, D and Metzger, JM (2011). Exercise and Muscular Dystrophy: Implications and Analysis of Effects on Musculoskeletal and Cardiovascular Systems. *Compr. Physiol.* **1**.
27. Lynch, GS, Rafael, JA, Chamberlain, JS and Faulkner, JA (2000). Contraction-induced injury to single permeabilized muscle fibers from mdx, transgenic mdx, and control mice. *Am J Physiol Cell Physiol* **279**: C1290–4.
28. Rybakova, IN, Patel, JR and Ervasti, JM (2000). The Dystrophin Complex Forms a Mechanically Strong Link between the Sarcolemma and Costameric Actin. *J. Cell Biol.* **150**: 1209–1214.
29. Ervasti, JM (2003). Costameres: The Achilles' heel of Herculean muscle. *J. Biol. Chem.* **278**: 13591–13594.
30. Klietsch, R, Ervasti, JM, Arnold, W, Campbell, KP and Jorgensen, AO (1993). Dystrophin-glycoprotein complex and laminin colocalize to the sarcolemma and transverse tubules of cardiac muscle. *Circ Res* **72**: 349–360.
31. Ohlendieck, K and Campbell, KP (1991). Dystrophin-associated proteins are greatly reduced in skeletal muscle from mdx mice. *J. Cell Biol.* **115**: 1685–1694.
32. Townsend, D, Blankinship, MJ, Allen, JM, Gregorevic, P, Chamberlain, JS and Metzger, JM (2007). Systemic administration of micro-dystrophin restores cardiac geometry and prevents dobutamine-induced cardiac pump failure. *Mol. Ther.* **15**: 1086–1092.
33. Street, SF (1983). Lateral transmission of tension in frog myofibers: a myofibrillar network and transverse cytoskeletal connections are possible transmitters. *J. Cell. Physiol.* **114**: 346–364.
34. Petrof, BJ, Shrager, JB, Stedman, HH, Kelly, AM and Sweeney, HL (1993). Dystrophin protects the sarcolemma from stresses developed during muscle

contraction. *Proc. Natl. Acad. Sci. U. S. A.* **90**: 3710–3714.

35. Bloch, RJ and Gonzalez-Serratos, H (2003). Lateral force transmission across costameres in skeletal muscle. *Exerc. Sport Sci. Rev.* **31**: 73–78.
36. Lovering, RM and De Deyne, PG (2004). Contractile function, sarcolemma integrity, and the loss of dystrophin after skeletal muscle eccentric contraction-induced injury. *Am. J. Physiol. Cell Physiol.* **286**: C230–C238.
37. Yasuda, S, Townsend, D, Michele, DE, Favre, EG, Day, SM and Metzger, JM (2005). Dystrophic heart failure blocked by membrane sealant poloxamer. *Nature* **436**: 1025–9.
38. Ramaswamy, KS, Palmer, ML, van der Meulen, JH, Renoux, A, Kostrominova, TY, Michele, DE, *et al.* (2011). Lateral transmission of force is impaired in skeletal muscles of dystrophic mice and very old rats. *J. Physiol.* **589**: 1195–208.
39. Tinsley, JM, Blake, DJ, Roche, a, Fairbrother, U, Riss, J, Byth, BC, *et al.* (1992). Primary structure of dystrophin-related protein. *Nature* **360**: 591–593.
40. Thomas, GD, Sander, M, Lau, KS, Huang, PL, Stull, JT and Victor, RG (1998). Impaired metabolic modulation of alpha-adrenergic vasoconstriction in dystrophin-deficient skeletal muscle. *Proc. Natl. Acad. Sci.* **95**: 15090–15095.
41. Brenman, JE, Chao, DS, Xia, H, Aldape, K and Bredt, DS (1995). Nitric oxide synthase complexed with dystrophin and absent from skeletal muscle sarcolemma in Duchenne muscular dystrophy. *Cell* **82**: 743–752.
42. Chang, WJ, Iannaccone, ST, Lau, KS, Masters, BS, McCabe, TJ, McMillan, K, *et al.* (1996). Neuronal nitric oxide synthase and dystrophin-deficient muscular dystrophy. *Proc. Natl. Acad. Sci. U. S. A.* **93**: 9142–9147.
43. Sander, M, Chavoshan, B, Harris, S a, Iannaccone, ST, Stull, JT, Thomas, GD, *et al.* (2000). Functional muscle ischemia in neuronal nitric oxide synthase-deficient skeletal muscle of children with Duchenne muscular dystrophy. *Proc. Natl. Acad. Sci. U. S. A.* **97**: 13818–13823.
44. Reiser, PJ, Kline, WO and Vaghy, PL (1997). Induction of neuronal type nitric

oxide synthase in skeletal muscle by chronic electrical stimulation in vivo. *J. Appl. Physiol.* **82**: 1250–1255.

45. Sandow, A (1973). Electromechanical transforms and the mechanism of excitation-contraction coupling. *J. mechanochemistry {&} cell Motil.* **2**: 193–207.
46. Lovering, RM, Roche, J a., Bloch, RJ and De Deyne, PG (2007). Recovery of Function in Skeletal Muscle Following 2 Different Contraction-Induced Injuries. *Arch. Phys. Med. Rehabil.* **88**: 617–625.
47. van Meer, G, Voelker, DR and Feigenson, GW (2008). Membrane lipids: where they are and how they behave. *Nat. Rev. Mol. Cell Biol.* **9**: 112–124.
48. Singer, SJ and Nicolson, GL (1972). The fluid mosaic model of the structure of cell membranes. *Science* **175**: 720–731.
49. DeLisi, C and Wiegel, FW (1983). Membrane fluidity and the probability of complement fixation. *J. Theor. Biol.* **102**: 307–22.
50. Evans, E and Needham, D (1987). Physical properties of surfactant bilayer membranes: thermal transitions, elasticity, rigidity, cohesion and colloidal interactions. *J. Phys. Chem.* **91**: 4219–4228.
51. Chabanel, a., Flamm, M and Sung, KLP (1983). Influence of cholesterol content on red cell membrane viscoelasticity and fluidity. *Biophys. J.* **44**: 171–176.
52. Lenaz, G (1987). Lipid fluidity and membrane protein dynamics. *Biosci. Rep.* **7**: 823–837.
53. Ramírez, OT and Mutharasan, R (1990). The role of the plasma membrane fluidity on the shear sensitivity of hybridomas grown under hydrodynamic stress. *Biotechnol. Bioeng.* **36**: 911–920.
54. Lentz, BR (1989). Membrane 'fluidity' as detected by diphenylhexatriene probes. *Chem. Phys. Lipids* **50**: 171–190.
55. Marguet, D, Lenne, P-F, Rigneault, H and He, H-T (2006). Dynamics in the plasma membrane: how to combine fluidity and order. *EMBO J.* **25**: 3446–3457.
56. Tanii, H, Huang, J, Ohyashiki, T and Hashimoto, K (1994). Physical-chemical-

activity relationship of organic solvents: Effects on Na+-K+-ATPase activity and membrane fluidity in mouse synaptosomes. *Neurotoxicol. Teratol.* **16**: 575–582.

57. Terry, A V, Buccafusco, JJ and Decker, MW (1997). Cholinergic channel activator, ABT-418, enhances delayed-response accuracy in rats. *Drug Dev. Res.* **40**: 304–312.
58. Mokri, B and Engel, AG (1975). Duchenne dystrophy: electron microscopic findings pointing to a basic or early abnormality in the plasma membrane of the muscle fiber. *Neurology* **25**: 1111–20.
59. Pestronk, A, Parhad, IM, Drachman, DB and Price, DL (1982). Membrane myopathy: morphological similarities to Duchenne muscular dystrophy. *Muscle Nerve* **5**: 209–214.
60. Ozawa, E, Hagiwara, Y and Yoshida, M (1999). Creatine kinase, cell membrane and Duchenne Muscular Dystrophy. *Mol Cell Biochem* **190**: 143–51.
61. Wrogemann, K and Pena, SDJ (1976). Mitochondrial Calcium Overload: a General Mechanism for Cell-Necrosis in Muscle Diseases. *Lancet* **307**: 672–674.
62. Burr, a R and Molkentin, JD (2015). Genetic evidence in the mouse solidifies the calcium hypothesis of myofiber death in muscular dystrophy. *Cell Death Differ.*: 1–11doi:10.1038/cdd.2015.65.
63. Matsuda, R, Nishikawa, A and Tanaka, H (1995). Visualization of dystrophic muscle fibers in mdx mouse by vital staining with Evans blue: evidence of apoptosis in dystrophin-deficient muscle. *J. Biochem.* **118**: 959–964.
64. Stedman, HH, Sweeney, HL, Shrager, JB, Maguire, HC, Panettieri, R a, Petrof, B, *et al.* (1991). The mdx mouse diaphragm reproduces the degenerative changes of Duchenne muscular dystrophy. *Nature* **352**: 536–539.
65. Bers, DM (2002). Cardiac excitation-contraction coupling. *Nature* **415**: 198–205.
66. Pratt, SJP, Shah, SB, Ward, CW, Inacio, MP, Stains, JP and Lovering, RM (2013). Effects of in vivo injury on the neuromuscular junction in healthy and dystrophic muscles. *J. Physiol.* **591**: 559–70.

67. Hopf, FW, Turner, PR, Denetclaw, WF, Reddy, P and Steinhardt, R a (1996). A critical evaluation of resting intracellular free calcium regulation in dystrophic mdx muscle. *Am. J. Physiol.* **271**: C1325–39.
68. Alderton, JM and Steinhardt, R a. (2000). Calcium influx through calcium leak channels is responsible for the elevated levels of calcium-dependent proteolysis in dystrophic myotubes. *J. Biol. Chem.* **275**: 9452–9460.
69. Imbert, N, Vandebrouck, C, Constantin, B, Duport, G, Guillou, C, Cognard, C, *et al.* (1996). Hypoosmotic shocks induce elevation of resting calcium level in duchenne muscular dystrophy myotubes contracting in vitro. *Neuromuscul. Disord.* **6**: 351–360.
70. Allen, DG and Whitehead, NP (2011). Duchenne muscular dystrophy--what causes the increased membrane permeability in skeletal muscle? *Int. J. Biochem. Cell Biol.* **43**: 290–4.
71. Gailly, P, De Backer, F, Van Schoor, M and Gillis, JM (2007). In situ measurements of calpain activity in isolated muscle fibres from normal and dystrophin-lacking mdx mice. *J. Physiol.* **582**: 1261–75.
72. Niebroj-Dobosz, I, Kornguth, S, Schutta, HS and Siegel, FL (1989). Elevated calmodulin levels and reduced calmodulin-stimulated calcium-ATPase in Duchenne progressive muscular dystrophy. *Neurology* **39**: 1610–1614.
73. Klee, CB, Crouch, TH and Krinks, MH (1979). Calcineurin: a calcium- and calmodulin-binding protein of the nervous system. *Proc. Natl. Acad. Sci.* **76**: 6270–3.
74. Kyrychenko, V, Poláková, E, Janíček, R and Shirokova, N (2015). Mitochondrial dysfunctions during progression of dystrophic cardiomyopathy. *Cell Calcium* **58**: 186–195.
75. Papa, S and Skulachev, VP (1997). Reactive oxygen species, mitochondria, apoptosis and aging. *Mol. Cell. Biochem.* **174**: 305–319.
76. Whitehead, NP, Yeung, EW and Allen, DG (2006). Muscle damage in mdx

(dystrophic) mice: role of calcium and reactive oxygen species. *Clin. Exp. Pharmacol. Physiol.* **33**: 657–662.

77. Shkryl, VM, Martins, AS, Ullrich, ND, Nowycky, MC, Niggli, E and Shirokova, N (2009). Reciprocal amplification of ROS and Ca2+ signals in stressed mdx dystrophic skeletal muscle fibers. *Pflugers Arch. Eur. J. Physiol.* **458**: 915–928.
78. Zhelev, D V. and Needham, D (1993). Tension-stabilized pores in giant vesicles: determination of pore size and pore line tension. *BBA - Biomembr.* **1147**: 89–104.
79. Krasieva, TB and Steinhardt, RA (2000). A Decrease in Membrane Tension Precedes Successful Cell-Membrane Repair **11**: 4339–4346.
80. Dai, J and Sheetz, MP (1995). Regulation of endocytosis, exocytosis, and shape by membrane tension. *Cold Spring Harb. Symp. Quant. Biol.* **60**: pp 567–571.
81. Sheetz, MP and Dai, J (1996). Modulation of membrane dynamics and cell motility by membrane tension. *Trends Cell Biol.* **6**: 85–89.
82. McNeil, PL and Steinhardt, RA (1997). Loss, restoration, and maintenance of plasma membrane integrity. *J. Cell Biol.* **137**: 1–4.
83. De Mello, W (1973). Membrane Sealing in Frog Skeletal-Muscle Fibers. *Proc. Natl. Acad. Sci.* **70**: 982–984.
84. Togo, T, Alderton, JM, Bi, GQ and Steinhardt, R a (1999). The mechanism of facilitated cell membrane resealing. *J. Cell Sci.* **112 (Pt 5**: 719–31.
85. Anderson, L V, Davison, K, Moss, JA, Young, C, Cullen, MJ, Walsh, J, *et al.* (1999). Dysferlin is a plasma membrane protein and is expressed early in human development. *Hum. Mol. Genet.* **8**: 855–861.
86. Han, R, Bansal, D, Miyake, K, Muniz, VP, Weiss, RM, McNeil, PL, *et al.* (2007). Dysferlin-mediated membrane repair protects the heart from stress-induced left ventricular injury. *J. Clin. Invest.* **117**: 1805–13.
87. Bansal, D, Miyake, K, Vogel, SS, Groh, S, Chen, CC, Williamson, R, *et al.* (2003). Defective membrane repair in dysferlin-deficient muscular dystrophy. *Nature* **423**: 168–172.

88. Lennon, NJ, Kho, A, Bacskai, BJ, Perlmutter, SL, Hyman, BT and Brown, RH (2003). Dysferlin Interacts with Annexins A1 and A2 and Mediates Sarcolemmal Wound-healing. *J. Biol. Chem.* **278**: 50466–50473.

89. Han, R and Campbell, KP (2007). Dysferlin and muscle membrane repair. *Curr. Opin. Cell Biol.* **19**: 409–416.

90. Sudhof, TC and Rothman, JE (2009). Membrane fusion: grappling with SNARE and SM proteins. *Science (80-.).* **323**: 474–477.

91. Stein, A, Radhakrishnan, A, Riedel, D, Fasshauer, D and Jahn, R (2007). Synaptotagmin activates membrane fusion through a Ca2+-dependent trans interaction with phospholipids. *Nat. Struct. Mol. Biol.* **14**: 904–911.

92. Bansal, D and Campbell, KP (2004). Dysferlin and the plasma membrane repair in muscular dystrophy. *Trends Cell Biol.* **14**: 206–213.

93. Mcneil, P (2009). Membrane repair redux : redox of MG53. *Nat. Cell Biol.* **11**: 9–11.

94. Cai, C, Masumiya, H, Weisleder, N, Matsuda, N, Nishi, M, Hwang, M, *et al.* (2009). MG53 nucleates assembly of cell membrane repair machinery. *Nat. Cell Biol.* **11**: 56–64.

95. Hwang, M, Ko, J-K, Weisleder, N, Takeshima, H and Ma, J (2011). Redox-dependent oligomerization through a leucine zipper motif is essential for MG53-mediated cell membrane repair. *Am. J. Physiol. Cell Physiol.* **301**: C106–C114.

96. Petrof, BJ, Shrager, JB, Stedman, HH, Kelly, a M and Sweeney, HL (1993). Dystrophin protects the sarcolemma from stresses developed during muscle contraction. *Proc. Natl. Acad. Sci. U. S. A.* **90**: 3710–4.

97. Drachman, DB, Toyka, KV and Myer, E (1974). Prednisone in Duchenne Muscular Dystrophy. *Lancet* **304**: 1409–1412.

98. Manzur, AY, Kuntzer, T, Pike, M and Swan, A (2008). Glucocorticoid corticosteroids for Duchenne muscular dystrophy. *Cochrane Database Syst. Rev.*doi:10.1002/14651858.CD003725.pub3.

99. Bach, JR, Campagnolo, DI and Hoeman, S (1991). Life satisfaction of individuals with Duchenne muscular dystrophy using long-term mechanical ventilatory support. *Am. J. Phys. Med. Rehabil.* **70**: 129–135.
100. Bach, JR and Martinez, D (2011). Duchenne muscular dystrophy: continuous noninvasive ventilatory support prolongs survival. *Respir. Care* **56**: 744–750.
101. Wolthers, OD and Pedersen, S (1990). *Short term linear growth in asthmatic children during treatment with prednisolone. BMJ* **301**, 145-148pp.
102. Baltgalvis, KA, Call, JA, Nikas, JB and Lowe, DA (2009). Effects of prednisolone on skeletal muscle contractility in mdx mice. *Muscle and Nerve* **40**: 443–454.
103. Avioli, L V (1993). Glucocorticoid effects on statural growth. *Br. J. Rheumatol.* **32 Suppl 2**: 27–30.
104. Markham, LW, Spicer, RL, Khoury, PR, Wong, BL, Mathews, KD and Cripe, LH (2005). Steroid therapy and cardiac function in duchenne muscular dystrophy. *Pediatr. Cardiol.* **26**: 768–771.
105. Ogata, H, Ishikawa, Y and Minami, R (2009). Beneficial effects of beta-blockers and angiotensin-converting enzyme inhibitors in Duchenne muscular dystrophy.[Erratum appears in J Cardiol. 2009 Apr;53(2):316]. *J. Cardiol.* **53**: 72–78.
106. Viollet, L, Thrush, PT, Flanigan, KM, Mendell, JR and Allen, HD (2012). Effects of angiotensin-converting enzyme inhibitors and/or beta blockers on the cardiomyopathy in duchenne muscular dystrophy. *Am. J. Cardiol.* **110**: 98–102.
107. Ishikawa, Y, Bach, JR and Minami, R (1999). Cardioprotection for Duchenne's muscular dystrophy. *Am. Heart J.* **137**: 895–902.
108. Bulfield, G, Siller, WG, Wight, PA and Moore, KJ (1984). X chromosome-linked muscular dystrophy (mdx) in the mouse. *Proc. Natl. Acad. Sci. U. S. A.* **81**: 1189–92.
109. Grady, RM, Teng, H, Nichol, MC, Cunningham, JC, Wilkinson, RS and Sanes, JR (1997). Skeletal and cardiac myopathies in mice lacking utrophin and dystrophin: a

model for Duchenne muscular dystrophy. *Cell* **90**: 729–38.

110. Capote, J, DiFranco, M and Vergara, JL (2010). Excitation-contraction coupling alterations in mdx and utrophin/dystrophin double knockout mice: a comparative study. *Am. J. Physiol. Cell Physiol.* **298**: C1077–86.
111. Sharp, NJ, Kornegay, JN, Van Camp, SD, Herbstreith, MH, Secore, SL, Kettle, S, *et al.* (1992). An error in dystrophin mRNA processing in golden retriever muscular dystrophy, an animal homologue of Duchenne muscular dystrophy. *Genomics* **13**: 115–121.
112. Kornegay, JN, Tuler, SM, Miller, DM and Levesque, DC (1988). Muscular dystrophy in a litter of golden retriever dogs. *Muscle Nerve* **11**: 1056–64.
113. Collins, C a. and Morgan, JE (2003). Duchenne's muscular dystrophy: Animal models used to investigate pathogenesis and develop therapeutic strategies. *Int. J. Exp. Pathol.* **84**: 165–172.
114. Jarmin, S, Kymalainen, H, Popplewell, L and Dickson, G (2014). New developments in the use of gene therapy to treat Duchenne muscular dystrophy. *Expert Opin. Biol. Ther.* **14**: 209–230.
115. Liu, M, Yue, Y, Harper, SQ, Grange, RW, Chamberlain, JS and Duan, D (2005). Adeno-associated virus-mediated microdystrophin expression protects young mdx muscle from contraction-induced injury. *Mol. Ther.* **11**: 245–256.
116. Foster, H, Sharp, PS, Athanasopoulos, T, Trollet, C, Graham, IR, Foster, K, *et al.* (2008). Codon and mRNA sequence optimization of microdystrophin transgenes improves expression and physiological outcome in dystrophic mdx mice following AAV2/8 gene transfer. *Mol. Ther.* **16**: 1825–32.
117. Zhang, Y, Yue, Y, Li, L, Hakim, CH, Zhang, K, Thomas, GD, *et al.* (2013). Dual AAV therapy ameliorates exercise-induced muscle injury and functional ischemia in murine models of Duchenne muscular dystrophy. *Hum. Mol. Genet.* **22**: 3720–9.
118. Harper, SQ, Hauser, MA, DelloRusso, C, Duan, D, Crawford, RW, Phelps, SF, *et al.* (2002). Modular flexibility of dystrophin: implications for gene therapy of

Duchenne muscular dystrophy. *Nat. Med.* **8**: 253–261.

119. Call, J a, Ervasti, JM and Lowe, D a (2011). TAT-μUtrophin mitigates the pathophysiology of dystrophin and utrophin double-knockout mice. *J. Appl. Physiol.* **111**: 200–5.
120. Gordon, BS, Lowe, D a and Kostek, MC (2014). Exercise increases utrophin protein expression in the mdx mouse model of Duchenne muscular dystrophy. *Muscle Nerve* **49**: 915–8.
121. Hirst, RC, McCullagh, KJA and Davies, KE (2005). Utrophin upregulation in Duchenne Muscular Dystrophy. *Acta Myol.* **24**: 209–215.
122. Perkins, KJ and Davies, KE (2002). The role of utrophin in the potential therapy of Duchenne muscular dystrophy. *Neuromuscul. Disord.* **12**.
123. Yue, Y, Liu, M and Duan, D (2006). C-terminal-truncated microdystrophin recruits dystrobrevin and syntrophin to the dystrophin-associated glycoprotein complex and reduces muscular dystrophy in symptomatic utrophin/dystrophin double-knockout mice. *Mol. Ther.* **14**: 79–87.
124. Yokota, T, Lu, QL, Partridge, T, Kobayashi, M, Nakamura, A, Takeda, S, *et al.* (2009). Efficacy of systemic morpholino exon-skipping in duchenne dystrophy dogs. *Ann. Neurol.* **65**: 667–676.
125. Sharp, PS, Bye-a-Jee, H and Wells, DJ (2011). Physiological characterization of muscle strength with variable levels of dystrophin restoration in mdx mice following local antisense therapy. *Mol. Ther.* **19**: 165–71.
126. Alter, J, Lou, F, Rabinowitz, A, Yin, H, Rosenfeld, J, Wilton, SD, *et al.* (2006). Systemic delivery of morpholino oligonucleotide restores dystrophin expression bodywide and improves dystrophic pathology. *Nat. Med.* **12**: 175–177.
127. Lu, QL, Rabinowitz, A, Chen, YC, Yokota, T, Yin, H, Alter, J, *et al.* (2005). Systemic delivery of antisense oligoribonucleotide restores dystrophin expression in body-wide skeletal muscles. *Proc. Natl. Acad. Sci. U. S. A.* **102**: 198–203.
128. Goyenvalle, A, Griffith, G, Babbs, A, Andaloussi, S El, Ezzat, K, Avril, A, *et al.*

(2015). Functional correction in mouse models of muscular dystrophy using exon-skipping tricyclo-DNA oligomers. *Nat. Med.*doi:10.1038/nm.3765.

129. Lu, Q-L, Cirak, S and Partridge, T (2014). What Can We Learn From Clinical Trials of Exon Skipping for DMD? *Mol. Ther. Nucleic Acids* **3**: e152.
130. Hoffman, EP and McNally, EM (2014). Exon-skipping therapy: a roadblock, detour, or bump in the road? *Sci. Transl. Med.* **6**: 230fs14.
131. Voit, T, Topaloglu, H, Straub, V, Muntoni, F, Deconinck, N, Campion, G, *et al.* (2014). Safety and efficacy of drisapersen for the treatment of Duchenne muscular dystrophy (DEMAND II): An exploratory, randomised, placebo-controlled phase 2 study. *Lancet Neurol.* **13**: 987–996.
132. Mendell, JR, Rodino-Klapac, LR, Sahenk, Z, Roush, K, Bird, L, Lowes, LP, *et al.* (2013). Eteplirsen for the treatment of Duchenne muscular dystrophy. *Ann. Neurol.* **74**: 637–647.
133. Mendell, JR, Goemans, N, Lowes, LP, Alfano, LN, Berry, K, Shao, J, *et al.* (2016). Longitudinal effect of eteplirsen versus historical control on ambulation in Duchenne muscular dystrophy. *Ann. Neurol.*doi:10.1002/ana.24555.
134. Lu, Q-L, Cirak, S and Partridge, T (2014). What Can We Learn From Clinical Trials of Exon Skipping for DMD? *Mol. Ther. Nucleic Acids* **3**: e152.
135. Ran, FA, Hsu, PD, Wright, J, Agarwala, V, Scott, DA and Zhang, F (2013). Genome engineering using the CRISPR-Cas9 system. *Nat. Protoc.* **8**: 2281–308.
136. Ran, FA, Hsu, PD, Lin, CY, Gootenberg, JS, Konermann, S, Trevino, AE, *et al.* (2013). Double nicking by RNA-guided CRISPR cas9 for enhanced genome editing specificity. *Cell* **154**: 1380–1389.
137. Nelson, CE, Nelson, CE, Hakim, CH, Ousterout, DG, Thakore, PI, Moreb, EA, *et al.* (2015). *In vivo genome editing improves muscle function in a mouse model of Duchenne muscular dystrophy*. *Science (80-.).* **5143**, 1-8pp.
138. Long, C, Amoasii, L, Mireault, AA, McAnally, JR, Li, H, Sanchez-Ortiz, E, *et al.* (2015). Postnatal genome editing partially restores dystrophin expression in a

mouse model of muscular dystrophy. *Science* **5725**: aad5725.

139. Tabebordbar, M, Zhu, K, Cheng, JKW, Chew, WL, Widrick, JJ, Yan, WX, *et al.* (2015). In vivo gene editing in dystrophic mouse muscle and muscle stem cells. *Science (80-.).* **5177**: 1–9.
140. Patel, K and Amthor, H (2005). The function of Myostatin and strategies of Myostatin blockade - New hope for therapies aimed at promoting growth of skeletal muscle. *Neuromuscul. Disord.* **15**: 117–126.
141. Nakatani, M, Takehara, Y, Sugino, H, Matsumoto, M, Hashimoto, O, Hasegawa, Y, *et al.* (2008). Transgenic expression of a myostatin inhibitor derived from follistatin increases skeletal muscle mass and ameliorates dystrophic pathology in mdx mice. *FASEB J.* **22**: 477–487.
142. Bogdanovich, S, Krag, TOB, Barton, ER, Morris, LD, Whittemore, L-A, Ahima, RS, *et al.* (2002). Functional improvement of dystrophic muscle by myostatin blockade. *Nature* **420**: 418–21.
143. Wagner, KR, Liu, X, Chang, X and Allen, RE (2005). Muscle regeneration in the prolonged absence of myostatin. *Proc. Natl. Acad. Sci. U. S. A.* **102**: 2519–2524.
144. Bish, LT, Sleeper, MM, Forbes, SC, Morine, KJ, Reynolds, C, Singletary, GE, *et al.* (2011). Long-term systemic myostatin inhibition via liver-targeted gene transfer in golden retriever muscular dystrophy. *Hum. Gene Ther.* **22**: 1499–1509.
145. Wagner, KR, Fleckenstein, JL, Amato, AA, Barohn, RJ, Bushby, K, Escolar, DM, *et al.* (2008). A phase I/IItrial of MYO-029 in adult subjects with muscular dystrophy. *Ann Neurol* **63**: 561–571.
146. Patel, K, Macharia, R and Amthor, H (2005). Molecular mechanisms involving IGF-1 and myostatin to induce muscle hypertrophy as a therapeutic strategy for Duchenne muscular dystrophy. *Acta Myol.* **24**: 230–241.
147. Schertzer, JD, Ryall, JG and Lynch, GS (2006). Systemic administration of IGF-I enhances oxidative status and reduces contraction-induced injury in skeletal muscles of mdx dystrophic mice. *Am. J. Physiol. Endocrinol. Metab.* **291**: E499–

505.

148. Filareto, A, Parker, S, Darabi, R, Borges, L, Iacovino, M, Schaaf, T, *et al.* (2013). An ex vivo gene therapy approach to treat muscular dystrophy using inducible pluripotent stem cells. *Nat. Commun.* **4**: 1549.

149. Cai, C, Masumiya, H, Weisleder, N, Pan, Z, Nishi, M, Komazaki, S, *et al.* (2009). MG53 regulates membrane budding and exocytosis in muscle cells. *J. Biol. Chem.* **284**: 3314–3322.

150. Cai, C, Masumiya, H, Weisleder, N, Matsuda, N, Nishi, M, Hwang, M, *et al.* (2009). MG53 nucleates assembly of cell membrane repair machinery. *Nat. Cell Biol.* **11**: 56–64.

151. Weisleder, N, Takizawa, N, Lin, P, Wang, X, Cao, C, Zhang, Y, *et al.* (2012). Recombinant MG53 Protein Modulates Therapeutic Cell Membrane Repair in Treatment of Muscular Dystrophy. *Sci. Transl. Med.* **4**: 139ra85–139ra85.

152. Song, R, Peng, W, Zhang, Y, Lv, F, Wu, H-K, Guo, J, *et al.* (2013). Central role of E3 ubiquitin ligase MG53 in insulin resistance and metabolic disorders. *Nature* **494**: 375–9.

153. Townsend, D, Yasuda, S, Chamberlain, J and Metzger, JM (2009). Cardiac consequences to skeletal muscle-centric therapeutics for Duchenne muscular dystrophy. *Trends Cardiovasc. Med.* **19**: 50–55.

154. Megeney, LA, Kablar, B, Perry, RL, Ying, C, May, L and Rudnicki, MA (1999). Severe cardiomyopathy in mice lacking dystrophin and MyoD. *Proc. Natl. Acad. Sci. U. S. A.* **96**: 220–225.

155. Politano, L, Nigro, V, Nigro, G, Petretta, VR, Passamano, L, Papparella, S, *et al.* (1996). Development of cardiomyopathy in female carriers of Duchenne and Becker muscular dystrophies. *JAMA* **275**: 1335–1338.

156. Melacini, P, Fanin, M, Danieli, GA, Fasoli, G, Villanova, C, Angelini, C, *et al.* (1993). Cardiac involvement in Becker muscular dystrophy. *J. Am. Coll. Cardiol.* **22**: 1927–34.

157. Hourdé, C, Joanne, P, Medja, F, Mougenot, N, Jacquet, A, Mouisel, E, *et al.* (2013). Voluntary physical activity protects from susceptibility to skeletal muscle contraction-induced injury but worsens heart function in mdx mice. *Am. J. Pathol.* **182**: 1509–18.

158. Townsend, D, Yasuda, S, Li, S, Chamberlain, JS and Metzger, JM (2008). Emergent dilated cardiomyopathy caused by targeted repair of dystrophic skeletal muscle. *Mol. Ther.* **16**: 832–5.

159. Townsend, D, Yasuda, S, Li, S, Chamberlain, JS and Metzger, JM (2008). Emergent dilated cardiomyopathy caused by targeted repair of dystrophic skeletal muscle. *Mol. Ther.* **16**: 832–5.

160. Batrakova, E V, Miller, DW, Li, SHU, Alakhov, VYU, Kabanov, A V, Elmquist, WF, *et al.* (2001). Pluronic P85 Enhances the Delivery of Digoxin to the Brain : In Vitro and in Vivo Studies **296**: 551–557.

161. Shaik, N, Giri, N and Elmquist, WF (2009). Investigation of the micellar effect of pluronic P85 on P-glycoprotein inhibition: cell accumulation and equilibrium dialysis studies. *J. Pharm. Sci.* **98**: 4170–90.

162. Venne, A, Li, S, Mandeville, R, Kabanov, A and Alakhov, V (1996). Hypersensitizing effect of pluronic L61 on cytotoxic activity, transport, and subcellular distribution of doxorubicin in multiple drug- resistant cells. *Cancer Res.* **56**: 3626–3629.

163. Krylova, OO and Pohl, P (2004). Ionophoric Activity of Pluronic Block Copolymers. *Biochemistry* **43**: 3696–3703.

164. Demina, T, Grozdova, I, Krylova, O, Zhirnov, A, Istratov, V, Frey, H, *et al.* (2005). Relationship between the structure of amphiphilic copolymers and their ability to disturb lipid bilayers. *Biochemistry* **44**: 4042–54.

165. Lee, RC, River, LP, Pan, FS, Ji, L and Wollmann, RL (1992). Surfactant-induced sealing of electropermeabilized skeletal muscle membranes in vivo. *Proc. Natl. Acad. Sci. U. S. A.* **89**: 4524–8.

166. Maskarinec, S a, Wu, G and Lee, KYC (2005). Membrane sealing by polymers. *Ann. N. Y. Acad. Sci.* **1066**: 310–20.

167. Frey, SL, Zhang, D, Carignano, M a, Szleifer, I and Lee, KYC (2007). Effects of block copolymer's architecture on its association with lipid membranes: experiments and simulations. *J. Chem. Phys.* **127**: 114904.

168. Wu, G, Majewski, J, Ege, C, Kjaer, K, Weygand, MJ and Lee, KYC (2005). Interaction between lipid monolayers and poloxamer 188: an X-ray reflectivity and diffraction study. *Biophys. J.* **89**: 3159–73.

169. Wang, J-Y, Chin, J, Marks, JD and Lee, KYC (2010). Effects of PEO-PPO-PEO triblock copolymers on phospholipid membrane integrity under osmotic stress. *Langmuir* **26**: 12953–61.

170. Cheng, C-Y, Wang, J-Y, Kausik, R, Lee, KYC and Han, S (2012). Nature of interactions between PEO-PPO-PEO triblock copolymers and lipid membranes: (II) role of hydration dynamics revealed by dynamic nuclear polarization. *Biomacromolecules* **13**: 2624–33.

171. Grover, FL, Heron, MW, Newman, MM and Paton, BC (1969). Effect of a Nonionic Surface-Active Agent on Blood Viscosity and Platelet Adhesiveness. *Circulation* **39**: I–249–252.

172. Hymes, AC, Safavian, MH, Gunther, T and Forsman, J (1971). The influence of an industrial surfactant pluronic F-68, in the treatment of hemorrhagic shock. *J. Surg. Res.* **11**: 191–197.

173. Mitsuno, T, Ohyanagi, H and Yokoyama, K (1984). Development of a perfluorochemical emulsion as a blood gas carrier. *Artif. Organs* **8**: 25–33.

174. Smith, CM, Hebbel, RP, Tukey, DP, Clawson, CC, White, JG and Vercellotti, GM (1987). Pluronic F-68 reduces the endothelial adherence and improves the rheology of liganded sickle erythrocytes. *Blood* **69**: 1631–6.

175. Adams-Graves, P, Kedar, A, Koshy, M, Steinberg, M, Veith, R, Ward, D, *et al.* (1997). *RheothRx (poloxamer 188) injection for the acute painful episode of sickle*

cell disease: a pilot study. Blood **90**, 2041-2046pp.

176. Ballas, SK, Files, B, Luchtman-Jones, L, Benjamin, L, Swerdlow, P, Hilliard, L, *et al.* (2004). Safety of purified poloxamer 188 in sickle cell disease: phase I study of a non-ionic surfactant in the management of acute chest syndrome. *Hemoglobin* **28**: 85–102.
177. Rodeheaver, GT, Kurtz, L and Kircher, BJ (1980). Pluronic F-68 ": A Promising New Skin Wound Cleanser **11**: 572–576.
178. Alexandridis, P and Hatton, TA (1995). Poly(Ethylene Oxide)-Poly(Propylene Oxide)-Poly(Ethylene Oxide) Block-Copolymer Surfactants in Aqueous-Solutions and at Interfaces - Thermodynamics, Structure, Dynamics, and Modeling. *Colloids Surfaces a-Physicochemical Eng. Asp.* **96**: 1–46.
179. Martindale, JJ and Metzger, JM (2014). Uncoupling of increased cellular oxidative stress and myocardial ischemia reperfusion injury by directed sarcolemma stabilization. *J. Mol. Cell. Cardiol.* **67**: 26–37.
180. Murphy, AD, McCormack, MC, Bichara, D a, Nguyen, JT, Randolph, M a, Watkins, MT, *et al.* (2010). Poloxamer 188 protects against ischemia-reperfusion injury in a murine hind-limb model. *Plast. Reconstr. Surg.* **125**: 1651–60.
181. Padanilam, JT, Bischof, JC, Lee, RC, Cravalho, EG, Tompkins, RG, Yarmush, ML, *et al.* (1994). Effectiveness of poloxamer 188 in arresting calcein leakage from thermally damaged isolated skeletal muscle cells. *Ann. N. Y. Acad. Sci.* **720**: 111–23.
182. Hannig, J, Zhang, D, Canaday, DJ, Beckett, M a, Astumian, RD, Weichselbaum, RR, *et al.* (2000). Surfactant sealing of membranes permeabilized by ionizing radiation. *Radiat. Res.* **154**: 171–7.
183. Greenebaum, B, Blossfield, K, Hannig, J, Carrillo, CS, Beckett, M a, Weichselbaum, RR, *et al.* (2004). Poloxamer 188 prevents acute necrosis of adult skeletal muscle cells following high-dose irradiation. *Burns* **30**: 539–47.
184. Emanuele, RM (1998). FLOCOR: a new anti-adhesive, rheologic agent. *Expert*

Opin. Investig. Drugs **7**: 1193–200.

185. Yusuf, S, Flather, M and Gent, M (1997). Effects of RheothRx on mortality, morbidity, left ventricular function, and infarct size in patients with acute myocardial infarction. *Circulation…* **96**: 192–201.

186. Schaer, GL, Spaccavento, LJ, Browne, KF, Krueger, KA, Krichbaum, D, Phelan, JM, *et al.* (1996). *Beneficial effects of RheothRx injection in patients receiving thrombolytic therapy for acute myocardial infarction. Results of a randomized, double-blind, placebo-controlled trial. Circulation* **94**, 298-307pp.

187. Townsend, D, Turner, I, Yasuda, S, Martindale, J, Davis, J, Shillingford, M, *et al.* (2010). Chronic administration of membrane sealant prevents severe cardiac injury and ventricular dilatation in dystrophic dogs. *J. Clin. Invest.* **120**: 1140–50.

188. Spurney, CF, Guerron, AD, Yu, Q, Sali, A, van der Meulen, JH, Hoffman, EP, *et al.* (2011). Membrane sealant Poloxamer P188 protects against isoproterenol induced cardiomyopathy in dystrophin deficient mice. *BMC Cardiovasc. Disord.* **11**: 20.

189. Quinlan, JG, Wong, BL, Niemeier, RT, McCullough, AS, Levin, L and Emanuele, M (2006). Poloxamer 188 failed to prevent exercise-induced membrane breakdown in mdx skeletal muscle fibers. *Neuromuscul. Disord.* **16**: 855–64.

190. Terry, RL, Kaneb, HM and Wells, DJ (2014). Poloxomer 188 has a deleterious effect on dystrophic skeletal muscle function. *PLoS One* **9**: e91221.

191. Collins, JM, Despa, F and Lee, RC (2007). Structural and functional recovery of electropermeabilized skeletal muscle in-vivo after treatment with surfactant poloxamer 188. *Biochim. Biophys. Acta* **1768**: 1238–46.

192. Walters, TJ, Mase, VJ, Roe, JL, Dubick, M a and Christy, RJ (2011). Poloxamer-188 reduces muscular edema after tourniquet-induced ischemia-reperfusion injury in rats. *J. Trauma* **70**: 1192–7.

193. Suzuki, N, Akiyama, T, Takahashi, T, Komuro, H, Warita, H, Tateyama, M, *et al.* (2012). Continuous administration of poloxamer 188 reduces overload-induced

muscular atrophy in dysferlin-deficient SJL mice. *Neurosci. Res.* **72**: 181–6.

194. Ng, R, Metzger, JM, Claflin, DR and Faulkner, JA (2008). Poloxamer 188 reduces the contraction-induced force decline in lumbrical muscles from mdx mice. *Am. J. Physiol. Cell Physiol.* **295**: C146–C150.

195. Markham, BE, Kernodle, S, Nemzek, J, Wilkinson, JE and Sigler, R (2015). Chronic Dosing with Membrane Sealant Poloxamer 188 NF Improves Respiratory Dysfunction in Dystrophic Mdx and Mdx/Utrophin-/- Mice. *PLoS One* **10**: e0134832.

196. Grindel, JM, Jaworski, T, Piraner, O, Emanuele, RM and Balasubramanian, M (2002). Distribution, metabolism, and excretion of a novel surface-active agent, purified poloxamer 188, in rats, dogs, and humans. *J. Pharm. Sci.* **91**: 1936–47.

197. Jewell, RC, Khor, SP, Kisor, DF, Lacroix, KAK and Wargin, WA (1997). Pharmacokinetics of RheothRx injection in healthy male volunteers. *J. Pharm. Sci.* **86**: 808–812.

198. Jewell, RC, Khor, SP, Kisor, DF, LaCroix, K a and Wargin, W a (1997). Pharmacokinetics of RheothRx injection in healthy male volunteers. *J. Pharm. Sci.* **86**: 808–12.

199. Singh-Joy, SD and McLain, VC (2008). Safety assessment of poloxamers 101, 105, 108, 122, 123, 124, 181, 182, 183, 184, 185, 188, 212, 215, 217, 231, 234, 235, 237, 238, 282, 284, 288, 331, 333, 334, 335, 338, 401, 402, 403, and 407, poloxamer 105 benzoate, and poloxamer 182 dibenzoate as use. *Int. J. Toxicol.* **27 Suppl 2**: 93–128.

200. Emanuele, M and Balasubramaniam, B (2014). Differential effects of commercial-grade and purified poloxamer 188 on renal function. *Drugs R. D.* **14**: 73–83.

201. Maskarinec, S a, Hannig, J, Lee, RC and Lee, KYC (2002). Direct observation of poloxamer 188 insertion into lipid monolayers. *Biophys. J.* **82**: 1453–9.

202. Maskarinec, S a. and Lee, KYC (2003). Comparative Study of Poloxamer Insertion into Lipid Monolayers †. *Langmuir* **19**: 1809–1815.

203. Firestone, MA, Wolf, AC and Seifert, S (2003). Small-angle X-ray scattering study of the interaction of Poly(ethylene oxide)-b-Poly(propylene oxide)-b-Poly(ethylene oxide) triblock copolymers with lipid bilayers. *Biomacromolecules* **4**: 1539–1549.

204. Cheng, C-Y, Wang, J-Y, Kausik, R, Lee, KYC and Han, S (2012). An ultrasensitive tool exploiting hydration dynamics to decipher weak lipid membrane-polymer interactions. *J. Magn. Reson.* **215**: 115–9.

205. Bates, FS and Fredrickson, GH (1999). Block Copolymers—Designer Soft Materials. *Phys. Today* **52**: 32.

206. Lodge, TP (2003). Block copolymers: Past successes and future challenges. *Macromol. Chem. Phys.* **204**: 265–273.

207. Batrakova, E V, Li, S, Alakhov, VY, Miller, DW and Kabanov, A V (2003). Optimal structure requirements for pluronic block copolymers in modifying P-glycoprotein drug efflux transporter activity in bovine brain microvessel endothelial cells. *J. Pharmacol. Exp. Ther.* **304**: 845–54.

208. Nawaz, S, Redhead, M, Mantovani, G, Alexander, C, Bosquillon, C and Carbone, P (2012). Interactions of PEO–PPO–PEO block copolymers with lipid membranes: a computational and experimental study linking membrane lysis with polymer structure. *Soft Matter* **8**: 6744.

209. Wang, J, Segatori, L and Biswal, SL (2014). Probing the association of triblock copolymers with supported lipid membranes using microcantilevers. *Soft Matter* **10**: 6417–24.

210. Wu, G and Lee, KYC (2009). Interaction of poloxamers with liposomes: an isothermal titration calorimetry study. *J. Phys. Chem. B* **113**: 15522–31.

211. Arnold, K, Zschoernig, O, Barthel, D and Herold, W (1990). Exclusion of poly(ethylene glycol) from liposome surfaces. *Biochim. Biophys. Acta* **1022**: 303–310.

212. Wang, J-Y, Marks, J and Lee, KYC (2012). Nature of interactions between PEO-

PPO-PEO triblock copolymers and lipid membranes: (I) effect of polymer hydrophobicity on its ability to protect liposomes from peroxidation. *Biomacromolecules* **13**: 2616–23.

213. Riess, G (2003). Micellization of block copolymers. *Prog. Polym. Sci.* **28**: 1107–1170.
214. Gohy, JF (2005). Block Copolymer Micelles. *Block Copolym. II* **190**: pp 65–136.
215. Zhao, MWC, Wang, Y, Xu, R, Winnik, MA and Croucher, MD (1991). Poly(styrene-ethylene oxide) Block Copolymer Micelle Formation in Water: A Fluorescence Probe Study': 1033–1040.
216. Batrakova, E V, Li, S, Li, Y, Alakhov, VY, Elmquist, WF and Kabanov, A V (2004). Distribution kinetics of a micelle-forming block copolymer Pluronic P85. *J. Control. Release* **100**: 389–97.
217. Holland, RJ, Parker, EJ, Guiney, K and Zeld, FR (1995). Fluorescence Probe Studies of Ethylene Oxide / Propylene Oxide Block Copolymers in Aqueous Solution **64**: 11981–11988.
218. Basu Ray, G, Chakraborty, I and Moulik, SP (2006). Pyrene absorption can be a convenient method for probing critical micellar concentration (cmc) and indexing micellar polarity. *J. Colloid Interface Sci.* **294**: 248–54.
219. Lopes, JR and Loh, W (1998). Investigation of Self-Assembly and Micelle Polarity for a wide Range of Ethylene Oxide-Propylene Oxide-Ethylene Oxide Block Copolymers in Water. *Langmuir* **14**: 750–756.
220. Batrakova, E V, Shengmin, L, Shu, L, Annie, V, Alakhov Valery and Kabanov, A V (1999). Fundamental relationships between the composition of pluronic block copolymers and their hypersensitization effect in MDR cancer cells. *Pharm. Res.* **16**: 1373–1379.
221. Kabanov, A V, Nazarova, IR, Astafieva, I V, Batrakova, E V, Alakhov, VY, Yaroslavov, AA, *et al.* (1995). Micelle Formation and Solubilization of Fluorescent Probes in Poly(oxyethylene-b-oxypropylene-b-oxyethylene) Solutions.

Macromolecules **28**: 2303–2314.

222. Abdel-Rahman, SM and Kauffman, RE (2004). The integration of pharmacokinetics and pharmacodynamics: understanding dose-response. *Annu. Rev. Pharmacol. Toxicol.* **44**: 111–136.
223. Rowland, M and Tozer, TN. Clinical Pharmacokinetics and Pharmacodynamics Concepts and Applications. *Pharm. Sci.*
224. Ingalls, CP, Warren, GL, Lowe, D a, Boorstein, DB and Armstrong, RB (1996). Differential effects of anesthetics on in vivo skeletal muscle contractile function in the mouse. *J. Appl. Physiol.* **80**: 332–40.
225. Call, J a, Warren, GL, Verma, M and Lowe, D a (2013). Acute failure of action potential conduction in mdx muscle reveals new mechanism of contraction-induced force loss. *J. Physiol.* **591**: 3765–76.
226. Pal, S, Milano, G and Roccatano, D (2006). Synthetic polymers and biomembranes. How do they interact? Atomistic molecular dynamics simulation study of PEO in contact with a DMPC lipid bilayer. *J. Phys. Chem. B* **110**: 26170–9.
227. Adhikari, U, Goliaei, A, Tsereteli, L and Berkowitz, ML (2016). Properties of Poloxamer Molecules and Poloxamer Micelles Dissolved in Water and Next to Lipid Bilayers: Results from Computer Simulations. *J. Phys. Chem. B*: acs.jpcb.5b11448doi:10.1021/acs.jpcb.5b11448.
228. Eagle, M, Bourke, J, Bullock, R, Gibson, M, Mehta, J, Giddings, D, *et al.* (2007). Managing Duchenne muscular dystrophy - The additive effect of spinal surgery and home nocturnal ventilation in improving survival. *Neuromuscul. Disord.* **17**: 470–475.
229. Moriuchi, T, Kagawa, N, Mukoyama, M and Hizawa, K (1993). Autopsy analyses of the muscular dystrophies. *Tokushima J. Exp. Med.* **40**: 83–93.
230. McNally, EM (2007). New approaches in the therapy of cardiomyopathy in muscular dystrophy. *Annu. Rev. Med.* **58**: 75–88.

231. Goyenvalle, A, Seto, JT, Davies, KE and Chamberlain, J (2011). Therapeutic approaches to muscular dystrophy. *Hum. Mol. Genet.* **20**.
232. Malerba, A, Sharp, PS, Graham, IR, Arechavala-Gomeza, V, Foster, K, Muntoni, F, *et al.* (2011). Chronic systemic therapy with low-dose morpholino oligomers ameliorates the pathology and normalizes locomotor behavior in mdx mice. *Mol. Ther.* **19**: 345–54.
233. Danialou, G, Comtois, a S, Dudley, R, Karpati, G, Vincent, G, Des Rosiers, C, *et al.* (2001). Dystrophin-deficient cardiomyocytes are abnormally vulnerable to mechanical stress-induced contractile failure and injury. *FASEB J.* **15**: 1655–7.
234. Spurney, CF, Guerron, AD, Yu, Q, Sali, A, van der Meulen, JH, Hoffman, EP, *et al.* (2011). Membrane sealant Poloxamer P188 protects against isoproterenol induced cardiomyopathy in dystrophin deficient mice. *BMC Cardiovasc. Disord.* **11**: 20.
235. Menke, A and Jockusch, H (1991). Decreased osmotic stability of dystrophin-less muscle cells from the mdx mouse. *Nature* **349**: 69–71.
236. Menke, A and Jockusch, H (1995). Extent of shock-induced membrane leakage in human and mouse myotubes depends on dystrophin **733**: 727–733.
237. Call, JA, Eckhoff, MD, Baltgalvis, KA, Warren, GL and Lowe, DA (2011). Adaptive strength gains in dystrophic muscle exposed to repeated bouts of eccentric contraction. *J. Appl. Physiol.* **111**: 1768–77.
238. Goudenege, S, Lamarre, Y, Dumont, N, Rousseau, J, Frenette, J, Skuk, D, *et al.* (2010). Laminin-111: a potential therapeutic agent for Duchenne muscular dystrophy. *Mol. Ther.* **18**: 2155–63.
239. Belanto, JJ, Mader, TL, Eckhoff, MD, Strandjord, DM, Banks, GB, Gardner, MK, *et al.* (2014). Microtubule binding distinguishes dystrophin from utrophin. *Proc. Natl. Acad. Sci. U. S. A.* **111**: 5723–8.
240. Roche, J a, Lovering, RM and Bloch, RJ (2008). Impaired recovery of dysferlin-null skeletal muscle after contraction-induced injury in vivo. *Neuroreport* **19**:

1579–1584.

241. Verma, M, Asakura, Y, Hirai, H, Watanabe, S, Tastad, C, Fong, GH, *et al.* (2010). Flt-1 haploinsufficiency ameliorates muscular dystrophy phenotype by developmentally increased vasculature in mdx mice. *Hum. Mol. Genet.* **19**: 4145–4159.

242. Arpke, RW, Darabi, R, Mader, TL, Zhang, Y, Toyama, A, Lonetree, CL, *et al.* (2013). A new immuno-, dystrophin-deficient model, the NSG-mdx4Cv mouse, provides evidence for functional improvement following allogeneic satellite cell transplantation. *Stem Cells* **31**: 1611–1620.

243. Rowland, M and Tozer, TN (2010). *Clinical pharmacokinetics and pharmacodynamics : concepts and application*.

244. McLennan, DN, Porter, CJH and Charman, S a (2005). Subcutaneous drug delivery and the role of the lymphatics. *Drug Discov. Today. Technol.* **2**: 89–96.

245. Turner, P V, Brabb, T, Pekow, C and Vasbinder, MA (2011). Administration of Substances to Laboratory Animals : Routes of Administration and Factors to Consider **50**.

246. Kabanov, A V, Batrakova, E V and Alakhov, VY (2002). Pluronic® block copolymers as novel polymer therapeutics for drug and gene delivery. *J. Control. Release* **82**: 189–212.

247. Kabanov, A V, Batrakova, E V and Miller, DW (2003). Pluronic® block copolymers as modulators of drug efflux transporter activity in the blood – brain barrier **55**: 151–164.

248. de Kretser, T a and Livett, BG (1977). Skeletal-muscle sarcolemma from normal and dystrophic mice. Isolation, characterization and lipid composition. *Biochem. J.* **168**: 229–237.

249. Otten, W, Iaizzo, P a and Eichinger, HM (1997). Effects of a high n-3 fatty acid diet on membrane lipid composition of heart and skeletal muscle in normal swine and in swine with the genetic mutation for malignant hyperthermia. *J. Lipid Res.*

38: 2023–2034.

250. Bagher, P, Duan, D and Segal, SS (2011). Evidence for impaired neurovascular transmission in a murine model of Duchenne muscular dystrophy. *J. Appl. Physiol.* **110**: 601–609.

251. Leung, DG, Herzka, DA, Thompson, WR, He, B, Bibat, G, Tennekoon, G, *et al.* (2014). Sildenafil does not improve cardiomyopathy in Duchenne/Becker muscular dystrophy. *Ann. Neurol.*doi:10.1002/ana.24214.

252. Mendell, JR, Campbell, K, Rodino-Klapac, L, Sahenk, Z, Shilling, C, Lewis, S, *et al.* (2010). *Dystrophin immunity in Duchenne's muscular dystrophy. N. Engl. J. Med.* **363**, 1429-1437pp.

253. Kabanov, A V, Batrakova, E V, Sriadibhatla, S, Yang, Z, Kelly, DL and Alakov, VY (2005). Polymer genomics: shifting the gene and drug delivery paradigms. *J. Control. Release* **101**: 259–71.

254. Bosnakovski, D, Xu, Z, Li, W, Thet, S, Cleaver, O, Perlingeiro, RCR, *et al.* (2008). Prospective isolation of skeletal muscle stem cells with a Pax7 reporter. *Stem Cells* **26**: 3194–3204.

255. Darabi, R, Gehlbach, K, Bachoo, RM, Kamath, S, Osawa, M, Kamm, KE, *et al.* (2008). Functional skeletal muscle regeneration from differentiating embryonic stem cells. *Nat. Med.* **14**: 134–143.

256. Heydemann, A, Huber, JM, Demonbreun, A, Hadhazy, M and McNally, EM (2005). Genetic background influences muscular dystrophy. *Neuromuscul. Disord.* **15**: 601–609.

257. Lechmann, T and Reinhart, WH (1998). The non-ionic surfactant Poloxamer 188 (RheothRx) increases plasma and whole blood viscosity. *Clin. Hemorheol. Microcirc.* **18**: 31–6.

258. Houang, EM, Haman, KJ, Filareto, A, Perlingeiro, RC, Bates, FS, Lowe, D a, *et al.* (2015). Membrane-stabilizing copolymers confer marked protection to dystrophic skeletal muscle in vivo. *Mol. Ther. — Methods Clin. Dev.* **2**: 15042.

259. Firestone, MA and Seifert, S (2005). Interaction of nonionic PEO-PPO diblock copolymers with lipid bilayers. *Biomacromolecules* **6**: 2678–2687.
260. Lee, B and Firestone, MA (2008). Electron Density Mapping of Triblock Copolymers Associated with Model Biomembranes : Insights into Conformational States and Effect on Bilayer Structure. *Biomacromolecules* **9**: 1541–1550.
261. Chang, L-C, Lin, C-Y, Kuo, M-W and Gau, C-S (2005). Interactions of Pluronics with phospholipid monolayers at the air-water interface. *J. Colloid Interface Sci.* **285**: 640–652.
262. Herron, TJ, Vandenboom, R, Fomicheva, E, Mundada, L, Edwards, T and Metzger, JM (2007). Calcium-independent negative inotropy by beta-myosin heavy chain gene transfer in cardiac myocytes. *Circ. Res.* **100**: 1182–1190.
263. Davis, J, Wen, H, Edwards, T and Metzger, JM (2007). Thin filament disinhibition by restrictive cardiomyopathy mutant R193H troponin i induces Ca2+-independent mechanical tone and acute myocyte remodeling. *Circ. Res.* **100**: 1494–1502.
264. Borgens, RB, Bohnert, D, Duerstock, B, Spomar, D and Lee, RC (2004). Subcutaneous tri-block copolymer produces recovery from spinal cord injury. *J. Neurosci. Res.* **76**: 141–54.
265. Wang, T, Chen, X, Wang, Z, Zhang, M, Meng, H, Gao, Y, *et al.* (2014). Poloxamer-188 Can Attenuate Blood-Brain Barrier Damage to Exert Neuroprotective Effect in Mice Intracerebral Hemorrhage Model. *J. Mol. Neurosci.*doi:10.1007/s12031-014-0313-8.
266. Cheung, ATW, Chan, MS, Ramanujam, S, Rangaswami, A, Curl, K, Franklin, P, *et al.* (2004). Effects of poloxamer 188 treatment on sickle cell vaso-occlusive crisis: computer-assisted intravital microscopy study. *J. Investig. Med.* **52**: 402–6.
267. Pembouong, G, Morellet, N, Kral, T, Hof, M, Scherman, D, Bureau, M-F, *et al.* (2011). A comprehensive study in triblock copolymer membrane interaction. *J. Control. Release* **151**: 57–64.
268. Khadka, NK, Cheng, X, Ho, CS, Katsaras, J and Pan, J (2015). Interactions of the

Anticancer Drug Tamoxifen with Lipid Membranes. *Biophys. J.* **108**: 2492–2501.

269. Loura, LMS and Ramalho, JPP (2011). Recent developments in molecular dynamics simulations of fluorescent membrane probes. *Molecules* **16**: 5437–5452.
270. Leekumjorn, S and Sum, AK (2006). Molecular simulation study of structural and dynamic properties of mixed DPPC/DPPE bilayers. *Biophys. J.* **90**: 3951–3965.
271. Leekumjorn, S and Sum, AK (2007). Molecular studies of the gel to liquid-crystalline phase transition for fully hydrated DPPC and DPPE bilayers. *Biochim. Biophys. Acta - Biomembr.* **1768**: 354–365.
272. Poghosyan, AA and Shahinyan, AA (2005). Constant Surface Tension and Simulation of DPPC Bilayers: The CHARMM and GROMACS Force Field Comparison. *Electron. J. Nat. Sci.* **1**: 39–43.
273. Bennett, WFD, Sapay, N and Tieleman, DP (2014). Atomistic simulations of pore formation and closure in lipid bilayers. *Biophys. J.* **106**: 210–219.
274. Kong, X, Qin, S, Lu, D and Liu, Z (2014). Surface tension effects on the phase transition of a DPPC bilayer with and without protein: a molecular dynamics simulation. *Phys. Chem. Chem. Phys.* **16**: 8434–40.
275. Feller, SE and Pastor, RW (1999). Constant surface tension simulations of lipid bilayers : The sensitivity of surface areas and compressibilities. *J. Chem. Phys.* **111**: 1281–1287.
276. Tieleman, DP, Leontiadou, H, Mark, AE and Marrink, SJ (2003). Simulation of pore formation in lipid bilayers by mechanical stress and electric fields. *J. Am. Chem. Soc.* **125**: 6382–6383.
277. Sharma, V, Stebe, K, Murphy, JC and Tung, L (1996). Poloxamer 188 decreases susceptibility of artificial lipid membranes to electroporation. *Biophys. J.* **71**: 3229–41.
278. Schrodinger Maestro Desmond 2.2 User Manual.
279. Marrink, SJ and Mark, AE (2001). Effect of Undulations on Surface Tension in Simulated Bilayers. *J. Phys. Chem. B* **105**: 6122–6127.

280. Rodriguez-espigares, I, Manuel, J, Guix, R, Martinez-seara, H, Giorgino, T and Carri, P (2013). MEMBPLUGIN tutorial : A hands-on introduction 1 Summary 2 Conditions for use of the MEMBPLUGIN tools.
281. Hezaveh, S, Samanta, S, De Nicola, A, Milano, G and Roccatano, D (2012). Understanding the interaction of block copolymers with DMPC lipid bilayer using coarse-grained molecular dynamics simulations. *J. Phys. Chem. B* **116**: 14333–14345.
282. Dinç, CÖ, Kibarer, G and Güner, A (2010). Solubility profiles of poly(ethylene glycol)/solvent systems. II. Comparison of thermodynamic parameters from viscosity measurements. *J. Appl. Polym. Sci.* **117**: 1100–1119.
283. Jähnig, F (1996). What is the surface tension of a lipid bilayer membrane? *Biophys. J.* **71**: 1348–1349.
284. Israelachvili, J (1997). The different faces of poly(ethylene glycol). *Proc. Natl. Acad. Sci. U. S. A.* **94**: 8378–8379.
285. Zhou, J, Ke, F, Tong, Y, Li, Z and Liang, D (2011). Solution behavior of copolymers with poly(ethylene oxide) as the 'hydrophobic' block. *Soft Matter* **7**: 9956.
286. Stepniewski, M, Pasenkiewicz-Gierula, M, Rog, T, Danne, R, Orlowski, A, Karttunen, M, *et al.* (2011). Study of PEGylated lipid layers as a model for PEGylated liposome surfaces: Molecular dynamics simulation and langmuir monolayer studies. *Langmuir* **27**: 7788–7798.
287. Collins, JM, Despa, F and Lee, RC (2007). Structural and functional recovery of electropermeabilized skeletal muscle in-vivo after treatment with surfactant poloxamer 188. *Biochim. Biophys. Acta* **1768**: 1238–46.
288. Maynard, C, Swenson, R, Paris, JA, Martin, JS, Hallstrom, AP, Cerqueira, MD, *et al.* (1998). *Randomized, controlled trial of RheothRx (poloxamer 188) in patients with suspected acute myocardial infarction. RheothRx in Myocardial Infarction Study Group. Am. Heart J.* **135**, 797-804pp.

289. Sieblist, C, Jenzsch, M and Pohlscheidt, M (2013). Influence of pluronic F68 on oxygen mass transfer. *Biotechnol. Prog.* **29**: 1278–88.
290. Hughes, LD, Rawle, RJ and Boxer, SG (2014). Choose your label wisely: water-soluble fluorophores often interact with lipid bilayers. *PLoS One* **9**: e87649.
291. Zanetti-Domingues, LC, Tynan, CJ, Rolfe, DJ, Clarke, DT and Martin-Fernandez, M (2013). Hydrophobic fluorescent probes introduce artifacts into single molecule tracking experiments due to non-specific binding. *PLoS One* **8**: e74200.
292. Nagel, a, Lehmann-Horn, F and Engel, a G (1990). Neuromuscular transmission in the mdx mouse. *Muscle Nerve* **13**: 742–9.
293. Dunn, JF, Bannister, N, Kemp, GJ and Publicover, SJ (1993). Sodium is elevated in mdx muscles: Ionic interactions in dystrophic cells. *J. Neurol. Sci.* **114**: 76–80.
294. Dunn, JF, Burton, KA and Dauncey, MJ (1995). Ouabain sensitive Na+ K+-ATPase content is elevated in mdx mice: Implications for the regulation of ions in dystrophic muscle. *J. Neurol. Sci.* **133**: 11–15.
295. Reggiani, C, Canato, M, Dal Maschio, M, Sbrana, F, Raiteri, R, Vassanelli, S, *et al.* (2010). Mechanical and electrophysiological properties of the sarcolemma of muscle fibers in two murine models of muscle dystrophy: Col6a1-/-and Mdx. *J. Biomed. Biotechnol.* **2010**.
296. Warren, GL, Ingalls, CP, Shah, SJ and Armstrong, RB (1999). Uncoupling of in vivo torque production from EMG in mouse muscles injured by eccentric contractions. *J. Physiol.* **515 (Pt 2**: 609–19.